

Experimental Investigation of Thermal Bowing for Concrete Insulated Wall Panels

by

Sergio Arevalo

A thesis submitted in partial fulfillment of the requirements for the degree of

Master of Science

in

STRUCTURAL ENGINEERING

Department of Civil and Environmental Engineering

University of Alberta

© Sergio Arevalo, 2019

Abstract

Precast concrete insulated wall panels (IWP) are thermally and structurally efficient systems commonly used in construction. Although their flexural performance has been studied extensively, there are limited studies on thermal bowing in IWP. Bowing causes unwanted deflections, stresses on the panel and connections, and gaps in structures on their corners (i.e. ‘fishmouth effect’). Due to the lack of experimental results, designers and modelers rely on prior experience when considering thermal bowing.

Four 6.1 m long IWP with 75 mm wythes and insulation were constructed. Each IWP has different diameters of Glass Fibre Reinforced Polymer (GFRP) shear connectors (9.5 to 16 mm) spaced at 610 mm in an X-arrangement. The shear connection stiffness was determined using push-through tests. Push-through results showed non-linear behaviour and quicker loss of stiffness as connector size increased. Based on push-through results it is more efficient to use smaller connectors (#3 bar) than larger connectors, as smaller (9.5 mm) connectors were capable of carrying 84% more stress than the 16 mm connectors. The resulting load-slip curves and stiffness of connectors to be used in understanding the thermal testing were also presented.

Furthermore, a thermal enclosure was fabricated to cause thermal bowing in IWP using connectors from the push-through test. Bowing was induced by heating the wythe inside the enclosure to temperature differentials over 20°C. In terms of displacement per °C, the results showed end slip behaviour decreased 9.2% with the use of higher sized connectors compared to lower sized connectors; however, increased 16% for bowing effect in higher sized connectors compared to lower sized connectors. This shows the stiffer connector’s ability to translate resistance to end slip, into forces that create bowing. The panel with stiffest connectors showed thermal loads of 182 kN (temperature differential of 20°C) caused loss of stiffness, cracking, and permanent deformation.

Acknowledgments

The completion of this thesis would not have been possible without the support and guidance of many parties.

First and foremost, I would like to acknowledge my parents, whose sacrifices and efforts in life carved the path towards opportunities that may have never otherwise presented themselves. I am proud to be their son, and this accomplishment is theirs, too.

To my family, Gisele, Adrien, and Diego, thank you for your companionship, and general belief in me. Thank you to Qing, whose support and positive words I could count on, even in the middle of the night when one might be expected to be asleep, and not writing about walls. Thank you for always encouraging me to be my best. To my friends, thank you for your encouragement. I expect you will all read the entirety of my thesis. There will be a quiz.

I am proud to have completed this work at the University of Alberta with support from the NSERC Discovery Grants Program for funding my research, Tufbar for GFRP donations, and Lafarge for insulation and WWM insulation. My work in the lab could not have been completed without the help of Greg Miller and Cam West. Thank you to the TRG group for helping cast the panels, Benedict for the “power play” assistance in the lab, Ian with further assistance in the lab, and Clayton for the constant assurance that all would be fine.

Finally, and most importantly, I would like to express my gratitude to my advisor, Dr. “Doug” Tomlinson, whose mentorship, expertise, and guidance proved invaluable throughout the whole of this process. Thank you for taking a chance on a keen, very green engineer in training. I finish this work feeling more inspired than ever by the noble work of engineering.

Table of Contents

1.	INTRODUCTION	1
1.1	Research Objective.....	2
1.2	Scope of Research	3
1.3	Thesis Organization.....	3
2.	LITERATURE REVIEW	5
2.1	Introduction	5
2.2	History	6
2.3	Structural Designations	7
2.3.1	Fully Composite Walls	7
2.3.2	Non-Composite Walls.....	7
2.3.3	Partially Composite Walls	8
2.4	Description of Insulated Wall Panels	9
2.4.1	Wythes	9
2.4.2	Insulation.....	10
2.4.3	Shear Connectors	10
2.5	Percent Composite Action (PCA)	12
2.5.1	Evaluating Composite Action.....	12
2.6	Structural Testing of Insulated Wall Panels.....	13
2.6.1	Flexural Testing	13
2.6.2	Direct Shear Push-Through Tests	14
2.7	Types of Shear Connectors	15
2.7.1	Concrete	15
2.7.2	Steel.....	16

2.7.3	Carbon Fibre Reinforced Polymer (CFRP).....	17
2.7.4	Glass Fibre Reinforced Polymer.....	17
2.7.5	Basalt Fibre Reinforced Polymer.....	18
2.8	Thermal Characteristics of Insulated Wall Panels	19
2.8.1	Thermal Performance.....	19
2.8.2	Coefficient of Thermal Expansion.....	21
2.8.3	Evaluation of Thermal Resistance “R” Value	22
2.9	Bowing of Panels	23
2.9.1	Environmental Causes of Bowing	24
2.9.2	Structural Causes of Bowing	25
2.9.3	Composite Action Influence on Bowing.....	26
2.9.4	Challenges with Bowing.....	26
2.10	Previous Thermal Experiments	27
2.11	Models of Insulated Wall Panels.....	29
2.12	Digital Image Correlation (DIC).....	30
2.13	Gaps in Literature Review.....	30
3.	EXPERIMENTAL INVESTIGATION OF CONNECTOR STIFFNESS UNDER DOUBLE SHEAR	32
3.1	Introduction	32
3.2	Push-Through Experimental Program.....	32
3.2.1	Materials	34
3.2.2	Push-Through Fabrication	37
3.2.3	Push-through Test Setup and Instrumentation.....	38
3.3	Push-Through Testing Results	39
3.3.1	DIC Analysis.....	40

3.3.2	Summary of Push-through Test Results	42
3.3.3	Stiffness Calculation Approaches	45
3.3.4	Stiffness Moving Approach Results	46
3.3.5	Stiffness Results.....	47
3.3.6	Effect of Parameters on Failure Mode	47
3.3.7	Effect of Parameters on Peak Load.....	48
3.3.8	Effect of Parameters on Proportional Limit.....	50
3.3.9	Effect of Parameters on Stiffness.....	50
3.3.10	Effect of Parameters on Deformability	52
3.4	Shear Flow of Connector Systems.	53
3.5	Chapter Conclusion	55
3.5.1	Recommendations.....	56
4.	EXPERIMENTAL INVESTIGATION OF THERMAL BOWING IN FULL-SCALE PRECAST CONCRETE INSULATED WALL PANELS.....	57
4.1	Introduction	57
4.2	Panel Description	59
4.3	Test Parameters	60
4.4	Fabrication.....	61
4.4.1	Materials	62
4.4.2	Lifting and Handling.....	64
4.5	Thermal Enclosure Setup and Instrumentation	65
4.5.1	Fabrication	65
4.5.2	Heating Source.....	65
4.5.3	Air Circulation	66
4.5.4	Supports	66

4.5.5	IWP Placement.....	68
4.5.6	Instrumentation	68
4.6	Testing Procedure.....	69
4.7	Results	70
4.7.1	Panel Temperature Response	71
4.7.2	Calculating Temperature Differential	73
4.7.3	End Slip.....	73
4.7.4	Thermal Bowing of IWP.....	77
4.7.5	Strains	80
4.7.6	Thermal Coefficient of Expansion.....	82
4.7.7	Thermal Bowing Comparison.....	83
4.8	Force on Shear Connectors	86
4.9	Limitations of Results	88
4.10	Chapter Conclusion	89
4.11	Recommendations	91
5.	SUMMARY AND CONCLUSIONS	92
5.1	Summary	92
5.2	Conclusions	92
5.3	Recommendation for Future Work	94
	References.....	96
	Appendix A – Formwork and Specimen Construction Process.....	104
	Appendix B – Push-through specimen load and stiffness plots.....	109
	Appendix C – Temperature plots	114
	Appendix D – Material properties	123
	Appendix E – Time plots	125

LIST OF TABLES

Table 2.1 Typical structural properties of connector materials (Rudd, 2017).....	15
Table 2.2 Thermal conductivity of typical insulated wall panel materials (Woltman, 2014)	19
Table 3.1 Push through test matrix	34
Table 3.2 Summary of push-through test results	40
Table 3.3 Summary of DIC analysis.....	41
Table 3.4 Summary of push-through test results for two shear connector systems.....	47
Table 3.5 Summary of push through failure modes.....	48
Table 3.6 Deformability index results for two shear connector system	53
Table 3.7 Shear flow for connection systems tested by various researchers	54
Table 4.1 Insulated wall panel thermal bowing test matrix	60
Table 4.2 Humidity of lab and outdoors	61
Table 4.3 Summary of Total End Slip during Heating Phase.....	76
Table 4.4 Summary of Total End Slip during Cooling Phase.....	76
Table 4.5 Summary of end slip slope.....	77
Table 4.6 Summary of midspan deflection and end slip.....	77
Table 4.7 Thermal bowing slope of IWP.....	80
Table 4.8 Summary of midspan deflection (bow) for different temperature differentials.....	80
Table 4.9 Summary of strains on hot wythe, hot wythe rebar, and cold wythe.....	81
Table 4.10 Summary of coefficient of thermal expansion.....	83

LIST OF FIGURES

Figure 1.1 Corner separation resulting from thermal bowing “Fishmouth” effect (CPCI Design Manual 5, 2017).....	2
Figure 2.1 Energy Demand in Canada for (a) residential and (b) commercial and institutional sectors (NRCan, 2016-2017)	5
Figure 2.2 Strain profile and deflected shape of IWP.....	8
Figure 2.3 Insulated wall panel key components (Rudd, 2017)	9
Figure 2.4 Stiff shear connectors (a) solid concrete regions, (b) embedded truss, and (c) grid or mesh (Tomlinson, 2015).....	11
Figure 2.5 Examples of flexible shear connectors: (a) Z-shaped steel connector, (b) M-shaped steel connector, (c) polypropylene pin connector, and (d) fibreglass vinyl-ester tie (Tomlinson, 2015)	12
Figure 2.6 Four-point bending test (Teixeria and Fam, 2017).....	14
Figure 2.7 Example of push through test (Kim et al., 2014)	15
Figure 2.8 Insulated wall panel showing cross section with stiffening concrete rib (Tomlinson et al., 2016)	16
Figure 2.9 Insulated wall panel FRP bent bar connectors (Salmon et al., 1997).....	18
Figure 2.10 Thermal resistance of connectors versus connector area (Sauter, 1991).....	20
Figure 2.11 Thermal mass effects for (a) various wall systems and (b) insulated wall panels (PCI Industry Handbook Committee, 2010)	21
Figure 2.12 (a) Zone method (b) Parallel flow method (Kim and Allard, 2014)	23
Figure 2.13 Thermal bowing on (a) non-composite panel (b) fully composite panel (Tomlinson, 2015).....	25
Figure 2.14 Concrete wall panels in storage (Losch, 2003)	25
Figure 2.15 (a) Hotbox schematic (b) removal of panel from the hot box (Woltman, 2014).....	27
Figure 2.16 (a) Full-scale thermal enclosure (b) back view with restraints of full-scale thermal enclosure (c) recommended method to measure wythe-slip (Post, 2006)	28
Figure 3.1 Push-through test specimen, all dimensions in mm.	34
Figure 3.2 (a) Stress strain curves of (a) 10M (black) and WWM (red) (b) insulation (c) GFRP bars (d) concrete cylinders.....	36

Figure 3.3 (a) Push through assembly showing shear connector and reinforcement arrangement (b) push-through formwork	37
Figure 3.4 (a) Push-through test setup (b) DIC surface on front face of specimen	38
Figure 3.5 General load-slip response of push-through test (Specimen 4B3)	39
Figure 3.6 DIC Images for bonded and unbonded specimen; (a) and (b) initial insulation debonding, (c) and (d) proportional limit, (e) and (f) ultimate failure (5B2 is bonded specimen; 5U2 is unbonded specimen).....	42
Figure 3.7 Average load deflection plots for (a) bonded and (b) unbonded with reported stiffness value at 0.25 mm deflection.....	44
Figure 3.8 Stiffness values from the moving approach at locations between 0.1 and 0.4 mm.....	46
Figure 3.9 Failure modes of push-through tests (a) concrete crushing (b) tension pull-out (c) compression connector concrete crushing (d) compression connector crushing.....	48
Figure 3.10 Effect of parameters on (a) peak load (b) peak load stress.....	49
Figure 3.11 Effect of parameters on (a) proportional limit load (b) proportional limit slip.....	50
Figure 3.12 Effect of parameters on stiffness	52
Figure 3.13 Effect of parameters on deformability.....	53
Figure 4.1 Thermal bowing on (a) fully composite panel (b) non-composite panel	57
Figure 4.2 Free body diagram mechanics of thermal bowing (a) unrestrained end slip (b) force transfer to connectors (c) deflected shape of bowed panel	58
Figure 4.3 IWP Design and shear connector layout; All dimensions in (mm) (a) top view (b) side view (c) cross section view.....	59
Figure 4.4 (a) IWP formwork (b) concrete pouring (c) IWP during stripping	62
Figure 4.5 Thermal enclosure overview (a) end cross section view (b) 3D view in sketchup (end of enclosure removed for clarity).....	62
Figure 4.6 Insulated wall panel lifting	64
Figure 4.7 Thermal enclosure heating construction process (a) thermal enclosure fabrication (b) heating blanket (c) circulation fans (d) LVDT (e) DIC opening (f) simple support (g) top cap of enclosure (h) thermal enclosure during test.....	67
Figure 4.8 Insulated wall panel reinforcement and instrumentation (a) reinforcement layout (b) strain gauge reinforcement (b) thermocouple placement.....	69
Figure 4.9 Thermal enclosure setup (a) top view (b) side view (c) right view.....	70

Figure 4.10 Temperature readings over test duration for IWP-4B (a) heating cycle (b) cooling cycle (c) transient vs steady state heating	71
Figure 4.11 IWP end slip on heating cycle and cooling cycle for north and south end of IWP...	74
Figure 4.12 IWP total end slip for heating (black) and cooling (gray) phases	75
Figure 4.13 IWP midspan deflection (bow) versus temperature differential heating (black) and cooling (gray) cycle.	78
Figure 4.14 Deflections from thermal differential for (a) midspan deflection (b) bowing profile at 5 °C increments	80
Figure 4.15 IWP midspan strain gauge on hot concrete wythe (a) IWP-3B (b) IWP-4U (c) IWP-4B (d) IWP-5B.....	82
Figure 4.16 Strain at midspan for a WWM beam, and an unreinforced beam	83
Figure 4.17 Midspan deflection with respect to connector stiffness of IWP	84
Figure 4.18 End slip with respect to connector stiffness of IWP.....	85
Figure 4.19 Retrieving force and stiffness, K, of each shear connector using total end slip	86
Figure 4.20 End slip and midspan deflection with respect to stiffness up to ΔT 25 °C.....	86
Figure 4.21 Estimated shear connector force on north side and south side of panel	87
Figure 4.22 Total estimated shear connector force with temperature differential.....	88

1. INTRODUCTION

Rising economic and space heating requirements have led to more research on improving the thermal performance of buildings, particularly exterior walls. These demands require structural components to be of high-quality assurance and aesthetically pleasing. At the same time, stricter energy use requirements are amplified in regions with extreme temperature ranges such as Canada. A promising solution that balances structural performance, architectural considerations, and thermal performance are precast concrete Insulated Wall Panels (IWP).

IWP have been continuously evolving over the last five decades. They are commonly used in building envelopes as either exterior cladding or load-bearing members in buildings. IWP are attractive to designers and owners as they combine aspects such as structural strength, high thermal mass, and low thermal energy transfer. They are commonly fabricated in precast concrete plants which is economical and allows for high quality assurance. IWP typically consist of two concrete wythes (layers) that sandwich a layer of rigid insulation. Shear connectors connect the wythes together. Depending on the stiffness of these shear connectors, IWP exhibit a wide range of structural behaviour between non-composite (i.e. wythes act independently) and composite (i.e. wythes act as a single unit). Higher composite action leads to cheaper panels that utilize material more efficiently (Hodicky et al. 2014). In the past, IWP utilized embedded concrete regions and steel connectors to connect wythes, however these created thermal bridges through the insulation and reduced the thermal performance. More recent research has focused on using Fibre Reinforced Polymers (FRP) in IWP as FRP combines good structural capacity with limited thermal bridging. With FRP it is possible to build a structurally efficient IWP with good thermal performance.

However, there are still concerns with the extreme temperature gradients IWP face and the thermal bowing that results. Thermal bowing is an out-of-plane deflection caused by the

temperature differential between the two surfaces of the wall, see Figure 1.1. Depending on the degree of composite action, temperature differentials cause relative slips between the wythes or bowing. IWP with lower levels of composite action will be subjected to more relative slip and less bowing, whereas a more composite IWP will slip less but bow more. Bowing is undesired as it induces unwanted deflections, applies stresses onto the IWP and connections, and can create a “fishmouth” effect at corners which interrupts the building envelope. Although IWP are commonly used, thermal bowing in IWP has not been investigated experimentally in detail and is currently estimated based on designer experience.

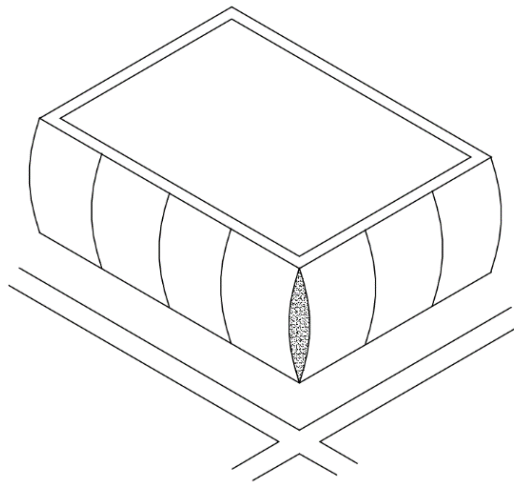


Figure 1.1 Corner separation resulting from thermal bowing “Fishmouth” effect (CPCI Design Manual 5, 2017)

1.1 Research Objective

The objective of this thesis is to evaluate thermal bowing of a precast concrete insulated wall panel with different levels of shear connector stiffness (i.e. composite action) that are representative of panels on the market. To achieve this objective, the following tasks need to be completed:

1. Conduct a literature review to understand the current state-of-the-art of IWP.
2. Evaluate the stiffness and strength of Glass FRP (GFRP) shear connectors that will be used for thermal bowing tests of full-scale panels using direct shear push through tests.

3. Construct four full scale (6.1 m long) insulated wall panels that are representative of those on the market. Each panel will have a different shear connection stiffness and one panel will have debonded insulation.
4. Design and construct a thermal enclosure and heating system that is able to induce a minimum of 20 °C thermal differential on the full-scale panels with the heat being evenly distributed along the panel length.
5. Record and analyze the relationship between temperature differential, thermal bowing, and relative wythe slip for each of the four full-scale simply supported IWP.
6. Compare the results from Tasks 2 and 5 to estimate the forces that thermal bowing places on shear connectors.

1.2 Scope of Research

The scope of this study is limited to experimentally evaluating thermal bowing in panels with different GFRP shear connector diameters. Other contributions to bowing such as humidity and creep are not investigated. The study focuses on 6.1 m long, non-prestressed reinforced concrete insulated wall panels that are simply supported. Data collected from the panel tests includes midspan deflection (i.e. bowing), relative slip between wythes, and temperature.

1.3 Thesis Organization

The structure of this thesis follows an experimental investigation to determine the relation between shear connector stiffness measured from direct shear push-through tests and the respective thermal bowing response of full-scale panels. The first stage of the experimental program is to fabricate and test 18 double-shear push-through specimens to evaluate stiffness that represent a range of partial-composite behaviour. The second stage of the experimental program is the construction of a thermal enclosure that will create a temperature differential by heating one IWP wythe and leaving the other wythe exposed to ambient laboratory temperature. The third stage is to construct

and test four full scale IWP under thermal differentials. Finally, the thermal bowing results are analyzed, and a relation between shear connection stiffness and thermal bowing is developed. The contents of the thesis are listed below:

Chapter 1: Introduction to the research program and outline of objectives and scope.

Chapter 2: A review of literature on IWP, shear connectors, and previous thermal testing done on IWP. Chapter 2 accomplishes *Task 1* of the research objective.

Chapter 3: The first stage of experimental work on evaluating stiffness of GFRP shear connectors through push-through tests. This chapter completes *Task 2* of the research objective.

Chapter 4: The second stage of experimental work focusing on the thermal bowing of IWP. A thermal enclosure was constructed, and then four IWP using known stiffness from the push-through tests are tested. Chapter 4 fulfills *Tasks 3, 4, 5, and 6* of the research objectives.

Chapter 5: Conclusions of the research program are presented.

References

Appendix A Construction process of formwork for push-through specimen and IWP

Appendix B Push-through specimen load deflection and stiffness plots for all specimens

Appendix C Temperature plots of heating and cooling cycle for all IWP

Appendix D Material properties

Appendix E Time plots of midspan deflection and end slip for all IWP

2. LITERATURE REVIEW

2.1 Introduction

Recent demands in construction require designers and architects to address increasing economic and environmental costs more than ever before. There is a shift in the construction industry to move from on-site construction to third-party fabrication shops to become economically competitive (Precast Concrete Institute (PCI), 2011). There is pressure to reduce the energy demands of buildings by developing more efficient building envelopes since space heating accounts for nearly 60% of the energy demands in Canadian commercial and residential buildings (Cuddihy et al., 2005) as shown in Figure 2.1 (NRCan, 2016-2017).

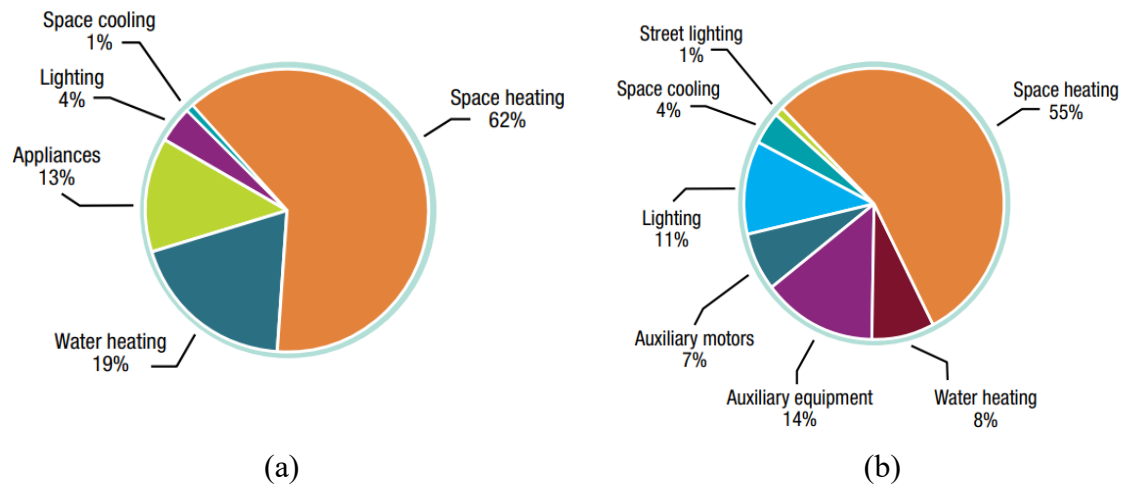


Figure 2.1 Energy Demand in Canada for (a) residential and (b) commercial and institutional sectors (NRCan, 2016-2017)

Double wythe panels address rising construction costs and building envelope demands with their modular capabilities and thermal efficiency. Double wythe panels consist of two reinforced or prestressed concrete wythes (layers) with an insulation layer between them. Shear connectors are used to transfer longitudinal shear between the concrete wythes.

Though IWP are commonly used, bowing of IWP under thermal loading is not well understood. Bowing is undesired as it induces unwanted deflections, applies stresses onto the IWP

and connections, and creates a “fishmouth” effect at corners which interrupts the building envelope. Bowing is a problematic topic in design as there is limited research on it (PCI, 2011). Losch (2003) noted the lack of data and opportunity to examine thermal bowing in IWP’s.

This chapter provides a background of research performed on precast concrete insulated wall panels (IWP). This background includes aspects such as IWP components, composite behaviour, shear connectors, structural response, and thermal bowing on double wythe panels.

2.2 History

IWP’s have become prevalent in North America over the last 60 years as architectural or structural elements in the commercial and industrial sectors (PCI, 2011). Walls built in the 1950s used various materials as insulation including lightweight concrete and mineralized wood, but these walls are thermally inefficient (Leung, 1984). Rigid foam insulation was then used beginning in the late 1950’s and into the 1960’s (Leabu, 1965). The panels used solid concrete zones to connect the wythes in the 1960s. Though these panels were structurally efficient, they had reduced thermal efficiency caused by thermal bridging through the solid concrete zones (Frankl, 2008).

In the 1980s, engineers began to prefer non-composite walls with metallic pin shear connectors to improve thermal efficiency and reduce bowing (Leung, 1984). Pin-type steel connectors are better than concrete regions at preventing thermal bridging, but better alternatives were sought to meet increasing energy demands. Later in the 1980s and in the 1990s, research shifted towards FRP connectors to reduce thermal bridging further. One of the first successful examples of this are the truss-shaped Glass FRP (GFRP) shear connectors developed by Salmon et al. (1997) and Einea et al. (1994). These authors observed that the panels are partially-composite under service load but had ultimate flexural strengths similar to fully composite panels. More recent research explored the different varieties of FRP including Carbon FRP (CFRP) grids

(Hassan and Rizkalla, 2010)), and Basalt FRP (BFRP) bars (Tomlinson, 2015). Furthermore, efforts have been made by researchers (Bai and Davidson, 2016; Gombeda et al, 2017; Tomlinson and Fam, 2016) to develop models that better predict the behaviour of IWPs under structural loads.

2.3 Structural Designations

Insulated wall panels are structurally designated based on the level of interfacial shear transferred between wythes. The three different classifications for an IWP are fully composite, partially composite, and non-composite.

2.3.1 Fully Composite Walls

Fully composite walls have complete longitudinal shear transfer between the wythes. In these walls, the two wythes act as one unit with a single neutral axis and maintain a single strain distribution as shown in Figure 2.2 (i.e. plane sections remain plane). Higher composite action leads to a higher stiffness and strength (PCI, 2011) and higher composite action is preferred as panels are cheaper to produce and utilizes materials more efficiently (Hodicky et al., 2014). However, this comes at a cost of creating thermal bridges when using steel or concrete connectors (PCI, 2011). Another concern is that the differential strain between wythes leads to significant bowing when there is a temperature or humidity gradient (Losch, 2003).

2.3.2 Non-Composite Walls

Non-composite walls are systems where the wythes act fully independently. This is shown in Figure 2.2 with the two wythes having separate neutral axes, each with tensile and compressive components. Generally, the interior wythe is structural while the exterior acts as an architectural façade (PCI, 2011). The lack composite action between wythes allows them to slip against one another which causes a decrease in strength and stiffness relative to fully composite wall.

However, walls with low to negligible composite action are more desirable for some designers as they have less thermal bridging (i.e. more thermally efficient) and have negligible bowing.

2.3.3 Partially Composite Walls

Partially composite walls behave in-between fully composite and non-composite walls. Practically, since panels are required to have connectors and no system is infinitely stiff, all panels are partially composite to some degree (PCI, 2011). Like with non-composite walls, each wythe has its own neutral axis. The differential strain (i.e. slip strain) between wythes accumulates along the panel length and results in relative slip. Unlike non-composite walls, the end slip depends on the level of composite action (in particular, stiffness of the shear connection). These panels are typically denoted by their percentage of fully composite walls with the slip between wythes being indicative of this percentage (Tomlinson and Fam, 2014). Lower slips indicate higher composite action, and vice versa. It is difficult to predict the structural behaviour of partially composite panels as it is heavily influenced by the longitudinal shear transferred between wythes (PCI 2011). To predict the shear transfer, the load-slip response of connectors needs to be understood and incorporated into deflection calculations, which requires significant iterations or testing (Tomlinson, 2015).

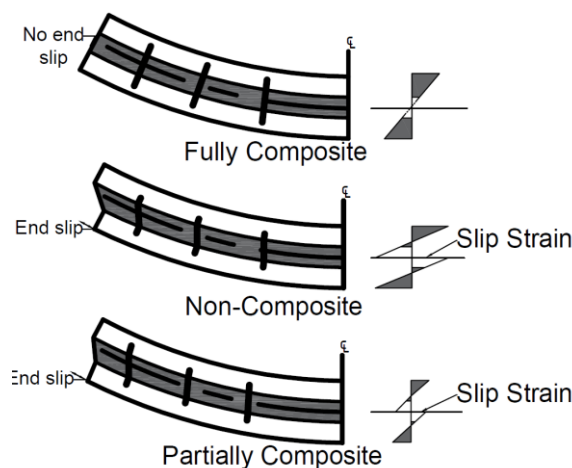


Figure 2.2 Strain profile and deflected shape of IWP

2.4 Description of Insulated Wall Panels

IWP's are typically composed of two concrete layers (wythes) with a layer of insulation between them (see Figure 2.3). The concrete layers and insulation are joined together with shear connectors. Panels can be as wide as 4.6 m and as tall as 23 m. Typically, the maximum size is governed by the capabilities of the plant, erection equipment, and transportation restrictions (PCI, 2011). Prestress on the wythes is often used to prevent cracking during handling and installation but is not required for shorter panels (PCI, 2011).

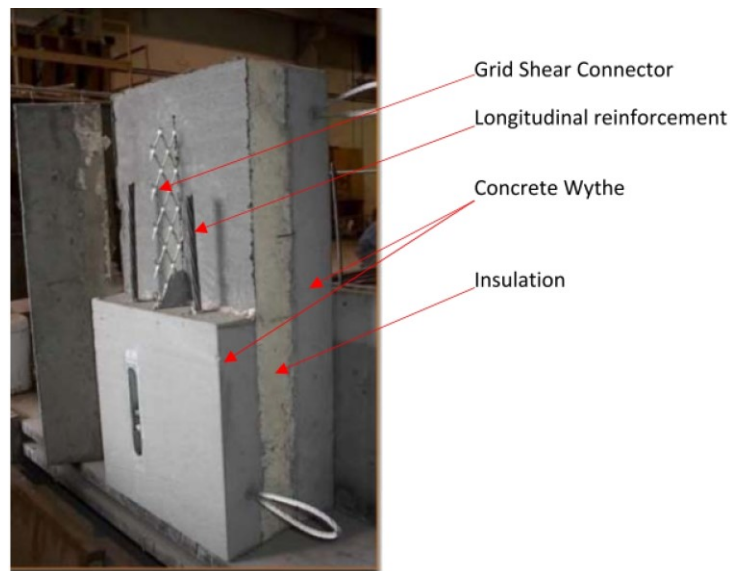


Figure 2.3 Insulated wall panel key components (Rudd, 2017)

2.4.1 Wythes

For load-bearing walls, the exterior concrete layer is often referred to as the façade wythe while the interior layer is often called the structural wythe. Wythes are made to be as thin as possible but are typically limited to 50 mm due to cover and fire requirements (PCI, 2011). The façade wythe is typically between 50-75 mm thick, while the interior wythe is typically between 50-150 mm thick. In panels with low degrees of composite action, the façade wythe is normally thinner than the interior wythe as it is designed to be non-loadbearing but serves an architectural function. However, as composite action increases, the façade wythe contributes more to the resistance of the

structural system and these panels tend to have wythes of equal thickness. Welded wire mesh is often used to meet minimum requirements for shrinkage and crack control. It is important to consider additional flexural stresses induced on panels during handling. For these cases, additional transverse reinforcement is detailed at the lifting points (PCI, 2011).

2.4.2 Insulation

Extruded (XPS) and expanded (EPS) polystyrene are the most common insulation foams used in IWP. The insulation layer is typically between 25 and 100 mm thick and acts as both a thermal and vapour barrier. The combination of the high R-value of the insulation and the high thermal mass of the concrete gives advantageous thermal resistance in IWP's relative to other exterior wall systems. Though the insulation has been shown to contribute to the flexural strength of a panel (Tomlinson and Fam, 2014), the insulation is often ignored as contributing to structural resistance after installation as the foam-concrete bond quality is unpredictable and may fail over time. Kim and You (2015) noted that the in-plane shear strength of IWP's with EPS foam is greater than those with XPS foam because of the rougher EPS surface. However, recent research indicates that roughening the surface of XPS drastically improves its structural performance meaning it can potentially be considered during design (Choi et al., 2015).

2.4.3 Shear Connectors

Shear connectors link the concrete wythes and insulation together. Connectors are made from materials including steel, FRP, plastic, and concrete (PCI, 2011). Traditional materials such as steel and concrete can achieve high degrees of composite behaviour and are widely available. However, steel and concrete have high thermal conductivities which leads to undesirable thermal bridging through the insulation. Currently, plastic or FRP connectors are often used to limit thermal bridging due to their lower thermal conductivity.

2.4.3.1 Stiff Shear Connectors

Shear connectors that develop high levels of composite action are defined as stiff connectors. Figure 2.4 shows common stiff connector geometries that have been explored in previous research. Solid concrete zones and steel trusses have been shown to develop high levels of composite behaviour (Pessiki and Mlynarczyk, 2003) but at the cost of compromising the thermal performance of the wall. However, FRP connectors arranged in either grid or truss formations can develop high composite behaviour without compromising the thermal performance (Salmon et al., 1997; Einea et al., 1994; Frankl, 2008). Regardless, a stiff shear connection has the drawback of inducing large differential strain between wythes, which induces bowing (Losch, 2003).

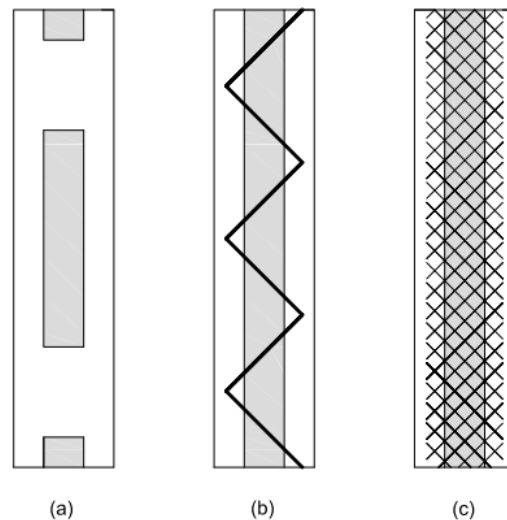


Figure 2.4 Stiff shear connectors (a) solid concrete regions, (b) embedded truss, and (c) grid or mesh (Tomlinson, 2015)

2.4.3.2 Flexible Shear Connectors

Flexible shear connectors are used in applications where non-composite behaviour is preferred. The primary function of flexible shear connectors is to prevent delamination of the façade wythe (Tomlinson 2015). Unlike stiff connectors, flexible connectors allow the wythes to slip relative to each other with minimal shear transfer, which limits bowing (Losch, 2003). Figure 2.5 shows

examples of flexible shear connectors such as Z-shaped steel connectors, M-shaped steel connectors, polypropylene pin connectors, and fibreglass vinyl-ester ties. Typically, non-composite walls have minimal thermal bridging concerns since the area of connectors relative to the wall area is very small. Bridging is even further reduced when FRP materials are used.

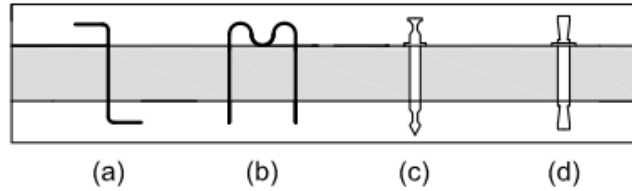


Figure 2.5 Examples of flexible shear connectors: (a) Z-shaped steel connector, (b) M-shaped steel connector, (c) polypropylene pin connector, and (d) fibreglass vinyl-ester tie (Tomlinson, 2015)

2.5 Percent Composite Action (PCA)

There is debate amongst designers on how to evaluate the composite behaviour of panels as it depends heavily on the shear connection configuration. PCA is also affected by the type of loading, and it has been shown that panels under high axial loads tend to have lower composite action than those under low axial loads (Tomlinson, 2015). Panels are classified as non-composite, partially composite, or fully composite depending on the PCA. The PCA is evaluated by comparing the stiffness or strengths of composite panels to theoretically fully composite panels, using strain compatibility, or measuring relative wythe slips.

2.5.1 Evaluating Composite Action

The two most common methods of evaluating composite action are based on moment resistance, k_u (PCI, 1997) and the stiffness at service loads, k_{EI} (Pessiki and Mlynarczyk, 2003).

$$k_u = \frac{M_{u,test} - M_{u,NC}}{M_{u,FC} - M_{u,NC}} \times 100\% \quad \text{Equation (1)}$$

$$k_{EI} = \frac{EI_{test} - EI_{NC}}{EI_{FC} - EI_{NC}} \times 100\% \quad \text{Equation (2)}$$

Where M_u refers to the ultimate moment, subscript *NC* refers to a non-composite panel, subscript *FC* refers to a fully composite panel, and subscript *test* refers to experimental results. Similarly, k_{EI} uses stiffness to calculate percentage of composite values, where *EI* represents the IWP's effective stiffness.

It is good practice to use both approaches (strength for ultimate limit states, stiffness for serviceability limit states) since the same connector arrangement can have large differences between the two. Alternative methods include measuring the composite action using wythe curvature (Hassan and Rizkalla, 2010), or by relative wythe slips (Naito et al., 2012).

2.6 Structural Testing of Insulated Wall Panels

The two most common structural testing set-ups for IWP's are four-point bending tests and direct shear push-through tests. Push-through tests are performed to obtain the shear-slip response of connection systems, including insulation effects. This method has the advantage of using smaller samples compared to four-point bending tests which allows more parameters to be investigated. Four-point bending is commonly used to study the overall flexural behaviour of walls where the connection shear-slip response interacts with the panel's flexural reinforcement.

2.6.1 Flexural Testing

Four-point bending tests are typically performed to analyze the flexural behaviour of IWPs. A typical experimental setup is shown in Figure 2.6. For IWPs, flexural testing has the advantage of determining structural properties of the entire system including the strength of the shear connection system, insulation contribution, failure mode of the panel, and composite action. Researchers have used four-point bending tests to investigate various connector arrangements (Tomlinson and Fam,

2014), how different shear connector materials behave (Pessiki and Mlynarczyk, 2003), and the effect of different insulation (Kim and You, 2015).

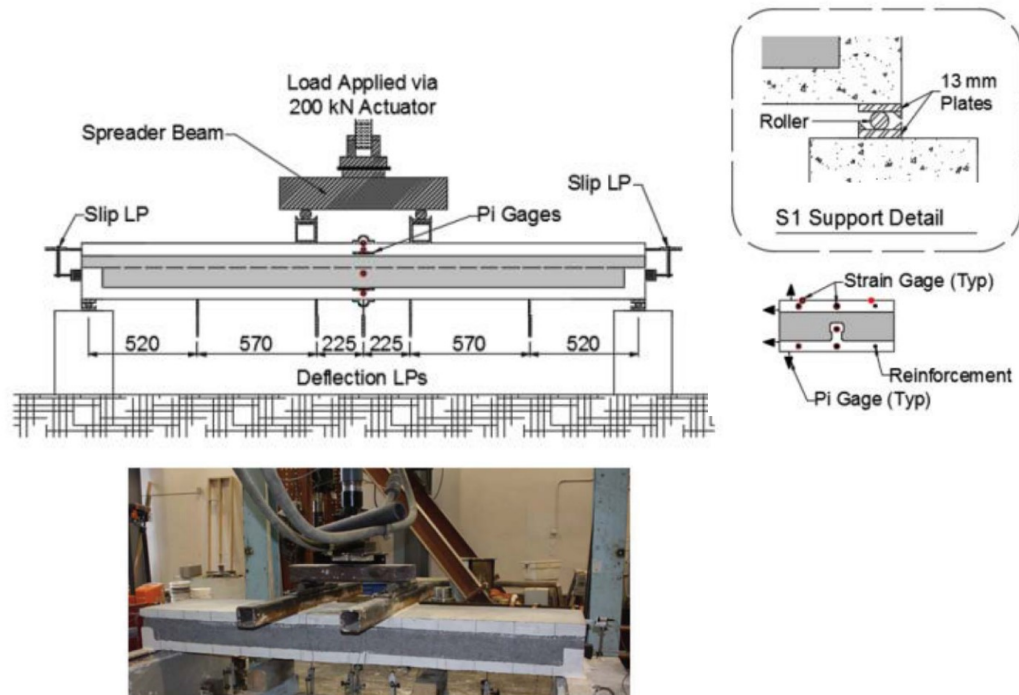


Figure 2.6 Four-point bending test (Teixeria and Fam, 2017)

2.6.2 Direct Shear Push-Through Tests

Push-through tests were traditionally used to determine the shear flow capacity of composite steel-concrete sections but these are also recommended to study shear connectors in IWP (Ekenel, 2013). The advantage with push-through tests is that a smaller specimen is used to investigate the response of specific shear connectors, as represented in Figure 2.7. Examples of research includes application of different connector types (Woltman et al, 2013), geometry of connectors (Naito et al., 2012) and orientation of connectors (Tomlinson et al, 2016).

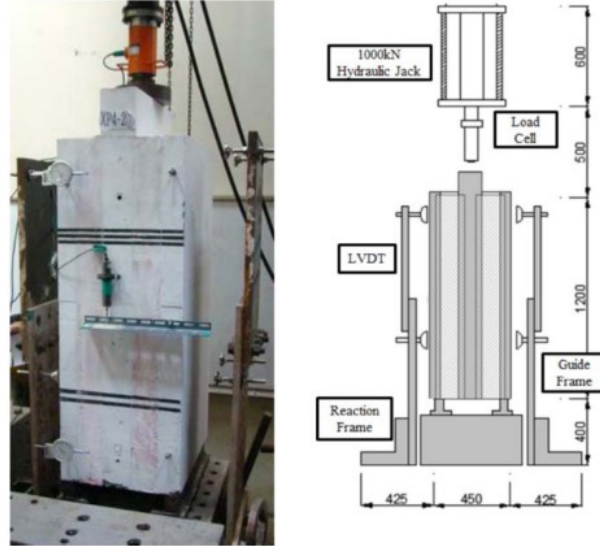


Figure 2.7 Example of push through test (Kim et al., 2014)

2.7 Types of Shear Connectors

Traditionally, concrete and steel were used as shear connectors. However, there is an increasing demand for other materials with better thermal properties. A summary of the structural properties of typical connector materials is provided in Table 2.1.

Table 2.1 Typical structural properties of connector materials (Rudd, 2017)

Material	Young's Modulus, GPa	Tensile Strength, MPa
Steel	200	450-680
Carbon FRP	120-580	1720-3690
Glass FRP	35-60	480-1600
Basalt FRP	45-70	1035-1650
Plastic	1.3-3.1	40

2.7.1 Concrete

In the 1960s, embedded concrete regions were used as shear connectors in double-tee IWP's. Pessiki and Mlynarczyk (2003), showed that solid concrete regions are effective for developing composite action, stiffness, and strength. However, this came at the cost of thermal efficiency as the solid regions created significant thermal bridging.

Alternatively, ribs or a reduced shear transfer distance balance thermal efficiency while retaining the high composite advantage of concrete (Frankl et al., 2011; Gleich, 2007), as shown in Figure 2.8. As rib thickness increases, composite action increases and vice versa. This is because the rib reduces the shear transfer length between wythes which makes the shear connectors stiffer (Tomlinson et al., 2016).

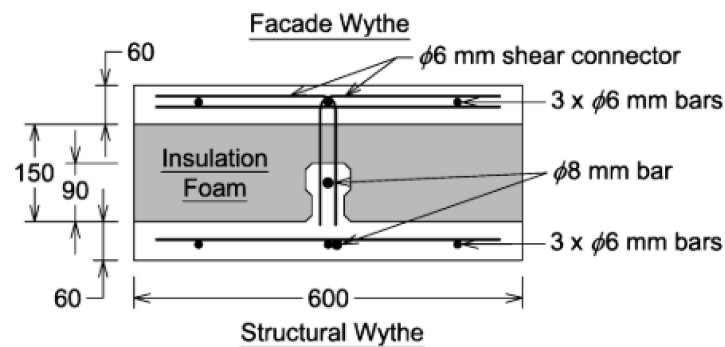


Figure 2.8 Insulated wall panel showing cross section with stiffening concrete rib (Tomlinson et al., 2016)

2.7.2 Steel

As mentioned, steel shear connectors are often used in IWP, but research has generally shifted towards using FRPs. Steel is desirable as it is well understood by designers, has relatively high stiffness and strength, and has ductile behaviour. However, designers should consider thermal bridging through steel connectors which lowers the thermal effectiveness of the building envelope.

Research at the University of Alberta was performed on Z-shaped steel plate connectors in eleven push-out tests. (Goudarzi et al., 2016). The web of the specimens was 160 mm, and the flange depth was 45 mm. Goudzardi et al. (2016) found that increasing the shear connector width improves the performance and increasing the width of the flange improves the breakout resistance of the connector. The primary failure mode was concrete pull-out. Goudzardi et al. (2016) recommends increasing the connector width instead of the thickness to improve the overall performance of the shear connection.

Tomlinson et al. (2016) tested 5.8 mm diameter truss-type steel connectors with varying insertion angles and found that connectors failed by yielding in tension or buckling in compression. The connection stiffness and strength increased as the connection insertion angle increased from 30° to 60° but the ductility of the connectors reduced.

2.7.3 Carbon Fibre Reinforced Polymer (CFRP)

CFRP has a stiffness comparable to steel and a significantly higher tensile strength compared to other materials. CFRP is also desirable in applications where corrosion resistance, weight, and thermal performance are a concern. However, CFRP is brittle (i.e. does not provide warning of failure) so it needs to be designed carefully and expensive relative to alternatives such as GFRP.

The majority of research on CFRP shear connectors comes from the North Carolina State University. In 2008, Frankl (2008) tested six 6.1 m tall by 3.7 m wide precast IWP's under combined vertical and lateral loads. The panels were fabricated with either EPS or XPS insulation. Frankl (2008) concluded that CFRP grid shear connectors can achieve nearly 100% composite action. The author also noted the importance of shear-grid quantity and configuration to achieve optimal structural response. Follow-up work by Hodicky et al. (2014) found that CFRP grid spacing corresponds to an increase in overall shear strength.

2.7.4 Glass Fibre Reinforced Polymer

GFRP has become popular as a shear connector as it has superior thermal performance compared to steel. GFRP has a high tensile strength and has stable properties under temperatures ranging between -40 and 50° C (Robert and Benmokrane, 2010). GFRP connectors (Salmon et al., 1997; Einea et al., 1994) are capable of achieving high degrees of composite action while improving on the thermal bridging created from steel (Figure 2.9). However, the low stiffness of GFRP leads to higher deflections under service loads compared to steel. Due to this, serviceability limit states

(e.g. deflection, crack control) often govern design rather than ultimate limit states. Another consideration, like with CFRP, is that GFRP is brittle and gives little to no warning of failure.

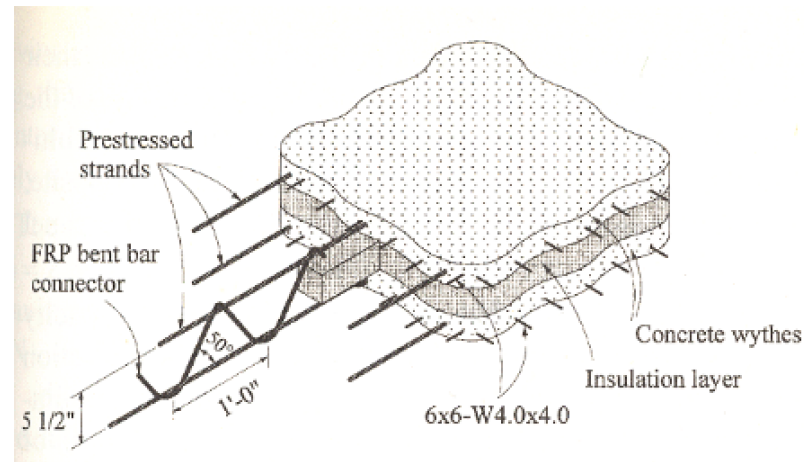


Figure 2.9 Insulated wall panel FRP bent bar connectors (Salmon et al., 1997)

Woltman et al. (2013) tested GFRP pin type connectors using 50 push-through tests and compared them to plastic and steel connectors. These connectors were designed to resist shear primarily from dowel action. It was observed that GFRP bars failed from internal delamination under flexural and shear stresses. It was also found that varying GFRP connector size and spacing had an insignificant effect on the average shear stress carried by connectors at failure (Woltman et al., 2013). Woltman et al. (2013) also found that the GFRP connectors' shear strength (60 to 112 MPa) was much lower than steel connectors (297-365 MPa) but significantly greater than polymer connectors (22-39 MPa). There was an insignificant effect on shear strength when varying the size, spacing, cross-section shape, or end treatment of the connectors.

2.7.5 Basalt Fibre Reinforced Polymer

Basalt FRP (BFRP) is cost-effective, highly resistant to fire (Sim et al., 2005), and performs better under freeze-thaw cycles than CFRP and GFRP (Shi et al., 2011). The cost of BFRP is similar to

GFRP and has stiffness and strength between GFRP and CFRP (Sim et al., 2005). However, Benmokrane et al (2014) have raised concerns with the long-term effects of moisture uptake and bond degradation of BFRP bars relative to GFRP.

Tomlinson et al. (2016) investigated BFRP shear connectors with varying insertion angles bar diameters, and quality of concrete-insulation bond. Increasing the insertion angle from 30 to 60° increased both load capacity and stiffness; larger connectors were able to carry considerably higher compressive stresses at failure than smaller connectors. However, unlike steel which yields in failure, BFRP connectors' dominant fail mode is by pull-out when under tension, meaning that increased embedment length or additional anchorage is recommended (Tomlinson et al., 2016).

2.8 Thermal Characteristics of Insulated Wall Panels

This section outlines considerations and research regarding the thermal performance of IWP's. Table 2.2 outlines typical thermal conductivities of components used in panels.

Table 2.2 Thermal conductivity of typical insulated wall panel materials (Woltman, 2014)

Material	Longitudinal Conductivity, k (W/mK)	Transverse Conductivity, k (W/mK)
Concrete¹ (normal density)	1.4-2.9	
Stainless Steel	9.4-21.2	
Mild Steel¹	45.3	
Extruded Polystyrene¹ (XPS)	0.029	
Expanded Polystyrene¹ (EPS)	0.033-0.037	
S-Glass Epoxy²	3.46	0.35
Ultra-high Modulus Carbon Epoxy²	121.1-129.8	1.04

¹(ASHRAE, 2001)

²(Mallick, 2007) adapted from (Freeman and Kuebeler, 1974)

³Perry's Chemical Engineer's Handbook page 500 or 2-461

2.8.1 Thermal Performance

In Canada, space heating accounts for nearly 60% of all energy use in residential and commercial sectors (NRCan, 2016-2017). Energy efficiency is becoming more important with the rising cost

and concerns of excessive energy use. IWPs are effective at reducing heating and cooling energy required in buildings (Post, 2006). The thermal performance of an IWP depends primarily on three variables: shear connector material and arrangement, insulation type and thickness, and interior wythe. The exterior wythe provides minimal resistance to heat transfer and has little effect on thermal performance since it lies outside the insulation (Woltman et al., 2014).

Shear connectors transfer heat through thermal bridging. Thermal bridging occurs when a component (e.g. shear connector) has higher thermal conductivity than the surrounding elements (e.g. insulation). McCall (1985) found that the thermal performance of an IWP decreases by up to 40% from thermal bridging through steel connectors and concrete regions penetrating the insulation. Traditional connectors (e.g. concrete and steel) have high thermal conductivity and are thermally inefficient (see Table 2.2), particularly in panels with high degrees of composite action. Research on FRP connectors has shown that they are structurally effective and also satisfy building envelope requirements compared to steel connectors, as shown in Figure 2.10 (Sauter, 1991).

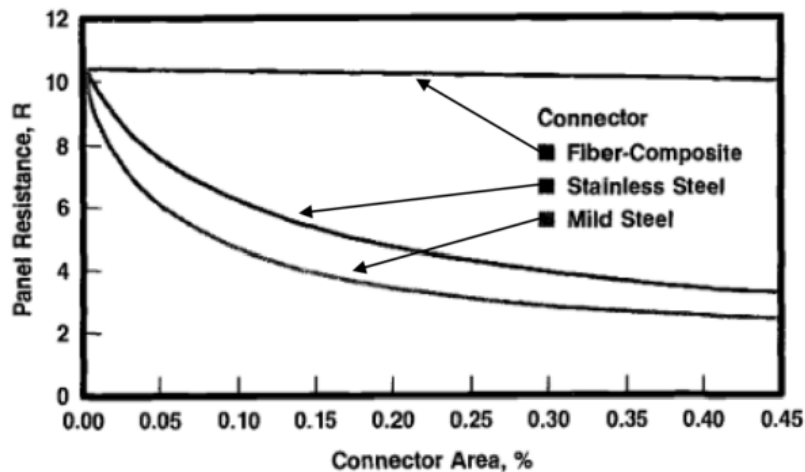


Figure 2.10 Thermal resistance of connectors versus connector area (Sauter, 1991)

Insulation (usually XPS or EPS) in modern IWP ranges between 25 and 100 mm thick. These insulation types serve as both vapour and thermal barriers, providing more heat resistance depending on their thickness. The thickness of the insulation depends on where the panel will be

installed. For instance, walls need to have a thermal resistance of RSI-4.76 (R-27) for buildings (NECB, 2017) in areas of northern climate such as Edmonton, Winnipeg, and Quebec City.

As mentioned, one advantage in thermal performance for IWP comes from the large thermal mass of the interior wythe. A wall with low thermal mass experiences interior temperature extremes close to that of the exterior if space heating is not provided (Woltman, 2014). Conversely, a building with high thermal mass requires more energy to heat or cool, resulting in reduced temperature extremes. Heat flow for two conventional walls and a concrete IWP is compared in Figure 2.11 (a). The IWP has better performance (i.e. smaller peak heating and cooling loads) than the other walls. Figure 2.11 (a) also illustrates thermal lag in IWPs, which is shown by the greater time shifts for heating and cooling. Figure 2.11 (b) shows that as the inner wythe thickness increases, heating and cooling loads decrease (PCI Industry Handbook Committee, 2010).

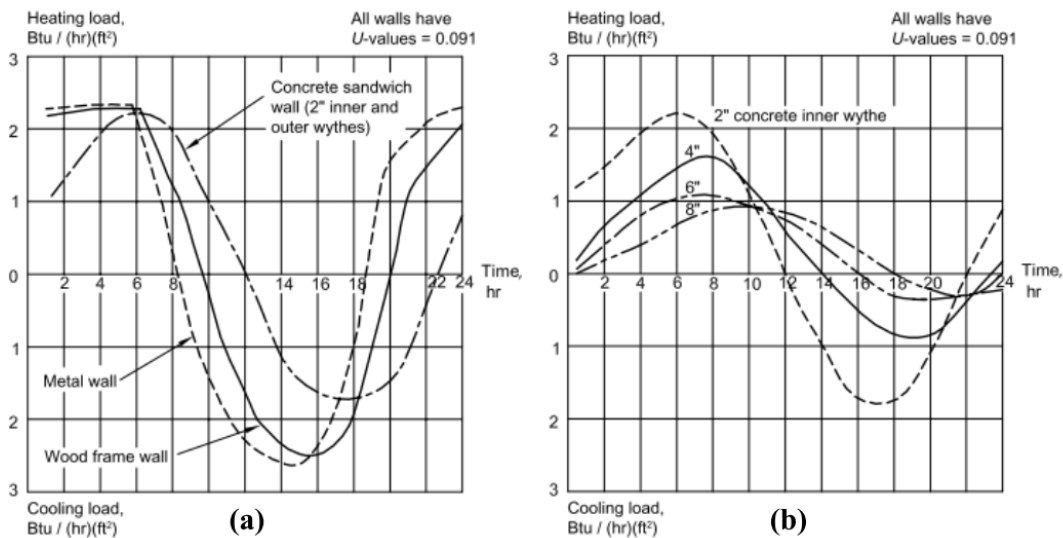


Figure 2.11 Thermal mass effects for (a) various wall systems and (b) insulated wall panels (PCI Industry Handbook Committee, 2010)

2.8.2 Coefficient of Thermal Expansion

The thermal coefficient of expansion represents the change in unit length per degree of temperature change. The humidity, temperature variation, and internal structure of the concrete all impact the

coefficient of expansion (Xia et al., 2017). When temperatures are lower and the moisture freezes, the coefficient of expansion becomes a function of ice and the concrete itself (Xia et al., 2017). Conversely, when the moisture turns to vapour from rising temperatures, high vapour pressure effects the coefficient of thermal expansion (Xia et al., 2017). Common implications on concrete resulting from the coefficient of thermal expansion include early-age cracking and serviceability (Sakyi-Bekoe, 2008).

2.8.3 Evaluation of Thermal Resistance “R” Value

The thermal resistance is defined as the “R-value” and is an important variable when considering the thermal performance of a panel. The RSI value ($\text{m}^2 \cdot \text{K}/\text{W}$ or, equally, $\text{m}^2 \cdot ^\circ\text{C}/\text{W}$) is calculated using Equation (3)

$$R = \frac{\Delta T}{Q} \quad \text{Equation (3)}$$

Where ΔT is the temperature differential (K or $^\circ\text{C}$) between the wythes, and Q is the heat flux (W/m^2) across the panel. Thermal resistance of panels is usually estimated according to ASHRAE Standard 90.1 (ASHRAE, 2010).

ASHRAE suggests three ways to evaluate the R-value of an exterior wall: parallel flow method, isothermal planes method, and the zone method. These methods treat the thermal resistances of the materials using an electrical resistance analogy and are arranged in parallel, series, or as a combination of the two to predict the R-value of the system (Lee and Pessiki, 2008). Later in this thesis, the zone method was used.

2.8.3.1 Zone Method

The zone method is the best technique in ASHRAE 90.1 to determine thermal resistance in systems with widely spaced thermal bridges (Lee and Pessiki, 2008). Figure 2.12(a) shows the panel

separated into two zones: an effective zone, W , and outside the effective zone with no presence of thermal discontinuity. The effective zone is calculated as follows:

$$W = m + 2d \quad \text{Equation (4)}$$

Where W is the width of the influence region (i.e. effective zone), m is the connector diameter, and d is the distance from the wall surface to the connector. However, Lee and Pessiki (2008), found that the zone width, W , overestimates R-values for metal-frames and IWP. They proposed a new zone width method to calculate R-value of IWP's more accurately (Lee and Pessiki, 2008).

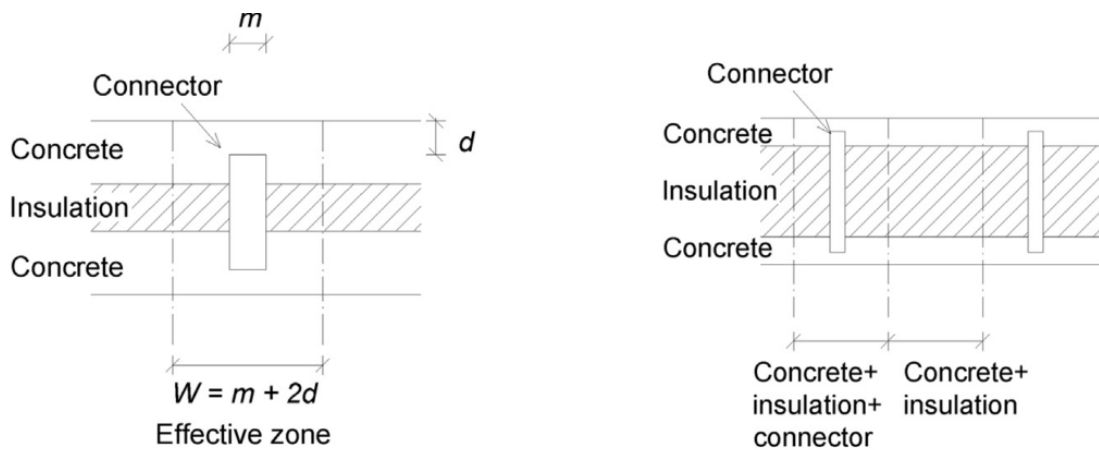


Figure 2.12 (a) Zone method (b) Parallel flow method (Kim and Allard, 2014)

2.9 Bowing of Panels

Losch (2003) summarized the phenomena of bowing in IWP's based on several factors that are grouped into either environmental or structural factors. Environmental factors include temperature and humidity. Structural factors include, creep, uneven prestress, and elastic modulus differences.

The amount of bowing is heavily affected by the composite action between wythes.

2.9.1 Environmental Causes of Bowing

2.9.1.1 Humidity

Lower humidity causes concrete to shrink faster; a consistent difference in humidity between the faces of the panel can induce bowing. This is commonly seen in northern climates, where the inside of a building is heated, generating lower humidity inside than there is outside. Similarly, areas that use air conditioning cause the inner wythe to dry faster, inducing an outward bow (Losch, 2003).

2.9.1.2 Thermal

Thermal bowing is the out-of-plane deflection caused by the thermal gradient between the outside and inside faces of a panel. This occurs because temperature changes cause materials to expand or contract. Typical coefficient of thermal expansion values for concrete range between 7.4 to 13×10^{-6} °C, and in certain mixes can reach as low as 4.0×10^{-6} °C (Kada, 2001). Thermal bowing is amplified in IWP's as there is a greater thermal gradient than in solid panels of equal thickness (PCI, 2011). In practice, panels are subjected cyclically to thermal bowing as panels exposed to the sun bow towards the sun, and vice versa for cold weather. The effect of thermal bowing is more severe in composite walls relative to non-composite or solid walls as shown in Figure 2.13. The temperature gradient creates curvature from the panel maintaining strain compatibility, whereas the non-composite panel is free to expand. Thermal bowing is undesired as it induces deflections and applied stresses onto the IWP and connections.

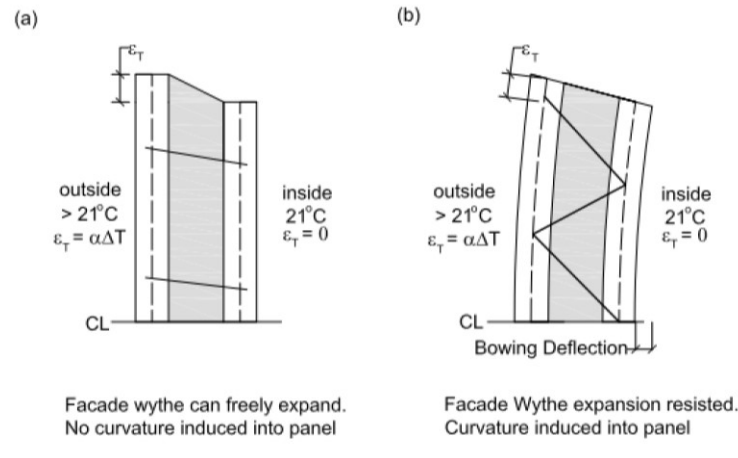


Figure 2.13 Thermal bowing on (a) non-composite panel (b) fully composite panel (Tomlinson, 2015)

2.9.2 Structural Causes of Bowing

2.9.2.1 Creep

The effect of creep is evident when concrete panels are stored in a horizontal position without proper support, as shown in Figure 2.17. The permanent deflection of the IWP that increases over time is known as creep. Due to this, PCI (2011) recommends lateral supports be included to minimize or to eliminate bowing due to creep in storage.

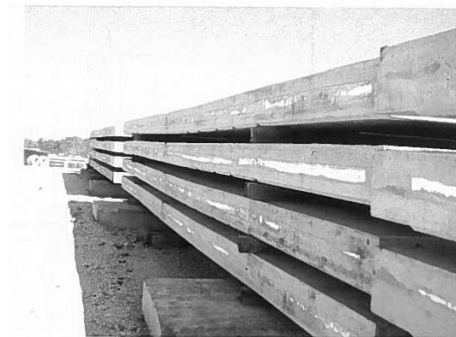


Figure 2.14 Concrete wall panels in storage (Losch, 2003)

2.9.2.2 Differences in Modulus of Elasticity of Concrete Between Wythes

If different concrete mixes are used in the two wythes of the panel, there exists the potential for differential shrinkage and bowing. This is a result of the difference in modulus of elasticity after

prestress transfer (Losch, 2003). It is possible to reduce or eliminate this effect by lowering the prestressing force in the wythe that has the lower modulus of elasticity (Losch, 2003).

2.9.3 Composite Action Influence on Bowing

In terms of structural effects, composite action between wythes, creep, and differences in elastic modulus of elasticity impact the magnitude of bowing on IWP's. Differential strain induces more bowing in panels with higher composite action (Losch, 2003). Examples of stiff connectors that develop high composite behaviour typically include steel trusses, solid concrete zones, or a combination of the two. Conversely, in non-composite panels, flexible connectors result in wythes that act largely independently. Because of this, non-composite panels do not exhibit bowing as significantly as a fully composite insulated wall panel. IWP's with low composite behaviour are often used in applications where bowing is unacceptable, such as cooler and freezer panels (Losch, 2003). However, most IWP's exhibit at least some degree of composite action from shear connectors or bonded insulation, so bowing is evident in all types of IWP's (PCI, 2011).

2.9.4 Challenges with Bowing

As highlighted, bowing is impacted by factors including differential wythe shrinkage, temperature effects, eccentric prestressing force, differential modulus of elasticity, and creep (PCI, 2011). Currently the PCI (2011) recognizes that predicting the amount of bowing is difficult and recommends that designers establish a reasonable and allowable magnitude of bowing based off experience. Designers are using a larger thermal gradient through the panel than the actual site's atmospheric temperature difference to get a reasonable estimate of panel bowing (PCI, 2011). However due to all the factors listed, bowing remains a complicated topic amongst designers as there is limited research available (PCI, 2011). Losch (2003) noted the lack of data and opportunity to examine further the effect of temperature differentials in IWP's.

2.10 Previous Thermal Experiments

Thermal testing on IWPs to date has focused on evaluating their R-value. Van Geem and Shirley (1987) tested three panels in a hot box and found that thermal lag for the panels (75 mm wythes) ranged from five to six hours and was not impacted by shear connector type. This result is due to the thermal storage capacity of concrete and the thermal resistance of the insulation (Van Geem and Shirley, 1987). Woltman et al. (2017) compared IWP with GFRP shear connectors to those with steel connectors in a hot box (Figure 2.15). Their results showed that steel connectors created significant thermal bridges, whereas GFRP connectors had minimal thermal bridging. In addition, there was no significant change in thermal resistance when GFRP connector size and spacing was changed, suggesting that bridging from GFRP connectors is small and localized (Woltman, 2014). FEM (Finite Element Method) was used by Lee and Pessiki (2004) to investigate the R-value of IWP with three concrete wythes, separated by two layers of rigid insulation. They found that the R-value of the three-wythe panel increases as the insulation overlap length increases. They also noted that the thickness of the concrete wythe does not have a significant effect on the R-value, whereas the insulation thickness was significant (Lee and Pessiki, 2004).

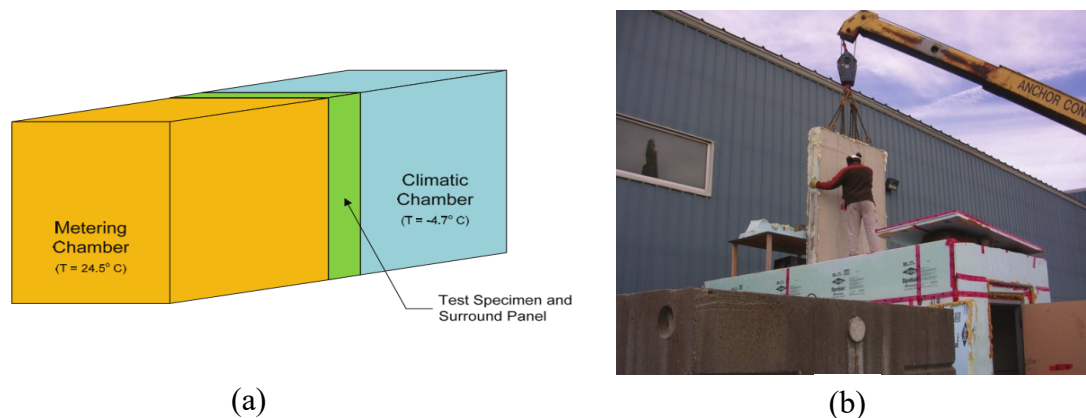


Figure 2.15 (a) Hotbox schematic (b) removal of panel from the hot box (Woltman, 2014)

In general, previous research focused on the heat transfer of IWP rather than bowing due to temperature differential. Post (2006) performed thermal and fatigue tests on 12.2 m (40 ft) IWP's subjected to a 55.6 °C (100°F) temperature gradient. This experiment is one of the few to study IWP's under thermal fatiguing and bowing. A thermal enclosure of foam insulation boards was built for the experiment, as shown in Figure 2.16. The panels were heated with two 10,257 W forced-air propane construction heaters to obtain a thermal gradient of 55.6°C. Results show that the displacement from thermal bowing was dependent on the level of fixity at the restrained end of the wall and the degree of composite action (Post, 2006). Post (2006) had three recommendations: to construct comparison specimens with no chemical bond between the insulation layer and wythes, represent the panel condition after years of thermal cycling, and provide a more efficient method to measure the wythe-slip, as depicted in Figure 2.16.

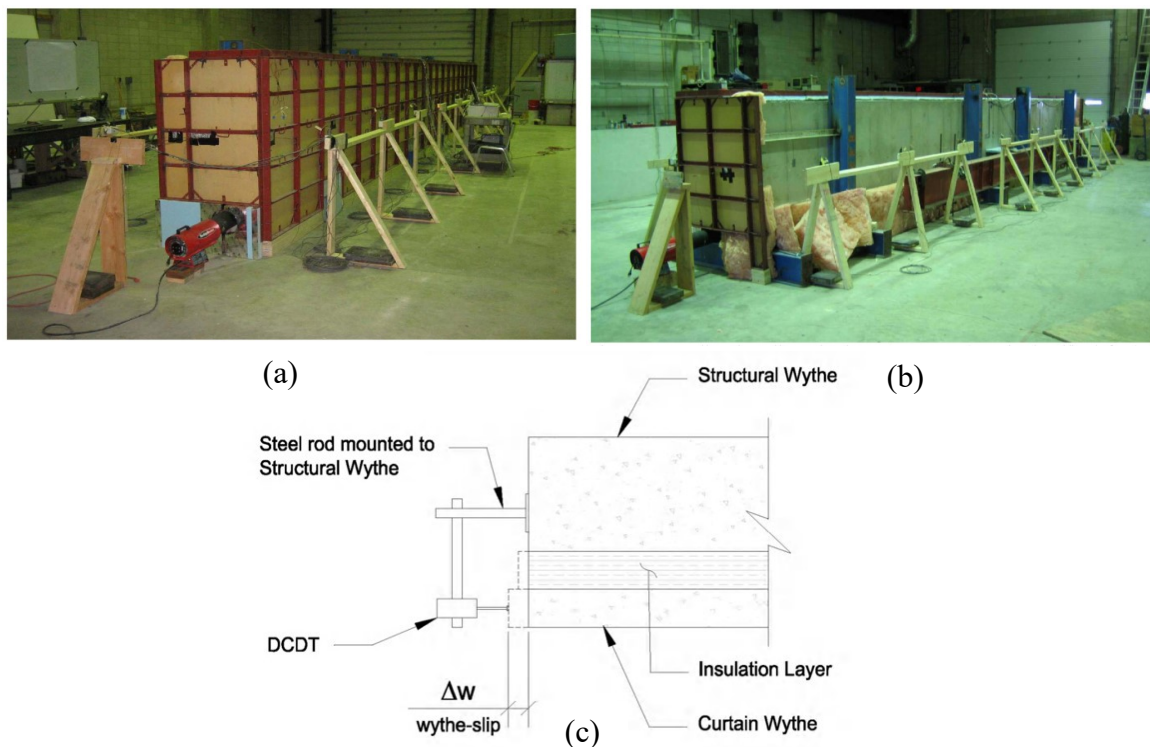


Figure 2.16 (a) Full-scale thermal enclosure (b) back view with restraints of full-scale thermal enclosure (c) recommended method to measure wythe-slip (Post, 2006)

2.11 Models of Insulated Wall Panels

The complexity of IWP behaviour has been a challenge for designers, and nowadays the current PCI design approach is considered obsolete (Bai and Davidson, 2016). Much of the work in the literature has focused on the experimental investigation into shear connector systems with limited research tailored to developing models for precast concrete IWP's.

Tomlinson (2015) developed a non-linear model for the bond-slip behaviour of the shear connection to account for partial composite behaviour at service and ultimate conditions for panels loaded under combined axial and flexural loads. The model was compared with experimental results and a parametric study was conducted. One notable finding is that composite action increases with panel length.

Bai and Davidson (2016) developed an analysis model for assessing partially composite walls under service loads (i.e. linear elastic properties). Because of the complexities in transverse and longitudinal interactions, Bai and Davidson (2016) provide a model that decouples composite behaviour into simplified subcases: transverse and longitudinal behaviour. They derived the longitudinal equation from Granholm's governing equations, which were derived for nailed timber structures. This allows for any properties of a shear connector to be inputted into the model.

In 2017, Gombeda et al (2017) provided a model to predict the behaviour of partially composite walls under out-of-plane loading. The authors note the difficulty of considering the connector constitutive properties, compatibility between the wythes, and connector location. Their model accounts for connector contribution based on its material properties and arrangement. An iterative approach to calculate relative tie deformations and shear forces is used to determine the percent composite behaviour between the wythes (Gombeda et al., 2017). The authors also developed an OpenSees model to demonstrate the accuracy of the model in predicting the interface slip and global flexural response (Gombeda et al., 2017). It is noted that the model is limited to

statically-determinate systems, and further research is required to develop efficient ways to use the model for indeterminate structures such as multi-span panels (Gombeda et al., 2017).

The existing models in the literature have focused more on structural loads instead of thermal loads. Factors such as the thermal lag and physical amount of bowing are still not well understood in terms of modeling.

2.12 Digital Image Correlation (DIC)

Recent advances in computing performance and high-resolution digital cameras have researchers looking towards using DIC to measure structural deformations. DIC compares a time-lapse series of photographs of a textured surface to a single reference image, with a grid of discrete patches added to each image afterwards using software. DIC tracks each patch based on the contrast provided by the textured surface and can detect movement reliably with sub-pixel accuracy (Dutton, 2012). DIC then uses the comparisons to determine information such as global displacements, relative displacements, and change in strain.

DIC has been used in geotechnical research to measure displacements (White et al., 2003). In structural engineering applications, DIC has been used for crack detection and width measurement during load cycling (Lecompte et al., 2006; Destrebecq et al., 2010), shear crack movement in reinforced concrete beams (Dutton, 2012), and shear deformations in IWPs with GFRP skins (Mathieson, 2015). In relation to IWP's, Tomlinson (2015) utilized DIC to examine wythe slip at the ends of a panel and validated the results against linear potentiometers.

2.13 Gaps in Literature Review

Despite the research discussed, there still exists gaps in current literature. Bowing in IWP's remains a complicated topic with little available information in current research. As most thermal experimental programs focus on the heat transfer, there still exists limited information regarding

thermal bowing on IWP's. Comparisons between the stiffness of varying IWP subjected to thermal bowing are limited. In addition, few studies which discuss the construction and use of a thermal enclosure for bowing tests are available. This thesis investigates the effect thermal bowing has on concrete IWP's with different shear connector stiffnesses experimentally.

3. EXPERIMENTAL INVESTIGATION OF CONNECTOR STIFFNESS UNDER DOUBLE SHEAR

3.1 Introduction

Precast concrete panels comprise of a layer of insulation surrounded by two layers of concrete. Shear connectors are required to connect and transfer longitudinal shear between wythes. To understand the shear connector behaviour, direct shear push-through testing is often conducted. Researchers such as Woltman et al. (2013), Tomlinson et al. (2016), and Naito et al (2012) have used push-through tests to evaluate shear connector systems and have used the resulting load-slip curves from push-through testing to provide important design information for understanding the role of shear connectors (i.e. connector strength and stiffness) in full walls. The stiffness of the shear connection system has a direct influence on the severity of thermal bowing in an IWP with bowing being more severe when shear connections are stiffer (i.e wall is more composite).

By varying composite action of the walls, the relation between thermal bowing and composite level can be investigated. The first step in this experimental program is to develop the load-slip behaviour of eighteen push-through samples with various shear connector diameters and insulation bond effectiveness to determine shear flow and stiffness. The push through tests will produce load-slip curves that are then used to understand the behaviour of the thermal bowing testing described in Chapter 4. Once the strength and stiffness of individual connectors are understood, thermal bowing will be investigated on each of the shear connector diameters types.

3.2 Push-Through Experimental Program

Eighteen push-through specimens were constructed, representing a subsection of the full-scale panels used for the thermal bowing tests in Chapter 4. The size of each push-through specimen is $600 \times 375 \times 300$ mm, with the concrete wythes and rigid XPS insulation having a thickness of 75

mm, representing typical thickness of wythes used in construction (Figure 3.1). The 600 mm length represents the centre-to-centre spacing of connectors used in the full-scale panels; the thickness, 375 mm, represents a back to back IWP, which ensures that connectors are loaded symmetrically during testing.

The shear connection considered in these tests has an “X” shape comprised of two 250 mm GFRP bars inserted at 45° to the face of the wall. The GFRP bars provided are a generic stock rather than commercial shear connectors as the connector test parameters and properties are easier to control and report. Each leg of the connector is embedded 71 mm into the respective wythe. GFRP was used as a shear connector as it has reduced thermal bridging relative to steel connectors and has been successfully used in walls tested in the past (Woltman et al, 2013; Salmon et al., 1997). The “X” shaped connector orientation ensures proper trussing action in both directions (i.e. compression, tension) and allows the connectors to be efficiently used to obtain their maximum peak loads. If only one bar is used (i.e. a diagonal connector rather than an “X” shape), lower connector failure stresses may result if the shear connector is loaded under compression or tension (Tomlinson et al., 2016).

Three nominal GFRP bar diameters (9.53, 12.7, and 15.8 mm) were tested. Six specimens were constructed for each bar diameter, with half including a polyethylene vapour barrier. Table 3.1 shows the experimental test matrix. Tests are identified with a 3-digit code. The first digit identifies the bar diameter with ‘3’, ‘4’, and ‘5’ denoting the #3 (9.53 mm), #4 (12.7 mm), and #5 (15.8 mm) bars. The second digit identifies the insulation bond quality with ‘B’ representing a bonded specimen (i.e. no vapour barrier), and ‘U’ representing an unbonded specimen (i.e with vapour barrier). The final digit denotes the number of the specimen (1, 2, or 3).

Table 3.1 Push through test matrix

Test Identifier	Nominal Bar Diameter, mm	Nominal Area (per bar), mm ²	Total Nominal Area (all 4 bars), mm ²	Insulation Bond
3B-1,2,3	9.52	71.2	285	Bonded
3U-1,2,3	9.52	71.2	285	Unbonded
4B-1,2,3	12.7	127	508	Bonded
4U-1,2,3	12.7	127	508	Unbonded
5B-1,2,3	15.9	199	796	Bonded
5U-1-2-3	15.9	199	796	Unbonded

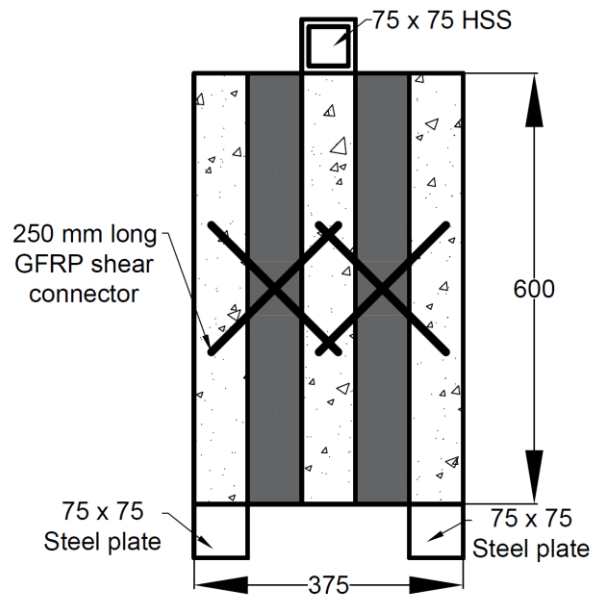


Figure 3.1 Push-through test specimen, all dimensions in mm.

3.2.1 Materials

Material stress-strain curves are provided in Figure 3.2. The considered material properties were concrete in compression (Figure 3.2 (d)), steel mesh and rebar in tension (Figure 3.2(a)), insulation in compression (Figure 3.2 (c)), and GFRP in tension (Figure 3.2 (b)). Peak capacities and stiffnesses for individual material tests are provided in Appendix D.

3.2.1.1 Concrete

Agilia self-consolidating concrete from Lafarge was used to construct the push-through specimens. The concrete had a maximum aggregate size of 9 mm and a spread of 740 mm (determined using a flow test immediately before casting following ASTM C1611 (ASTM, 2018)). The average

concrete strength at 28-days was 52 MPa with a standard deviation of 0.015 MPa. The strength was determined based on ASTM C39 provisions using 100 mm × 150 mm cylinders cast at the same time as the push-through and IWP panels (ASTM, 2001). The average Young's Modulus of the concrete, determined with a compressometer, at 28 days was 23.5 GPa with a standard deviation of 2.43 GPa.

3.2.1.2 Steel Reinforcement

Each wythe was reinforced with a smooth steel welded wire mesh (WWM) with a diameter of 5.76 mm (area of 26.1 mm²) and spacing of 100 mm in both directions. The WWM yield and ultimate stresses were 494 and 512 MPa with standard deviations of 4.53 and 18.7 MPa respectively.

The yield and ultimate strength of the 10M bars (used in conjunction with the WWM in the full-scale walls discussed in Chapter 4) were 415 and 616 MPa with a standard deviation of 11.8 and 5.11 MPa respectively. Both the WWM and 10M had an average Young's Modulus of 200 GPa, with standard deviations of 4.07 and 4.53 GPa respectively. The 10M bars reached a strain of 0.2 before rupturing, see Figure 3.2.

Push-through specimens were only reinforced with a WWM and had a reinforcement ratio, ρ , of 0.0035 as calculated in Equation (5).

$$\rho = \frac{A_s}{bh} = \frac{(26.1 \times 9)}{300(225)} = 0.00348 \quad \text{Equation (5)}$$

Where A_s is the total reinforcement cross sectional area, b is the specimen width, and h is the total concrete thickness.

3.2.1.3 Insulation

Extruded polystyrene rigid foam (XPS) from Dow PANELMATE™ was used as insulation. The insulation's compressive strength was 0.253 MPa with a standard deviation of 0.01 MPa. The R-value reported by the manufacturer is 7.2 per 25 mm (inch).

3.2.1.4 GFRP Shear Connectors

GFRP rebar was provided by TufBar and used as connectors. The connectors were 250 mm long and arranged in a “X” shape (Figure 3.3). The diameters (9.53, 12.7, and 15.8 mm) were tested. Tensile tests were performed based on ASTM D7205 on the three GFRP diameters to determine structural properties. The average tensile strength of the GFRP was 1420 MPa with a standard deviation of 202 MPa. The tensile modulus was 60.5 GPa with a standard deviation of 4.81 GPa. All three diameters had similar Young’s Modulus and tensile strength.

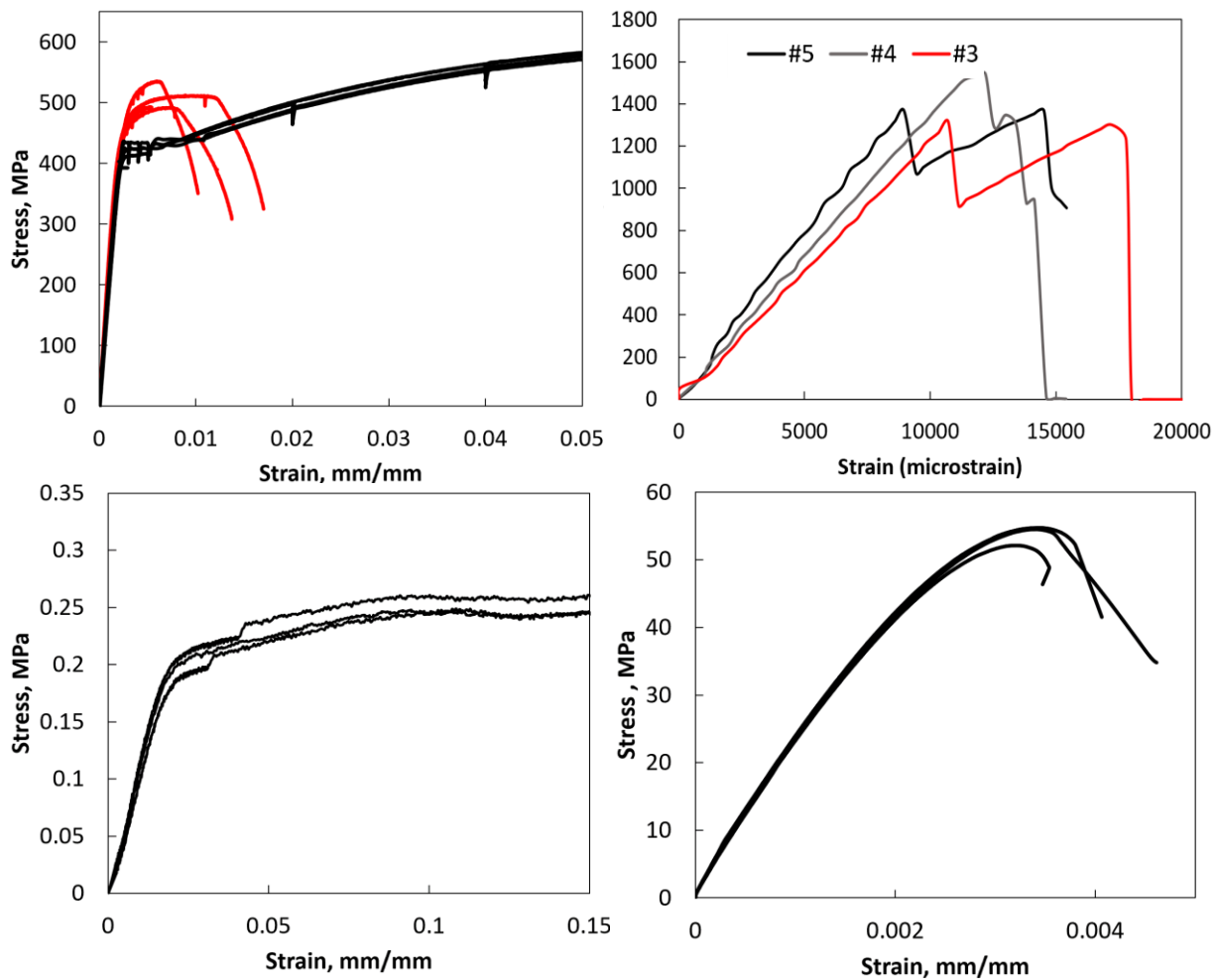


Figure 3.2 (a) Stress strain curves of (a) 10M (black) and WWM (red) (b) insulation (c) GFRP bars (d) concrete cylinders

3.2.2 Push-Through Fabrication

To reduce footprint in the lab, the push-through formwork was assembled vertically, see Figure 3.3. Three 2440 mm long sets of formworks were cut and assembled. Each set of push-through formwork contained six specimens.

To assemble the specimens, XPS insulation was cut to the dimension of the formwork. Pilot holes with a diameter 3 mm lower than the GFRP diameter were drilled at the connector location, and corresponding GFRP shear connectors were inserted tight into the foam. Each push-through formwork contained two sets of the X-shaped push-through specimens to simulate an IWP back to back, see Figure 3.3, and placed into the formwork as a package (Figure 3.3). The welded wire mesh was placed at mid-depth in each concrete wythe to provide reinforcement representative of a full-scale panel. A 38×89 mm wood brace was screwed to the top of the formwork to prevent uplift from the insulation during pour.

The specimens cured in the formwork under a plastic sheet and the formwork was stripped after 14 days. Specimens were allowed to cure in ambient lab conditions for a minimum of 28 days prior to testing. More details on the construction process are found in Appendix A



Figure 3.3 (a) Push through assembly showing shear connector and reinforcement arrangement (b) push-through formwork

3.2.3 Push-through Test Setup and Instrumentation

The push-through specimens were tested under double-shear (Figure 3.4). The two outer wythes were supported at their base with 75×75 mm steel supports with space between them to allow the insulation layers to pass through. Two steel side supports (320×300 mm with 20 mm thickness) were placed and clamped on either side of the push-through specimen to prevent rotation of the wythes. The specimens were loaded using a 360 kN actuator under stroke control at 1 mm/min until 15 mm of slip was reached, which is well beyond peak load for all tests. Two 25 mm Linear Variable Differential Transformers (LVDT) were mounted on the front and back of the specimen to measure relative slip between the wythes. A region on the front face of the specimen was painted white, and then sprayed in an irregular pattern using flat black spray paint to enable the use of DIC. A Canon EOS Rebel T6 camera (image size 5184×3456 pixels) was fixed 1 m away from the specimen and photos were taken at 10 second intervals during the test. Two dimensional DIC analysis was completed using GOM Correlate software.

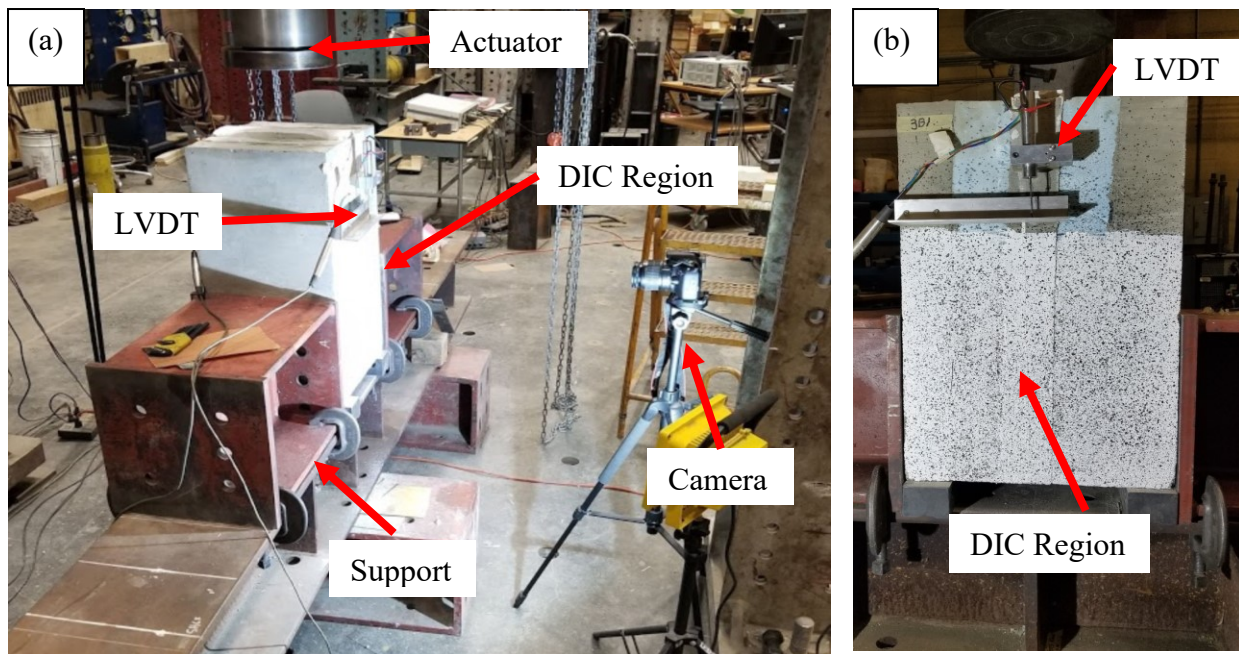


Figure 3.4 (a) Push-through test setup (b) DIC surface on front face of specimen

3.3 Push-Through Testing Results

The following section reviews the results of the push-through test on 18 specimens. Note that the reported loads are for the entire specimen, which consists of two pairs of shear connectors. The load carried by a single connector pair (i.e. one “X”) is half of the values reported in this chapter.

Figure 3.5 shows the load-slip response of specimen 4B3, which is representative of the response observed in these tests. The point when the linear behaviour changes to non-linear is the proportional limit. This point was usually indicated audibly during the test (e.g. insulation bond failure or GFRP crackling noise). After this point, the stiffness decreased steadily until the peak load was reached. The peak load is defined as the maximum load that the specimen sustained. After the peak load, there was a sudden loss in load followed by a residual capacity.

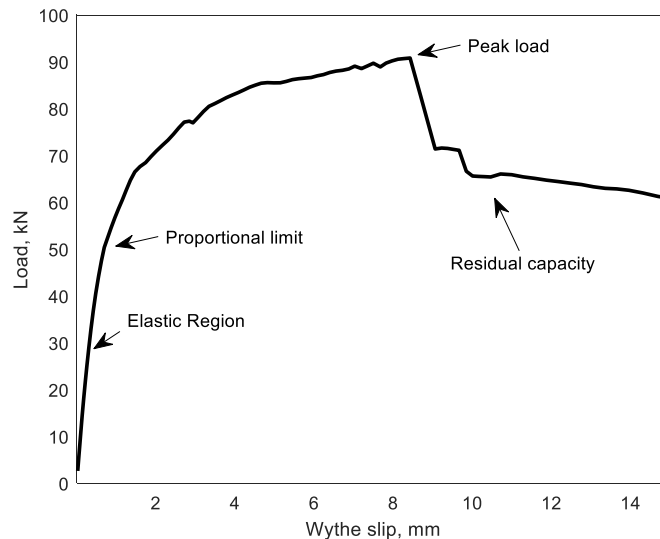


Figure 3.5 General load-slip response of push-through test (Specimen 4B3)

Table 3.2 presents a summary of the load for two connection systems and corresponding slip at the proportional limit and peak load from LVDT results. The elastic region is linear and typically ranged between 0 to 0.5 mm of slip depending on shear connector diameter size. The stiffness to be used in thermal bowing calculation is calculated from this region in section 3.3.5.

Table 3.2 Summary of push-through test results

Test Specimen ID	Proportional limit ² , kN	Displacement at proportional limit, mm	Peak Load ² , kN	Displacement at Peak Load, mm	Stiffness at deflection of 0.25 mm, kN/mm
3B1	48.6	0.84	59.4	7.86	58.4
3B2	37.2	0.76	61.6	4.74	50.1
3B3	33.4	0.51	67.9	4.37	51.3
3U1	44.9	0.79	55.0	3.46	46.4
3U2	21.0	0.36	53.4	4.15	40.4
3U3	40.6	0.97	48.0	1.46	29.1
4B1	35.9	0.56	86.4	2.97	62.6
4B2	40.2	0.38	72.5	3.02	91.6
4B3	41.3	0.49	90.9	8.47	63.9
4U1	38.4	0.41	75.4	8.15	60.6
4U2	31.8	0.31	92.3	2.59	77.3
4U3	31.9	0.44	96.9	4.28	53.4
5B1	32.3	0.23	95.7	4.42	89.3
5B2	67.1	0.34	83.5	10.6	84.8
5B3	31.6	0.26	106.7	3.97	89.5
5U1	23.7	0.18	111.8	4.27	28.9 ¹
5U2	24.1	0.13	101.4	2.24	104.5
5U3	29.6	0.16	87.3	1.17	88.6

¹ Specimen 5U1 insulation bond splits at early deflection and so reports lower stiffness

² All reported loads are for two “X” shaped shear connector systems (i.e. total load read by the load cell)

3.3.1 DIC Analysis

Table 3.3 shows the results of the DIC analysis. The three main areas that were considered with DIC were the initial insulation debonding, the proportional limit, and the peak load. DIC photos were taken at these three points of interest and the slip, and corresponding load were related. An advantage with DIC is that the slip when initial insulation debonding occurs is able to be clearly identified, which is not possible with LVDTs. Figure 3.6 shows visually the insulation debonding from the concrete on the debonded specimens compared to its bonded specimen.

Table 3.3 Summary of DIC analysis

Specimen ID	Initial insulation debonding		Proportional limit		Peak Load	
	Slip, mm	Load, kN ²	Slip, mm	Load, kN ²	Slip, mm	Load, kN ²
3B1	0.31	13.1	1.43	50.7	7.52	59.4
3B2	0.30	10.5	1.38	41.0	5.23	60.9
3B3	0.67	22.9	1.65	42.6	4.28	67.5
3U1	0.21	7.54	1.74	49.7	4.01	55.1
3U2	0.14	1.46	2.52	47.2	7.46	54.4
3U3	0.14	3.64	2.23	47.1	2.23	47.1
4B1	0.39	19.2	2.94	82.5	4.32	86.7
4B2	0.16	6.28	1.34	44.7	3.46	71.2
4B3	0.35	14.4	1.46	52.4	11.4	90.8
4U1	0.24	9.66	1.70	54.7	9.53	75.5
4U2	0.17	7.5	1.25	50.8	5.12	92.5
4U3	0.29	11.6	1.39	58.9	5.17	96.9
5B1	0.17	13.4	1.54	69.7	5.1	95.3
5B2	¹	¹	0.14	58.7	10.8	82.3
5B3	0.22	0.11	0.79	51.2	4.19	106.6
5U1	0.08	4.59	0.43	25.5	4.41	111.7
5U2	0.02	6.7	0.64	65.3	2.41	101
5U3	0.07	7.2	1.35	83.9	3.65	87.3

¹ Specimen data for this region is corrupt

² All reported loads are for two “X” shaped shear connector systems (i.e. total load read by the load cell)

The slip at initial insulation debonding decreases as connector diameter increases. The average debonding slips for 3B, 4B, and 5B tests were 0.43, 0.30, and 0.19 mm respectively. This reflects a 40% decrease in slip from 3B to 4B, and a 36% decrease from 4B to 5B. For unbonded specimens the average debonding slips were 0.16, 0.24, and 0.06 mm for the 3U, 4U, and 5U bars respectively. This result shows a relative decrease in wythe slip of 0.26, 0.07, and 0.13 mm for the 3U, 4U, and 5U tests relative to the comparable bonded specimens. The trend shows that connector size and bond quality have an impact on the initial insulation debonding slip. As the connector size increases, the pullout or buckling capacity increases (tension or compression failure mode respectively), and the concrete to insulation interface then becomes the initial point of failure; this results in insulation debonding becoming more evident with higher connector sizes.

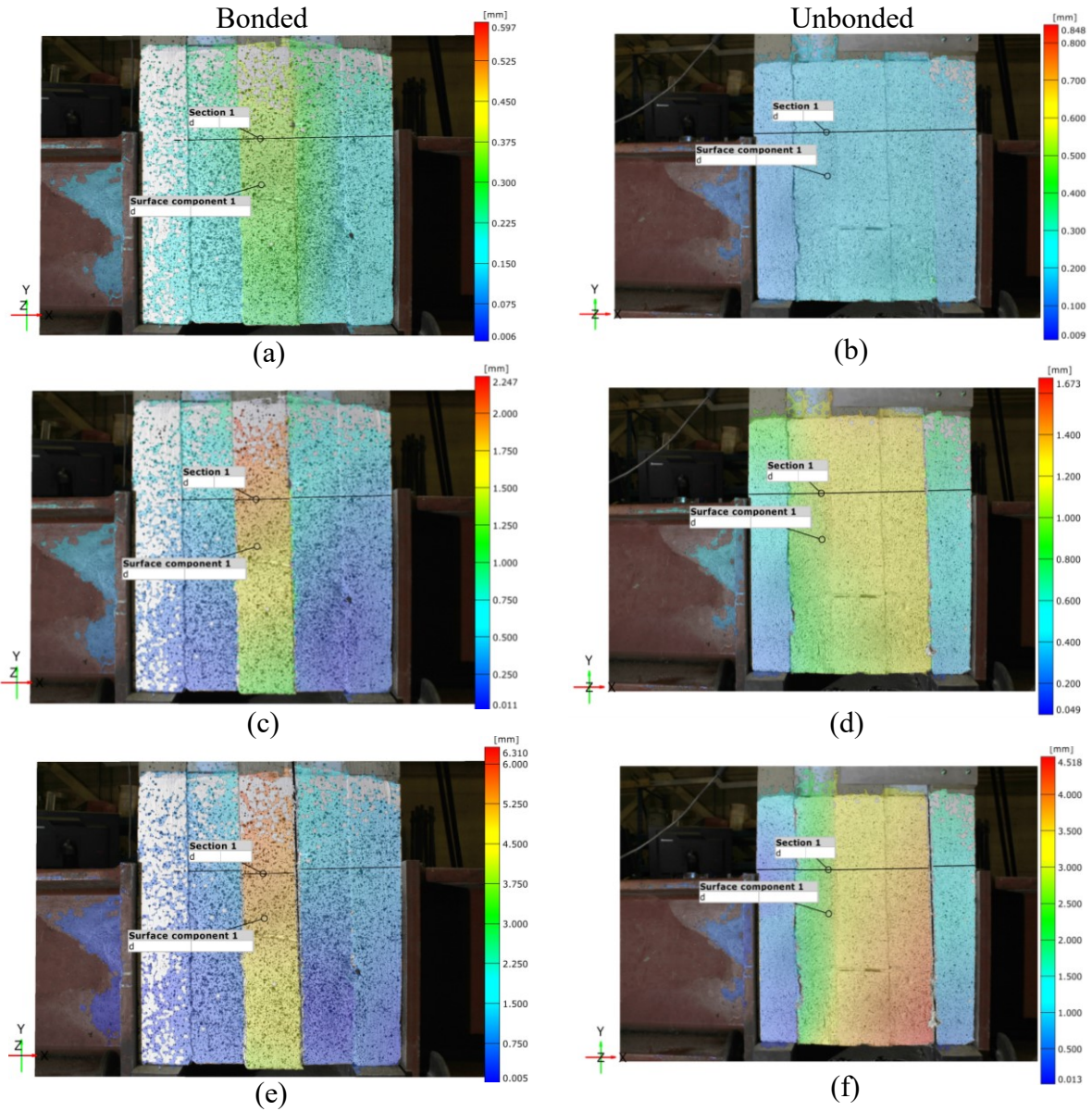


Figure 3.6 DIC Images for bonded and unbonded specimen; (a) and (b) initial insulation debonding, (c) and (d) proportional limit, (e) and (f) ultimate failure (5B2 is bonded specimen; 5U2 is unbonded specimen)

3.3.2 Summary of Push-through Test Results

3.3.2.1 #3 GFRP Shear Connector Results Summary

The average peak load for the 3B specimens was 62.9 kN with a deviation of 4.41 kN. The slip at peak load averaged 5.66 mm with a deviation of 1.91 mm. The average proportional limit was 39.7

kN with a deviation of 7.91 kN and occurred at an average slip of 0.703 mm with a deviation of 0.172 mm.

The average peak load for the 3U specimens was 52.1 kN with a deviation of 3.66 kN. The slip at peak load averaged 3.02 mm with a deviation of 1.39 mm. The average proportional limit was 35.5 kN with a deviation of 12.7 kN and occurred at an average slip of 0.706 mm with a deviation of 0.313 mm.

3.3.2.2 #4 GFRP Shear Connector Results Summary

The average peak load for the 4B specimens was 83.2 kN with a deviation of 9.59 kN. The slip at peak load averaged 4.82 mm with a deviation of 0.465 mm. The average proportional limit was 39.1 kN with a deviation of 2.85 kN and occurred at an average slip of 0.476 mm with a deviation of 0.091 mm.

The average peak load for the 4U specimens was 88.2 kN with a deviation of 11.3 kN. The slip at peak load averaged 5.01 mm with a deviation of 2.85 mm. The average proportional limit was 34.0 kN with a deviation of 3.78 kN and occurred at an average slip of 0.386 mm with a deviation of 0.068 mm.

3.3.2.3 #5 mm GFRP Shear Connector Results Summary

The average peak load for the 5B specimens was 95.3 kN with a deviation of 11.6 kN. The slip at peak load averaged 6.33 mm with a deviation of 3.70 mm. The average proportional limit was 43.6 kN with a deviation of 20.3 kN and occurred at an average slip of 0.276 mm with a deviation of 0.057 mm.

The average peak load for the 5U specimens was 100.1 kN with a deviation of 12.3 kN. The slip at peak load averaged 2.56 mm with a deviation of 1.57 mm. The average proportional

limit was 25.8 kN with a deviation of 3.29 kN and occurred at an average slip of 0.156 mm with a deviation of 0.0251 mm.

3.3.2.4 Overall Averaged Load-slip Response of Shear Connector Tests

To calculate the loads and stiffness, the average of the LVDT and DIC results was taken for both bonded and unbonded specimens. This is further averaged by the three tests per bonded and unbonded specimen. The overall average responses are plotted in Figure 3.7.

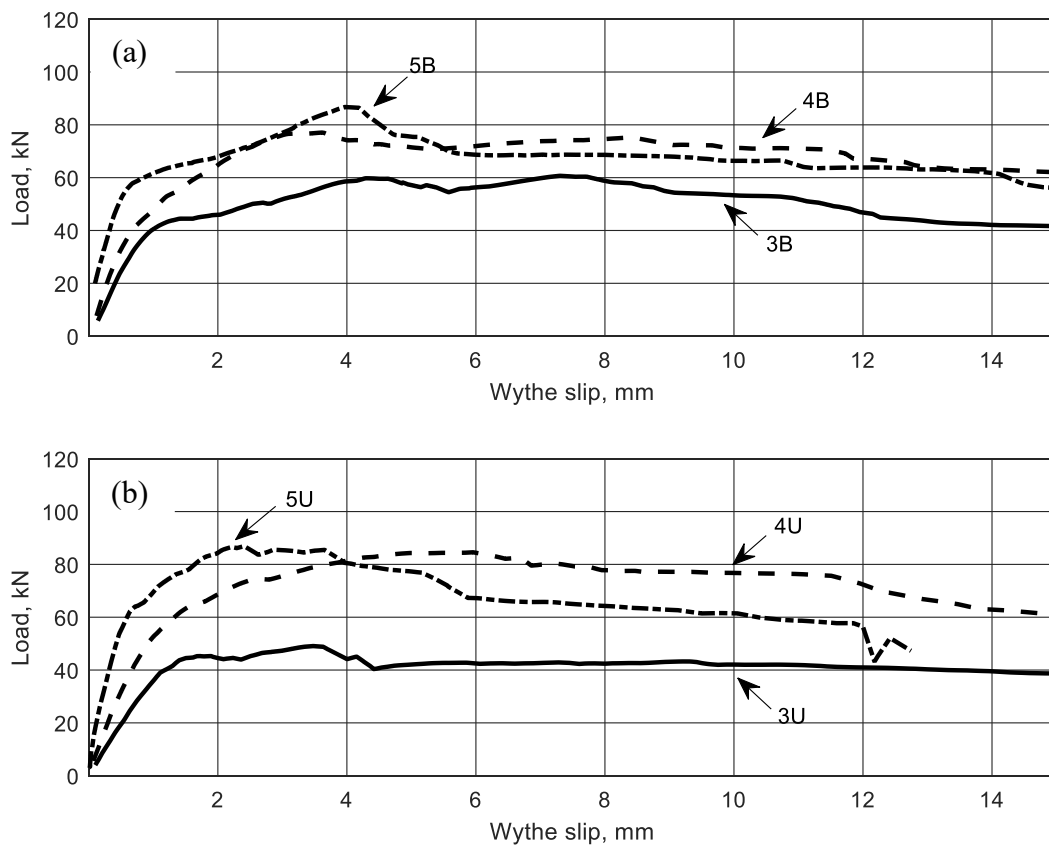


Figure 3.7 Average load deflection plots for (a) bonded and (b) unbonded with reported stiffness value at 0.25 mm deflection

3.3.3 Stiffness Calculation Approaches

The stiffness of the shear connection system is the primary property of interest for thermal bowing since connection stiffness affects how much shear transfers between wythes under the thermal loading observed in Chapter 4. Two approaches were used to evaluate the elastic stiffness of the push-through tests: the moving approach and the secant approach.

3.3.3.1 Moving Approach

The stiffness, k , is defined as the force over displacement in Equation (6). MATLAB was used to calculate the stiffness at a deflection “ i ”. The stiffness, k_i was calculated using Equation (6).

$$k_i = \frac{F_{i+5} - F_{i-5}}{\Delta_{i+5} - \Delta_{i-5}} \quad \text{Equation (6)}$$

Where F_{i+5} and F_{i-5} are the loads at the particular point at an interval of five elements ahead of the point and behind the point. Similarly, Δ_{i+5} and Δ_{i-5} are the deflections five elements ahead of point i and five elements behind point i respectively. One element represents a distance of 0.01 mm.

3.3.3.2 Stiffness Methodology Secant Approach

A secant method was also used to determine the stiffness of the specimens. This method is later found to be the most appropriate for evaluating the connection stiffness under the thermal loading seen in Chapter 4 (up to 20 kN for the #3 and 33 kN for the #5 bar respectively for one “X” set of connectors). The secant method is calculated using Equation (7).

$$k_{secant} = \frac{F_{0.4peak} - F_{0.1peak}}{\Delta_{0.4peak} - \Delta_{0.1peak}} \quad \text{Equation (7)}$$

The secant is taken between 10 and 40% of the peak load, $F_{0.1peak}$ and $F_{0.4peak}$, following a similar method to determine the Young’s Modulus of concrete cylinders. The corresponding slip

at relative to the peak loads are $\Delta_{0.1peak}$ $\Delta_{0.4peak}$. If the proportional limit is greater than 40% of the ultimate load, then the secant between $F_{0.1peak}$ and the proportional limit load is taken.

3.3.4 Stiffness Moving Approach Results

Stiffness values from the moving approach for slips between 0.15 and 0.40 mm were investigated. The stiffness at 0.25 mm slip is presented as the stiffness of the specimen in Table 3.2. This point is chosen to ignore the initial 0.1 mm slip (Figure B.4 of Appendix B) of the plots that show high variation, which is known as the “toe”. The toe results from settlement of the support and specimen and does not reflect the actual response of the system. The variation in the toe is amplified as the shear connector size increases. After the toe, stiffness stabilizes at 0.2 mm slip as shown in Figure 3.8. Beyond this point, specimens show signs of separation from insulation and lose stiffness (i.e. pass the proportional limit). The slip at the proportional limit decreases as bar size increases; the stiffness at 0.25 mm best represents the initial stiffness prior to the proportional limit for all tests.

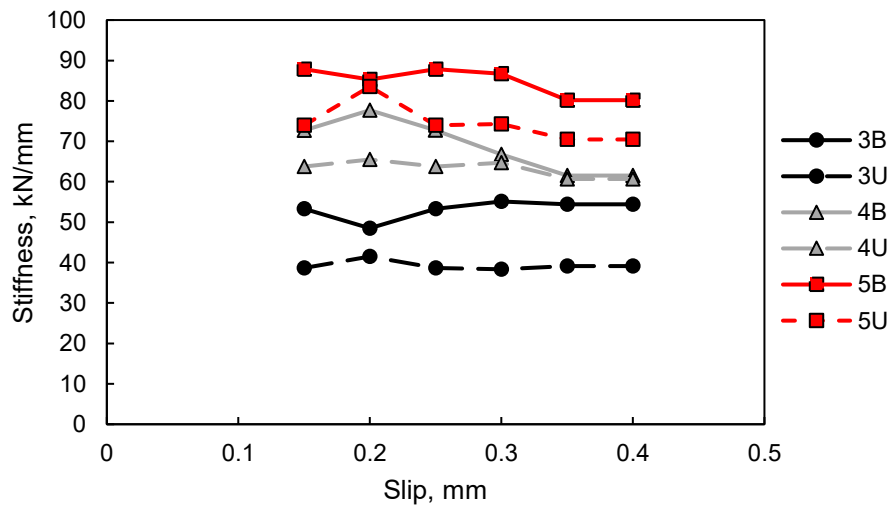


Figure 3.8 Stiffness values from the moving approach at locations between 0.1 and 0.4 mm.

3.3.5 Stiffness Results

Table 3.4 summarizes the average stiffness at a slip of 0.25 mm (moving method), and the secant method for the #3, #4, and #5 bars respectively by taking the average of the LVDT and DIC data for all three specimens of each type.

The moving method standard deviation for bonded specimens was 15.3, 19.7, and 23.5 kN/mm for 3B, 4B, and 5B respectively. For the unbonded, the deviation was 16.6, 24.1, and 47.5 kN/mm for the 3U, 4U, and 5U respectively.

The secant method standard deviation for bonded specimens was 14.6, 20.2, and 15.1. kN/mm for the 3B, 4B, and 5B respectively. The unbonded specimen deviation was 16.6, 25.9, and 52.8 kN/mm for the 3U, 4U, and 5U respectively.

Table 3.4 Summary of push-through test results for two shear connector systems

Specimen Type	#3 bar Stiffness, kN/mm	#4 bar Stiffness, kN/mm	#5 bar Stiffness, kN/mm
Moving method			
Bonded	53.3	72.7	87.9
Unbonded	38.6	63.8	74.0
Secant method			
Bonded	54.1	84.6	99
Unbonded	41.0	65.5	78.7

3.3.6 Effect of Parameters on Failure Mode

After completion of the push-through tests, the specimens were ripped open and examined for failure modes. Table 3.5 presents a summary of the failure mode for the push-through specimens. The #3 bar's failure mode consisted of the compression connector shear failure, tension connector pull-out and compression connector concrete crushing. The #4 shear connectors failed by tension connector pull-out and compression connector concrete crushing. The #5 shear connectors all had concrete crushing failure. Figure 3.9 shows examples of these four failure modes. Multiple failure modes were evident as the specimens were loaded to slips of 15 mm. This led to challenges identifying the first failure mode for the specimens.

Table 3.5 Summary of push through failure modes

SPECIMEN ID	FAILURE MODES			
	Compression connector shear failure	Tension connector pull-out	Compression connector concrete crushing	Concrete crushing
3B1	x	x		
3B2			x	
3B3		x	x	
3U1	x			
3U2		x		
3U3	x			
4B1		x	x	
4B2			x	
4B3				
4U1		x		
4U2		x		
4U3			x	
5B1				x
5B2				x
5B3				x
5U1				x
5U2				x
5U3				x

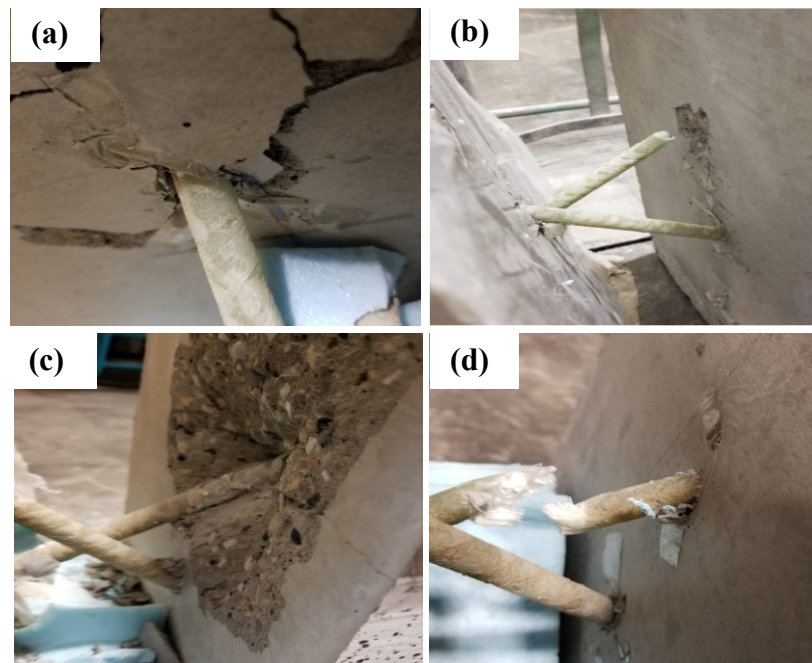


Figure 3.9 Failure modes of push-through tests (a) concrete crushing (b) tension pull-out (c) compression connector concrete crushing (d) compression connector crushing.

3.3.7 Effect of Parameters on Peak Load

Peak load average increased by 32% (20.3 kN) from 3B to 4B, and by 14% (12.0 kN) from 4B to 5B. For unbonded specimens this increase was 69% (36.1 kN) from 3U to 4U, and 14% (11.9 kN)

from 4U to 5U. This relation shows a nonlinear increase in peak load as shear connector size increases. However, Figure 3.10 (a) shows limited gains from #4 to #5, indicating that the #4 bar is most efficient for peak loads.

The axial stress carried by the shear connectors, σ_{SC} , was estimated using Equation (8).

$$\sigma_{SC} = \frac{P_{peak}}{nA_{SC} \sin \theta} \quad \text{Equation (8)}$$

Where P_{peak} is the peak load, θ is the insertion angle (45° in all tests). A_{SC} is the nominal connector area, and n is the number of bars (4 in all tests). Eq. (8) assumes small deformations and that the force is transferred entirely by truss action. Previous work (Tomlinson et al. 2016), indicates that this assumption is valid for truss-type connectors similar to the ones tested here.

As connector size increased, failure stress decreased. For bonded tests, the bar stress at failure decreased by 26% from 3B to 4B, and 37% from 4B to 5B (340, 252, and 185 MPa for 3B, 4B, and 5B respectively). For unbonded tests the decrease was 4.8% from 3U to 4U, and 27% from 4U to 5U bar (281, 267, and 194 MPa for 3U, 4U, and 5U respectively). Based on this, it is more efficient to use more, smaller connectors (such as #3) than fewer larger connectors since smaller connectors carry higher stresses before failure. Tomlinson et al (2016), who studied smaller connectors, noted that bars larger than 4 or 6 mm were more efficient, which indicates that the #3 bar (9.52 mm) may be the most efficient size for this type of connector.

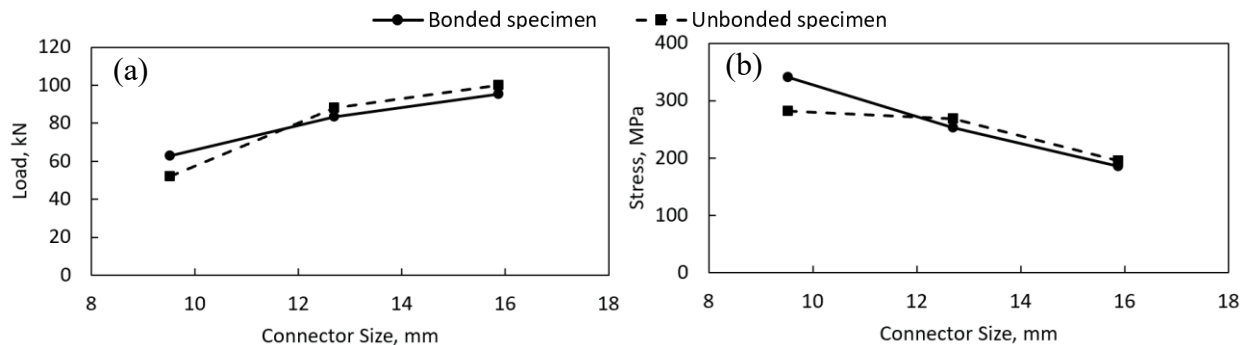


Figure 3.10 Effect of parameters on (a) peak load (b) peak load stress

3.3.8 Effect of Parameters on Proportional Limit

Proportional limit average load was more affected by bonding quality rather than connector size. From 3B to 3U the proportional limit decreased by 11.9% (4.23 kN), from 4B to 4U the proportional limit decreased 14.9% (5.1 kN), and from 5B to 5U decreased 69.2% (17.8 kN).

The slip at the proportional limit decreased as connector size increased. For bonded specimens, the decrease in slip was 32.2% (0.23 mm) from 3B to 4B and 41.9% (0.20 mm) from 4B to 5B. Similarly, for unbonded specimen slip, the decrease was 45.2% (0.32 mm) from 3U to 4U and 59.4% (0.23 mm) from 4U to 5U. There was also a decrease in the proportional limit slip from bonded to unbonded specimens. Slip decreased 0.47% from 3B to 3U, 18.8% from 4B to 4U, and 43.3% from 5B to 5U. This trend was also observed in the DIC analysis. The proportional limit is the point where connector response becomes non-linear; the results show this point occurring at earlier slips as connector size increases. This earlier slip indicates loss of stiffness for higher diameter bars. In the case of bowing, the loss of stiffness is more likely to lead to non-linear behaviour, which may cause permanent deflections in panels subject to thermal bowing.

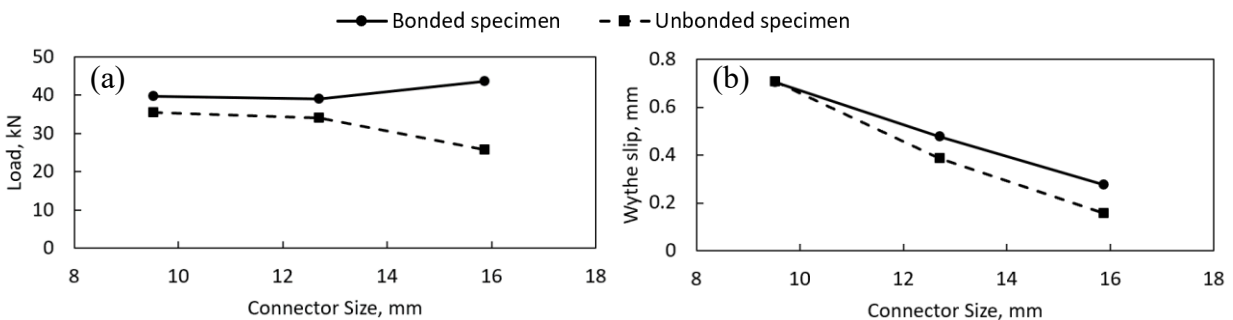


Figure 3.11 Effect of parameters on (a) proportional limit load (b) proportional limit slip

3.3.9 Effect of Parameters on Stiffness

Two stiffness calculation approaches were used: the moving method and the secant method. The moving method used the stiffness at 0.25 mm slip to avoid the initial “Toe” and non-linear response after the proportional limit. This stiffness increased with connector diameter and decreased from

bonded to unbonded specimens. The bonded specimen stiffness increased 36.4% (19.4 kN/mm) from 3B to 4B and increased 65.3% (25.2 kN/mm) from 4B to 5B. For unbonded specimens, the increase was 20.9% (15.2 kN/mm) from 3U to 4U and increased 15.9% (10.2 kN/mm) from 4U to 5U. The decrease from bonded to unbonded specimen was 27.5% (14.7 kN/mm), 12.2% (8.9 kN/mm), and 15.8% (13.9 kN/mm) for the #3, #4, and #5 bars respectively.

The secant method was the second method used in this study. These values better represent the connector forces (25 to 40% of peak load) observed during thermal loading in Chapter 4 compared to the moving method. Similar to the moving method, stiffness increased as connector size increased, and decreased in stiffness from bonded to unbonded specimens. The bonded specimen stiffness increased 56.3% (42.8 kN/mm) from 3B to 4B and increased 59.6 % (29.5 kN/mm) from 4B to 5B. For unbonded specimens, stiffness increased 16.9% (14.1 kN/mm) from 3U to 4U and increased 20.0% (25.1 kN/mm) from 4U to 5U. The decrease from bonded to unbonded specimens was 24.1% (12 kN/mm), 22.5% (25.3 kN/mm), and 20.5% (14.3 kN/mm) for the #3, #4, and #5 bars respectively.

The two methods show similar results in terms of unbonded specimens, and a small difference between the #4 and #5 bars. Both methods show that stiffness increases with connector size. However, there is a diminishing return when it comes to increasing bar size from #4 to #5 for stiffness; the #4 bar is the most efficient bar size if high stiffness is desired.

The debonding of insulation shows significant stiffness decrease with respect to its bonded counterpart. The secant method shows more of an effect compared to the moving method. This is due to the secant method using a wider range of slip (10 to 40% of proportional limit slip) compared to the incremental method (over 0.1 mm of slip) of the moving approach. Both methods show the significance of the bond between insulation and concrete regarding stiffness.

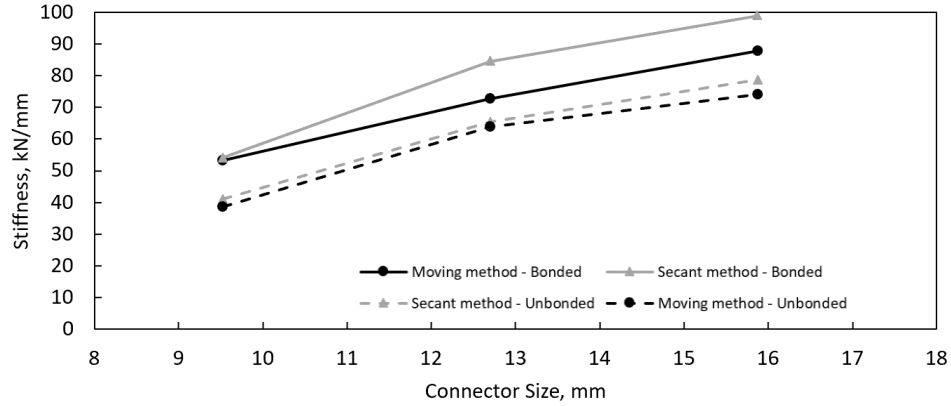


Figure 3.12 Effect of parameters on stiffness

3.3.10 Effect of Parameters on Deformability

The deformability index, DI , of the specimens was calculated using Equation (9). Deformability is used in FRP reinforced systems to evaluate how much warning of failure is expected. There are several approaches for finding DI (Tomlinson, 2015). This approach was used due to its simplicity.

$$DI = \frac{P_{peak} \times \Delta_{peak}}{P_{PL} \times \Delta_{PL}} \quad \text{Equation (9)}$$

Where P_{peak} and Δ_{peak} is the peak load and slip at peak load; P_{PL} and Δ_{PL} are the proportional limit load and slip at proportional load.

The DI shows a non-linear trend as connector size increases. For bonded specimens, there was a 137% increase from 3B to 4B, and a 79.8% increase from 4B to 5B. The non-linear behaviour is magnified for the unbonded specimens. The increase from 3U to 4U was 125% and 342% from 4U to 5U.

Deformability shows the difference in peak load and peak slip with respect to proportional limit and slip. Though simple to calculate, this approach may give misleading results in some situations. For instance, part of the reason for the jump in DI from 4U to 5U is that both the proportional limit load and slip for 5U was considerably lower than that for 4U. This has a skewing effect for the 5U tests and gives a very high DI relative to the other tests. That said, the trend still

shows that *DI* increases with connector size, and if the insulation is debonded. A higher *DI* provides more warning of failure via non-linearity; larger connectors give more warning of failure.

Table 3.6 Deformability index results for two shear connector system

Specimen Type	#3 bar DI	#4 bar DI	#5 bar DI
Bonded	22.3	53.2	96
Unbonded	31.4	70.8	313

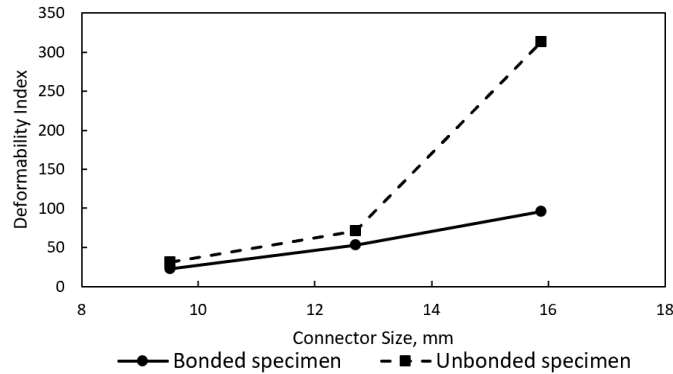


Figure 3.13 Effect of parameters on deformability

3.4 Shear Flow of Connector Systems.

Table 3.7 shows a comparison of shear flow for connectors from four studies: the current study (Arevalo), Woltman et al. (2013), Tomlinson et al. (2016), Kim and You (2015). The shear connectors in this study have higher shear flow compared to the 9.53 mm and 12.7 mm connectors tested by Woltman et al. (2013) and the 8 mm connectors tested by Tomlinson et al. (2016). This increase in shear flow is a result of the specimens in this study utilizing truss action, whereas Woltman et al. (2013) relied on dowel action and Tomlinson et al. (2016) used smaller bars. The GFRP grid tested by Kim and You (2015) has a similar shear flow to the #3 and #4 bars (45 kN/m to 75 kN/m). The general implication of this is that specimens from Woltman et al. (2013) and Tomlinson et al. (2016) are less composite by strength, whereas Kim and You (2015) would see similar composite action by strength. Similar trends are expected for shear connection stiffness

though stiffness results from other studies are not readily available so a direct comparison for stiffness was not be made.

Table 3.7 Shear flow for connection systems tested by various researchers

Study	Specimen ID	Material	Diameter, mm	Maximum Load, kN	Shear Flow, kN/m		
Current (Arevalo)	3B1	GFRP	9.53	29.7	49.5		
	3B2			30.8	51.3		
	3B3			33.95	56.6		
	3U1			27.5	45.8		
	3U2			26.7	44.5		
	3U3			24	40.0		
	4B1		12.7	43.2	72.0		
	4B2			36.25	60.4		
	4B3			45.45	75.8		
	4U1			37.7	62.8		
	4U2			46.15	76.9		
	4U3			48.45	80.8		
	5B1		15.8	47.85	79.8		
	5B2			41.75	69.6		
	5B3			53.35	88.9		
	5U1			55.9	93.2		
5U2	50.7	84.5					
5U3	43.65	72.8					
Woltman et al. (2013)	P1 (5 SC)	Steel	4.97	30.65	6.8		
	P2 (11 SC)	GFRP	6.35	54.8	5.5		
	P3 (11 SC)			39.15	4.0		
	P4 (5 SC)			38.3	8.5		
	P5 (5 SC)		9.53	35.85	8.0		
	P6 (5 SC)			37.1	8.2		
	P7 (5 SC)			27.4	6.1		
	P8 (7 SC)			42	6.7		
	P9 (3) SC			12.7	37.75	14.0	
Tomlinson (2016)	B45C4			BFRP	4	2.85	5.7
	B45T4	6.45	12.9				
	B45C6	4.92	9.84				
	B45C6a	20.75	41.5				
	B45T6	6	12.11		24.22		
	B45T6a		20.95		41.9		
	B45C8		8		10.19	20.38	
	B45T8				15.68	31.36	
	S45Ca		Steel		5.8	17.9	35.8
	S45T					9.58	19.16
S45Ta	22.44	44.88					
Kim and You (2015)	EPS 35	GFRP Mesh	35 mm spacing	-	58.7		
	EPS 53		53 mm spacing	-	62.5		
	XPSS 35		35 mm spacing	-	76.2		
	XPSS 53		53 mm spacing	-	40.5		

3.5 Chapter Conclusion

This chapter discussed the push-through experimental program to investigate shear connectors used in thermal bowing tests. Shear connectors of #3 (9.53 mm), #4 (12.7 mm), and #5 (15.8 mm) size were investigated to evaluate their stiffness and strength. The following was observed:

1. Peak loads increased as connector size increased and decreased if the insulation was debonded. However, the connector failure stress decreased as connector size increased. The results show that the lower diameter connectors (#3, #4) are more efficient (i.e. reach higher stress) compared to the #5 bar. Higher sized connectors show failure by concrete blowout, resulting in lower failure stress.
2. The proportional limit load was not affected by connector size but decreased as specimens were debonded compared to respective bonded specimens. The slip at the proportional limit decreased as connector size increased. Based on proportional limit slip, smaller connectors are more efficient at staying in the elastic region as compared to the #5 bar which showed lower slip. This effect was amplified when moving from bonded to unbonded specimens (up to 67% from #5B to #5U) which indicates the ability of the concrete to insulation bond at maintaining elasticity of the system.
3. Deformability increased with both connector size and if insulation was unbonded. Deformability provides warning of failure; this indicates that larger connectors are recommended if serviceability is less of a concern and warning prior to failure is desired. It is noted that though larger bars have more deformability, their proportional limit slip was much lower than the other bars. This results in higher (and potentially misleading) deformability indices for the larger connectors.
4. Two methods of calculating stiffness were utilized, the moving method and the secant method. Both methods had similar results, though the secant method better represents the

effect of thermal loads that the shear connectors are subject to in the thermal bowing tests. Connector size increase shows diminishing returns in terms of stiffness when going from #4 to #5 bar. Similar thermal bowing behaviour and loads may result for these two connectors as compared to the #3 bar.

3.5.1 Recommendations

Several recommendations are concluded based on the results presented in this chapter:

1. Test smaller and larger connectors to confirm if the diminishing effect of stiffness for these connectors is observed over a wider range of connection systems.
2. Confirm if EPS insulation has a similar effect as XPS insulation. This is important as the debonding effects of the #4 and #5 bar can become varied compared to the #3 bar.
3. Cycling the load after the proportional limit to see if changes occur (e.g. change in stiffness, permanent deformation). This will also allow the response of specimens to cycling load to be evaluated.
4. Perform strain energy analysis on the load-slip results. This will be a more accurate prediction at warning of specimen compared to deformability. This is because deformability is impacted by the proportional limit slip.

4. EXPERIMENTAL INVESTIGATION OF THERMAL BOWING IN FULL-SCALE PRECAST CONCRETE INSULATED WALL PANELS

4.1 Introduction

Insulated wall panels used as exterior walls are subjected to temperature changes that result in thermal expansion or contraction of the exterior wythe. The thermal movement results in a combination of relative slip between the wythes and bowing (i.e. out-of-plane displacement along the panel length). Depending on the shear connection system stiffness, different bowing and relative wythe slips can be expected. For a non-composite panel, end slip will be unrestrained as the shear connectors do not contribute any resistance, which results in no bowing (see Figure 4.1). However, for a fully composite panel, large bowing will occur but no slip as the shear connectors are stiff enough to completely restrain end slip.

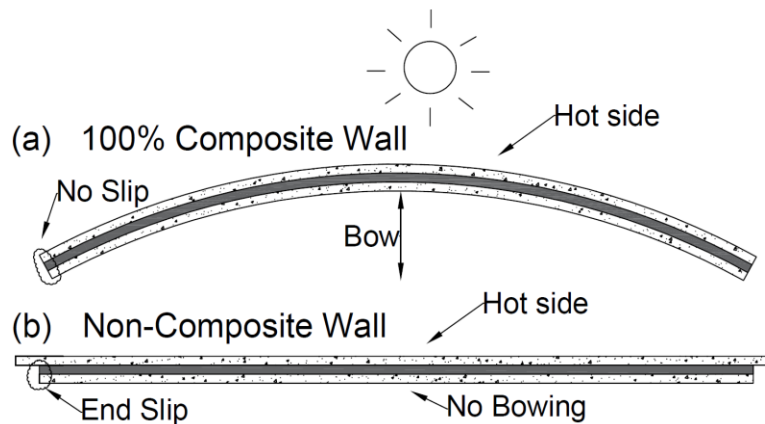


Figure 4.1 Thermal bowing on (a) fully composite panel (b) non-composite panel

In the 1980's, the market for IWP shifted to non-composite to avoid issues related to bowing and thermal bridging. The thermal insulation in IWP creates a greater thermal gradient than that in walls made of a single solid material, causing an increase in curvature and thus bowing (Post, 2006). Bowing is undesirable as it induces unwanted deflections, applies stresses onto the wall panel and connections, and can create a “fishmouth” effect at corners which interrupts the building envelope. Although commonly used, thermal bowing in these panels has been rarely investigated

experimentally and is currently estimated based on designer experience (PCI, 2011). Designers are using a larger thermal gradient through the panel than the actual site's atmospheric temperature difference to get a reasonable estimate of panel bowing (PCI 2011).

Bowing causes bending and shear forces in the panel that are transferred through shear connectors, see Figure 4.2. Slip is caused if one wythe expands relative to the other (Figure 4.2 (a)). Slip is a result of accumulating differential strain (slip strain) from one wythe to the next (Tomlinson, 2015). The desire to slip engages the connectors which resist slip by transferring longitudinal shear force between the wythes (Figure 4.2(b)). This force transfer results in curvature (and thus bowing) of the panel (Figure 4.2(c)). The amount of shear transferred is a function of the connector stiffness with stiffer connection systems resulting in more bowing and less slip.

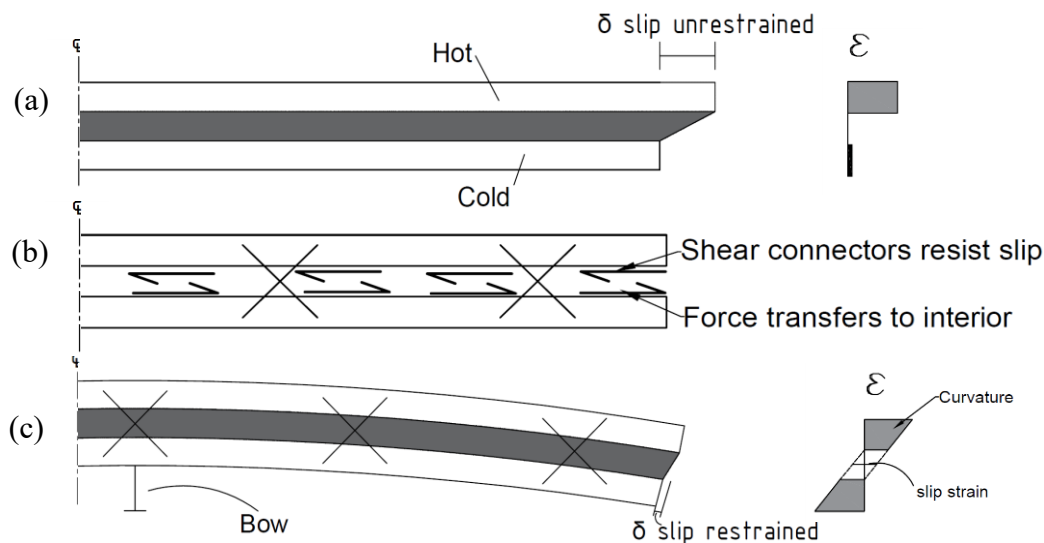


Figure 4.2 Free body diagram mechanics of thermal bowing (a) unrestrained end slip (b) force transfer to connectors (c) deflected shape of bowed panel

Four full-scale (6.1 m long) panels with varying diameters of GFRP shear connectors and insulation bond configurations were constructed and tested to experimentally evaluate thermal bowing in a simply-supported partially composite IWP similar in design to panels available on the market. The focus of the experimental program is on the thermal contributions to bowing on an isolated panel without consideration of other factors (e.g. creep, humidity, connections).

A thermal enclosure was built to run the tests. This enclosure was used to induce thermal gradients of up to 30°C in the test panels. This gradient simulates conditions often experienced in Canada. It is important to understand how connector stiffness (i.e. degree of stiffness-based composite action) affects bowing of IWPs. The composite action of the walls was varied by changing the shear connector arrangement.

4.2 Panel Description

The layout of the panels is shown in Figure 4.3. Reinforcement, wythe/insulation thickness, and panel length were selected to be representative of walls currently on the market. All IWPs were 6.1 m long and 590 mm wide. This length was chosen to show more evidence of bowing compared to shorter panels. The concrete wythes were 75 mm thick and sandwich a 75 mm of XPS insulation. The IWPs were reinforced with welded wire mesh and 10M rebar with a reinforcement ratio of 0.0081 (calculation presented later). Ten ‘X’ shaped GFRP connectors using the same materials and layout as the ones in Chapter 3 were inserted at 610 mm spacing along each wall.

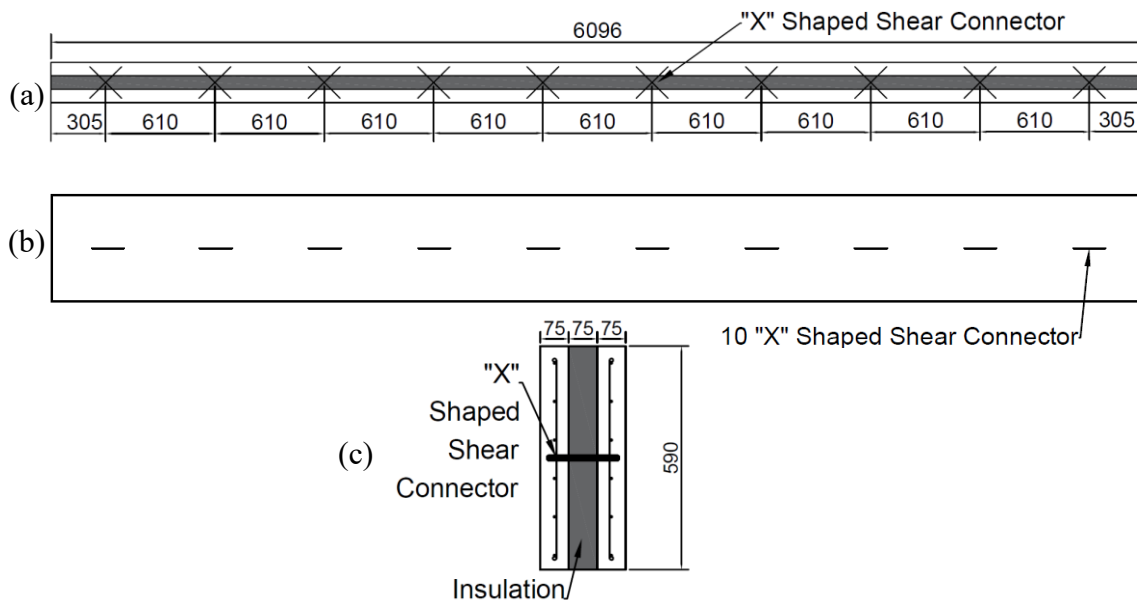


Figure 4.3 IWP Design and shear connector layout; All dimensions in (mm) (a) top view (b) side view (c) cross section view.

4.3 Test Parameters

Three panels with GFRP shear connectors were constructed with either 9.52 (IWP-3B), 12.7 (IWP-4B), or 15.9 mm (IWP-5B) diameter connectors (Table 4.1). This size range was used to investigate thermal bowing response for various degrees of partial composite action. The fourth panel (IWP-4U) used 12.7 mm shear connectors but also had the insulation debonded from the concrete with a thin polyethelene sheet to examine the insulation-concrete bond effect on thermal bowing.

Table 4.1 Insulated wall panel thermal bowing test matrix

ID	Connector diameter, mm	Insulation Bond	Shear connector reinforcement ratio, ρ_{sc}	Stiffness per shear connector, kN/mm (from secant method, Chapter 3)	Days tested after cast
IWP-3B	9.52 (#3)	Bonded	0.000396	27.1	176
IWP-4B	12.7 (#4)	Bonded	0.000704	42.3	143
IWP-4U	12.7 (#4)	Unbonded	0.000704	32.8	184
IWP-5B	15.9 (#5)	Bonded	0.00110	49.5	137

Humidity readings taken in the lab and outdoors on the University of Alberta campus at 12:00 PM were taken with a humidity sensor over several days are shown in Table 4.2. The weather when humidity was taken was similar to that during the test dates. This showed a consistent humidity of 33% in the lab. Lower humidity causes the concrete to shrink faster; a consistent difference between the wythes leads to bowing. In the case of the lab, humidity was relatively low to cause further bowing.

Table 4.2 Humidity of lab and outdoors

Date	Location A - Structures Lab at Location of Wall Panels		Location B – University of Alberta Quad, in front of CCIS Building Entrance	
	Humidity (%)	Temperature (°C)	Humidity (%)	Temperature (°C)
7/15/2019 Monday	43	23	35	29
7/17/2019 Wednesday	46	23	34	36
7/19/2019 Friday	45	25	32	34
7/22/2019 Monday	42	24	35	32
7/24/2019 Wednesday	45	23	36	28
7/26/2019 Friday	44	25	31	35

4.4 Fabrication

The insulated wall panels were cast on their side due to lab space restrictions, see Figure 4.4. Casting the panels this way allows formwork to take a lower footprint, enables multiple concrete wythes to be poured at once, allows better control of the locations of instrumentation, and eliminates tilt-up loads. Two sets of IWP forms were assembled with a length of 6100 mm (20 ft), each set of forms held two panels, accommodating four IWP total. Braces were cut and inserted at 400 mm spacing to maintain a level straight wall and resist lateral pressure during pour. In addition, brace pieces were placed at 1 m on centre spacing on top to prevent insulation uplift during casting.

To assemble the specimens, XPS insulation was cut to the dimension of the formwork. The WWM was welded together from three segments due to availability of mesh sizes and was placed in each concrete wythe to provide minimum reinforcement. Additional boundary reinforcement of 10M rebar was welded on the top and bottom of the WWM (i.e. on the sides of the finished panels). The “X” shape GFRP shear connectors were then placed at 610 mm spacing through the insulation. For ease of construction, the “X” shaped GFRP connectors were assembled together with the insulation and connected with chairs as a single package to drop into the formwork. Two lifting anchors were placed 1.5 m from each end of the IWP to allow for handling of the walls in the lab. Concrete was then placed evenly throughout the formwork, and then troweled for a smooth finish.

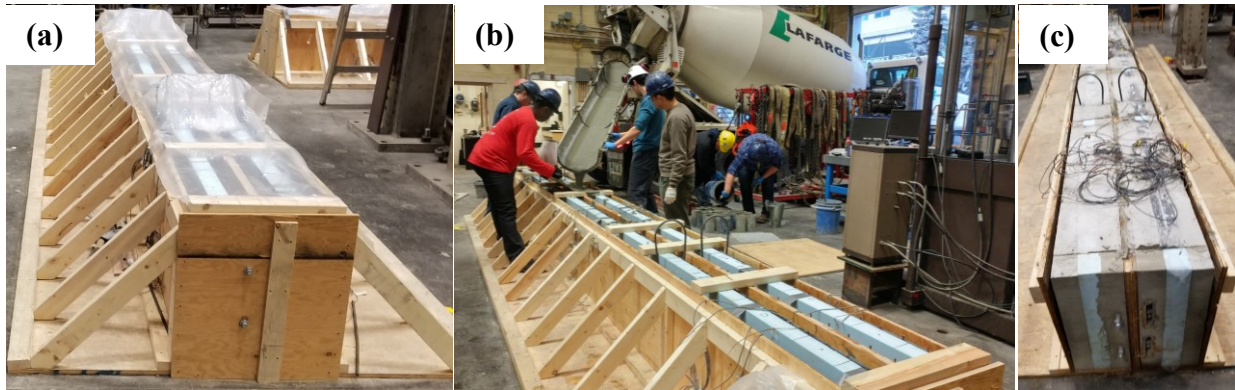


Figure 4.4 (a) IWP formwork (b) concrete pouring (c) IWP during stripping

A thermal enclosure (Figure 4.5) was built over the wall, with one wythe of the wall exposed to ambient laboratory temperature (cold wythe), while the other wythe (hot wythe) is exposed to elevated temperatures to induce bowing.

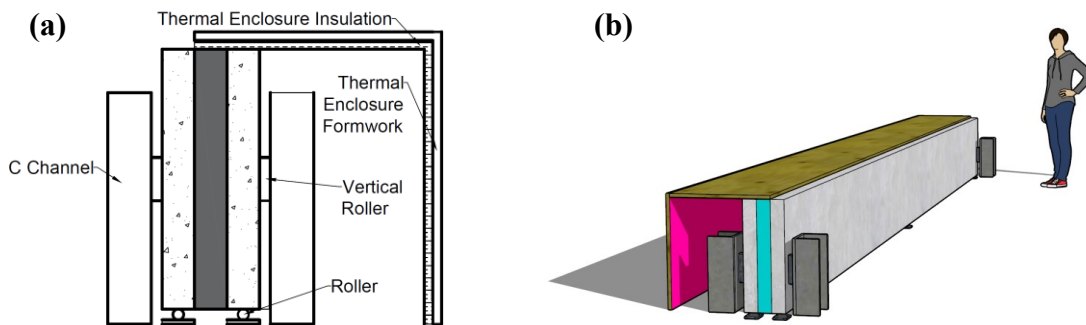


Figure 4.5 Thermal enclosure overview (a) end cross section view (b) 3D view in sketchup (end of enclosure removed for clarity).

4.4.1 Materials

Both the push-through (presented in Chapter 3) and the full-scale specimens used the same concrete mix, insulation, and reinforcement. A summary is provided here; more details, including stress-strain relationships, are given in Chapter 3.

4.4.1.1 Concrete

The average concrete strength and Young's Modulus at 28-days was 52 MPa and 23.5 GPa respectively. Thermal expansion tests were done on the concrete and are reported later on (Section 4.7.6)

4.4.1.2 Steel Reinforcement

Each wythe was reinforced with a plain (i.e. no deformations) steel welded wire mesh (WWM) with a diameter of 5.76 mm (area of 26.1 mm²) and spacing of 100 mm in both directions. The WWM yield and ultimate stresses were 494 and 512 MPa. The yield and ultimate strength of the 10M bars were 415 and 616 MPa respectively. Both the WWM and 10M had an average Young's Modulus of 200 GPa. The reinforcement ratio of the walls, ρ is found using Equation (10).

$$\rho = \frac{A_s}{bh} = \frac{(12 \times 26.1 + 4 \times 100)}{590(150)} = 0.00809 \quad \text{Equation (10)}$$

Where A_s is the total area of steel in the panel cross section, b is the panel width, and h is the concrete thickness through the panel cross section.

4.4.1.3 Insulation

Extruded polystyrene (XPS) was used in the panels. The compressive strength of the insulation was 0.253 MPa. The density of the insulation was 28.8 kg/m³ with an R-value of 7.2 per 25 mm (inch). Further information is provided in Appendix D.

4.4.1.4 GFRP Shear Connectors

GFRP shear connectors were 250 mm long and arranged in an "X" shape (see Figure 3.3 for more detail). Three diameters (9.53, 12.7, and 15.8 mm) were used and correspond to #3, #4, and #5 bar designations respectively. The average tensile strength and elastic modulus of the GFRP was 1420 MPa and 60.5 GPa respectively.

4.4.1.5 Thermal Properties

The thermal conductivities of the insulation and GFRP were 0.029 and 0.125 W/m·K respectively. Insulation properties were taken from Table 2.2 and GFRP properties were provided by the manufacturer. Using the zone width method from Lee and Pessiki (2008), the estimated R-value of the IWPs used in thermal testing is 3.55 m²K/W.

4.4.2 Lifting and Handling

A 10-ton overhead crane was used to move IWPs around the Morrison Structural Lab. “U” bent 10M bars with embedment greater than 300 mm were used as lifting hooks placed 1.5 m from the ends of the wall. This location was selected to minimize bending moments from panel self-weight during handling. Each panel weighs approximately 1.2 tonnes and it was determined that the handling moments were much lower than the panel’s cracking moment. Figure 4.6 shows a panel being lifted during stripping.



Figure 4.6 Insulated wall panel lifting

4.5 Thermal Enclosure Setup and Instrumentation

A thermal enclosure was constructed to investigate IWP bowing under temperature differentials up to 30° C. The enclosure's purpose was to create a temperature differential by heating one wythe ('hot wythe') while leaving the other exposed to lab ambient temperature ('cold wythe').

4.5.1 Fabrication

Plywood with 19 mm thickness and mineral wool batt insulation (Rockwool) were used to maintain heat in the thermal enclosure, as shown in Figure 4.7(a). Plywood provided a frame to support the insulation and fixtures (e.g. heating source) for the enclosure. The mineral wool insulation was placed on the surface of the plywood closest to the heating surface as well as used to fill gaps and limit heat loss through the enclosure and maintain a steady heat flow. The enclosure is closed with a 19 mm (0.75 in) plywood piece on top with a layer of Rockwool under to seal off potential air gaps Figure 4.7(h).

4.5.2 Heating Source

The heat was provided by two silicone rubber heaters (3875 W/m²) of 609 mm (24 in) length and 304 mm (12 in) width. The heaters were attached to two aluminum sheets that radiated the heat outwards. The two heaters were mounted onto the enclosure using 9.53 mm threaded bars at the corner of the aluminum sheet, see Figure 4.7(b). The heaters are capable of being heated up to 200°C but a controller was used as a thermostat to ensure that the heat inside the enclosure would not exceed 65°C with the use of a thermocouple inside the enclosure. If this temperature was exceeded, then the heaters would turn off. After preliminary testing, it was determined that the heaters should be placed 2032 mm (i.e. one third of panel length) from each end of the enclosure to better provide even heat distribution along the length of the test panel.

4.5.3 Air Circulation

Fans were used to circulate the radiated heat from the heaters to the rest of the enclosure to create a more even temperature distribution along the panel length. Circulation was provided by two 119 mm (4.69 in) fans as shown in Figure 4.7(c). These fans were mounted at the centre of the enclosure beside the heating blankets.

4.5.4 Supports

Two $100 \times 100 \times 50$ mm steel plates with a grid of ball bearings were used as supports at the end of the panel (Figure 4.7(f)). The ball bearings were placed such that they would sit beneath the bearing surface of the IWP. This simple support was used to allow the wall to rotate out-of-plane at the ends while providing a surface to bear on. Two vertical 25 mm diameter steel pipes of 780 mm length were used at the panel ends to provide a surface along the panel's height to rotate about.

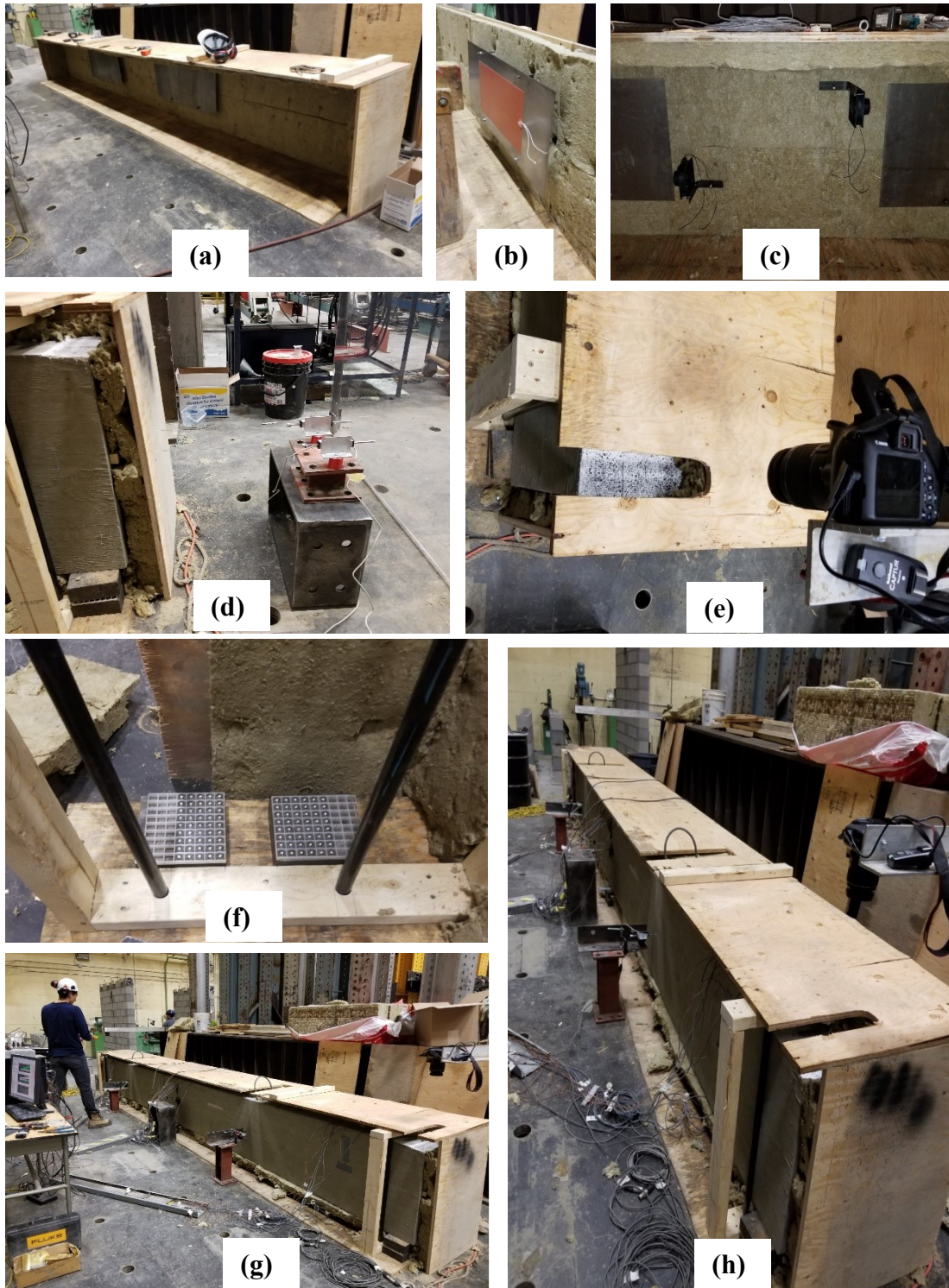


Figure 4.7 Thermal enclosure heating construction process (a) thermal enclosure fabrication (b) heating blanket (c) circulation fans (d) LVDT (e) DIC opening (f) simple support (g) top cap of enclosure (h) thermal enclosure during test

4.5.5 IWP Placement

A 10-ton crane was used to lift the IWP into the enclosure and place it on the support. The vertical pipes were used as guides to place the panel in the correct location. Once the IWP was set in place, mineral wool batt insulation is placed on around all of the panel edges to limit heat loss through the enclosure. A lid was then placed on top of the panel to seal the enclosure, see Figure 4.7(g).

4.5.6 Instrumentation

Strain gauges for the reinforcement were prepared and installed along four locations in the panel cross section, and thermocouples were installed along three cross sections of the panel, see Figure 4.8. Reinforcement strain gauges were placed on the top and bottom 10M bar and concrete surface gauge at the midpoint of the panel. These gauges measured the strain profile through the panel during testing. Uniaxial 120Ω and 2 mm length strain gauges were used on the reinforcement; uniaxial 350Ω and 50 mm length strain gauges were used on the concrete.

Type K Thermocouples measured temperature on the concrete surface, as well as at the insulation-concrete interface. Thermocouples were used to measure the temperature gradient throughout three cross sections of the panel during the experiment, (South, Midspan, and North in Figure 4.8).

The LVDTs (50 mm) were mounted on steel supports to measure end slip and bowing displacements along the length of the panel as shown in Figure 4.6. Five LVDTs were placed along the length of the wall, two at the supports, and three at third points to measure the bowing profile. End slip was measured by placing two LVDT's at the end to track the movement of the hot and cold wythe of the IWP, (Figure 4.7(d)). All LVDT sizes were between 25 mm to 50 mm as the predicted displacements were expected be less than 20 mm during testing.

DIC was also used to measure end slip at the end. A Nikon D5200 camera is placed at the south end and a Canon EOS Rebel T6 at the north end of the panel to take photos. An aluminum

angle bracket was used to mount cameras over top of 100×250 mm cut openings (Figure 4.7(e)) of the lid of the enclosure to take photos for DIC. Photos of 3456 × 5184 size (Canon) and 3000 × 4496 size (Nikon) were taken at a rate of one per minute throughout the heating phase of the testing.

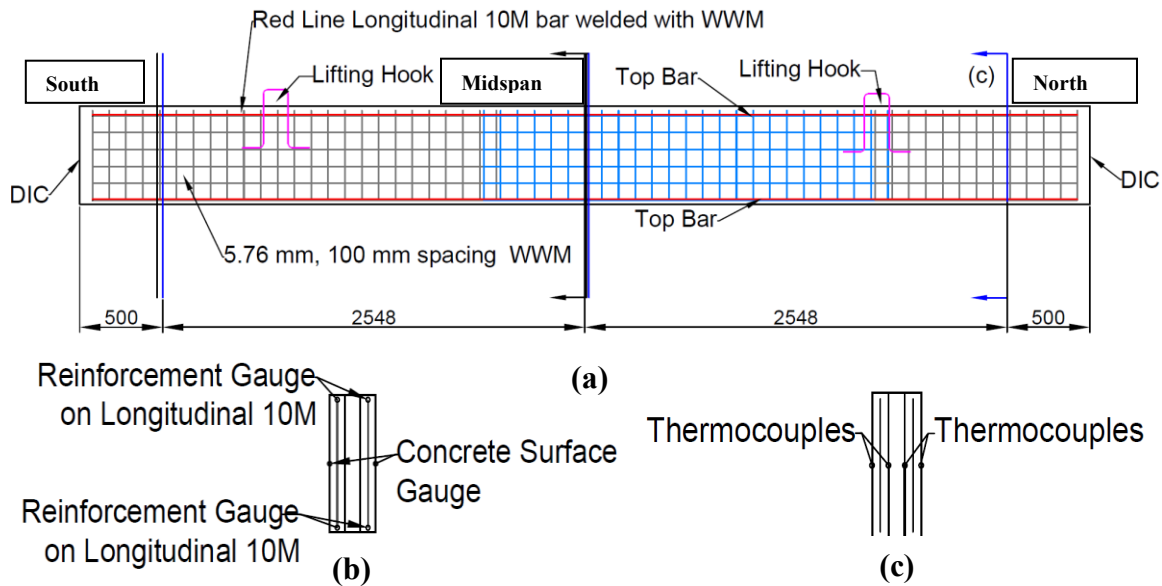


Figure 4.8 Insulated wall panel reinforcement and instrumentation (a) reinforcement layout (b) strain gauge reinforcement (b) thermocouple placement

4.6 Testing Procedure

The testing procedure consists of a heating and cooling cycle. LVDTs and strain gauges were calibrated before each test. Typically, heating cycles were started between 8:30 AM to 9:00 AM and would last until lab closure at 4:00 PM. This time window was sufficient to achieve a thermal gradient of at least a minimum of 20 °C and up to 30 °C for each panel. Supervision was required throughout this process to monitor rate of heating and for safety. After the heating cycle was complete, the heaters were turned off and the panel was allowed to cool down naturally. Data was recorded during the cool down process which took on average 48 hours. DIC only remained active for the heating phase since camera battery power was lost early into the cooling cycles. Apart from

testing the four walls, an initial heating test was done on IWP-5B to determine the optimal spacing of the heaters. IWP-3B required two tests, as the first one reached a temperature 33 °C (temperature differential of 13 °C) before a lab power failure occurred (unrelated to these tests). All data was sampled every ten seconds.

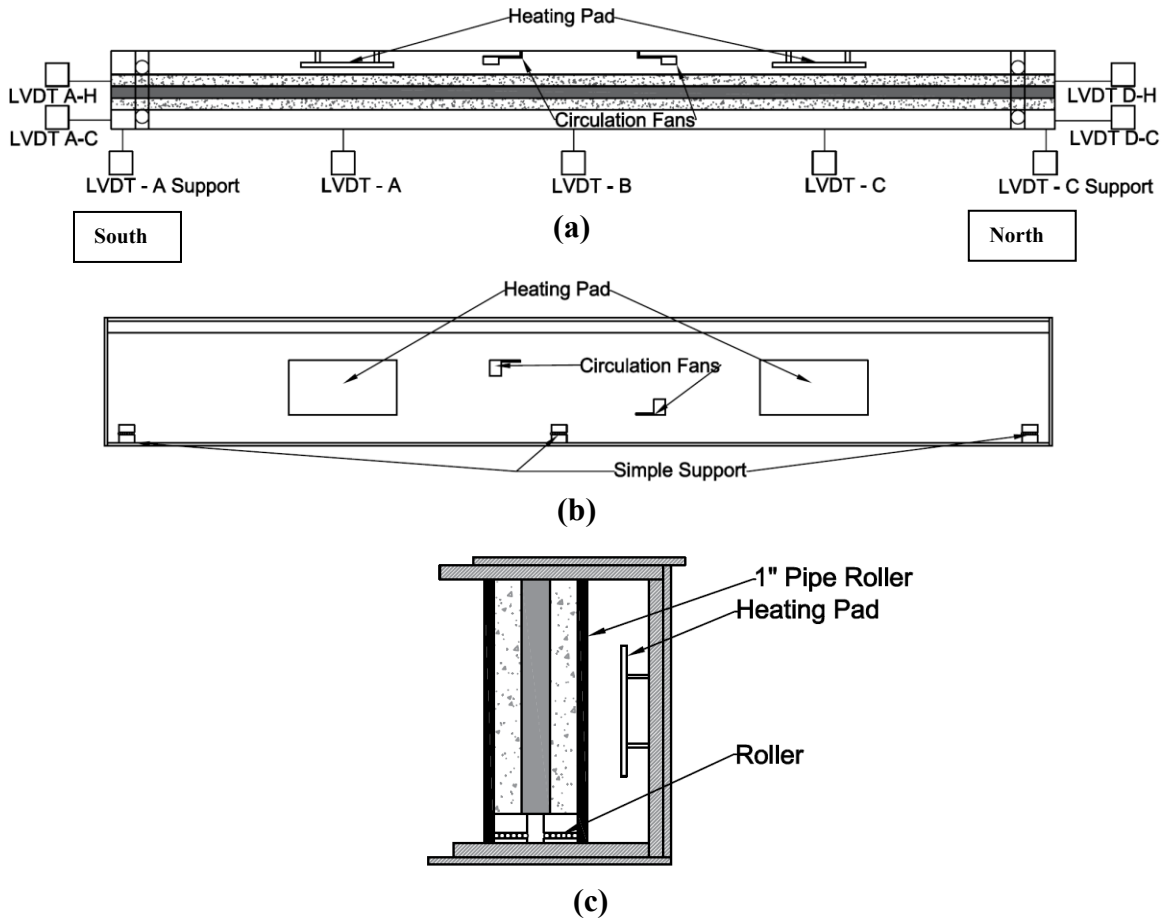


Figure 4.9 Thermal enclosure setup (a) top view (b) side view (c) right view

4.7 Results

The following section outlines the results obtained for each wall in terms of bowing, end slip, and strains through heating and cooling. Temperature trends and differential is discussed first. The

deflection response (i.e. end slip and midspan deflection) of the panels connectors is then discussed. Lastly, strains and estimate forces carried by the connectors is investigated.

4.7.1 Panel Temperature Response

The temperature recorded by all 12 thermocouples in both the heating and cooling cycle of IWP-4B is shown in Figure 4.10. This panel is shown to illustrate the thermal response during a test.

The other panels generally had similar responses and these responses are shown in Appendix C.

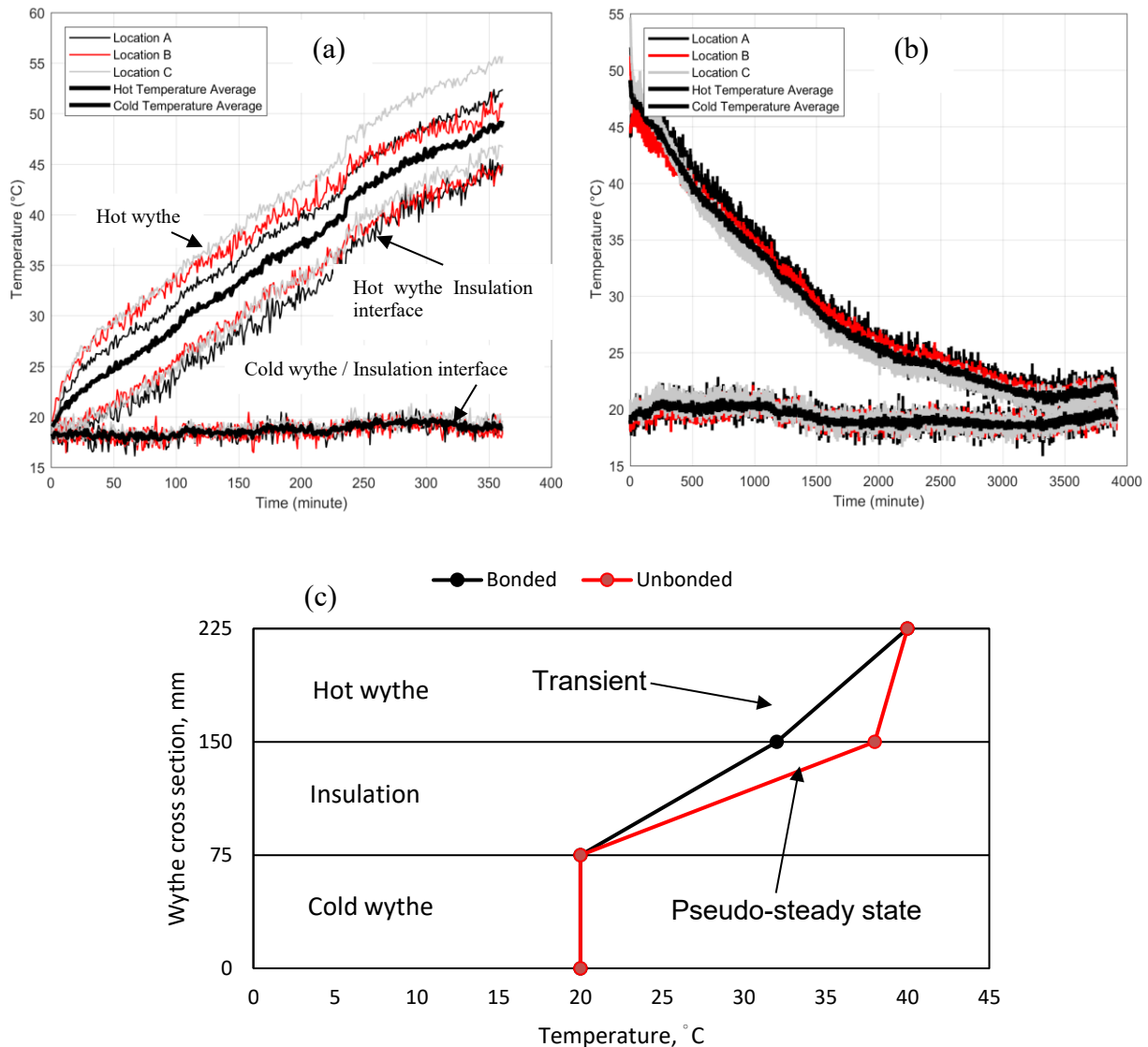


Figure 4.10 Temperature readings over test duration for IWP-4B (a) heating cycle (b) cooling cycle (c) transient vs steady state heating

The temperature readings in the panel were split into hot wythe and cold wythe behaviour. A linear temperature distribution through each wythe is assumed. This assumption has been used by researchers when evaluating temperature profiles in concrete bridge girders (Avid, 2018).

The cold wythe and cold wythe-insulation interface temperature remained steady at room temperature (~ 20 °C). Slight fluctuations (± 1 °C) were evident as the lab temperature varied slightly throughout the day.

The hot wythe and the hot wythe insulation-interface temperatures increased steadily during the heating phase but the hot wythe-insulation interface temperatures lagged about 100 minutes behind the hot wythe surface. This thermal lag is caused by the thermal storage capacity of the concrete and effective thermal resistance of the IWP. As a result of this initial thermal lag, there was a consistent temperature difference between the hot surface of the wythe and the following insulation-concrete interface throughout the heating process. The thermal lag in the heat cycle causes additional curvature and results in additional bowing of the panels relative to a panel with the same average temperature but equal temperature through the wythe.

The difference in heating for the panels was split into two phases, transient heating and pseudo-steady state heating (Figure 4.10 (c)). It was noted throughout the heating process that the bonded panels (i.e IWP-3B, 4B, 5B) showed transient temperature profiles during heating, whereas IWP-4U had a temperature profile that acts closer to a steady-state situation (i.e. similar temperatures through the wythe). This implies that, at a similar surface temperature, the steady state (IWP-4U) is subjected to higher thermal loads compared to the bonded panels (IWP-3B, 4B, 5B). This increase in heat for IWP-4U is believed to be due to the vapour barrier's ability to absorb and retain heat, and sealing of insulation, causing the hot wythe to heat more.

However, during cooling the bonded walls showed transient temperature profiles for only the first 80 minutes; temperature in the hot wythe was essentially consistent through its thickness beyond this point. As there is no active heat source, the enclosure was changed from transient to pseudo-steady state since the cooling period (48 hours) was slow enough for these conditions to develop.

4.7.2 Calculating Temperature Differential

To compare results between panels, the temperature differential, ΔT , between the two wythes was required. Four thermocouples were placed through the panel cross section (surface of hot wythe, hot wythe/insulation interface, cold wythe/insulation interface, surface of cold wythe) at three locations along the panel (see Figure 4.6). The temperature difference, ΔT , is calculated as the difference between the average temperature of the six thermocouples in the hot wythe, T_{hot} , and the average temperature of the six thermocouples in the cold wythe, T_{cold} .

$$\Delta T = T_{hot} - T_{cold} \quad (11)$$

This average temperature differential between the wythes, ΔT , is the temperature differential that is discussed over the course of this chapter.

4.7.3 End Slip

End slip results was discussed in terms of end slip at the north and south ends of the wall. End slip was a result of the panels inability to completely transfer forces caused by thermal expansion of the hot wythe. Less end slip is expected for stiffer connectors and vice versa. The sum of the two end slips during the heating and cooling cycles are reported in Tables 4.3 and 4.4 respectively.

4.7.3.1 North and South End Slip

Figure 4.11 shows the end slip through the heating and cool process for the north and south end of each IWP. Slips ranged from 1 mm (south end) to 1.5 mm (north end), as shown in Figure 4.11.

These slips are higher than average proportional limit slips seen in Chapter 3 (0.703 mm for #3 connector and 0.386 mm for IWP-5B).

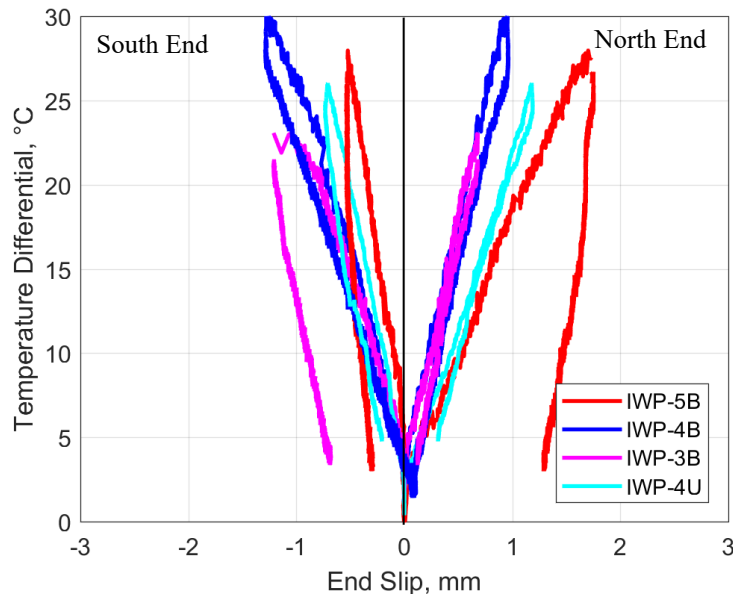


Figure 4.11 IWP end slip on heating cycle and cooling cycle for north and south end of IWP

The north end slip showed a dominant behaviour from IWP-5B and IWP-4U in compared to the south end slip. The south slip showed the most end slip in increasing order of IWP-5B, IWP-4U, IWP-4B, and IWP-3B respectively. For cool down, IWP-4B and IWP-4U follow the same trend as the heating cycle whereas IWP-5B and IWP-3B showed permanent slip as they cooled down. The suspected cause of this trend for IWP-5B and IWP-3B was due to these panels being cycled; prior cycling is believed to have caused these two panels to have permanent deformation. Since these slips were higher than proportional limit slips from Chapter 3, it is expected that the connectors experienced non-linear deformation.

4.7.3.2 Total End Slip

The total end slip of all the IWP are shown in Figure 4.12 and values reported in Tables 4.3 and 4.4. At a ΔT of 20 °C the total slip ranged from 1.32 to 1.49 mm. The trend here showed higher end slip for IWP-5B and IWP-4U, however it is noted that these two specimens also showed the

most slip during the thermal lag phase (0.209 and 0.191 mm at 5 °C). To reduce the effect of the lag region, the slope between 50 and 80% of the maximum end slip is calculated and reported in Table 4.5. This method better gives a representation as changes in temperature are more gradual in a real system; typically, there is no sudden initial jump in temperature over a 30-minute period. The slope showed a decreasing trend in end slip for panels with stiffer connectors. This indicates IWP-3B is resisting the longitudinal thermal expansion force the least and compared to IWP-5B.

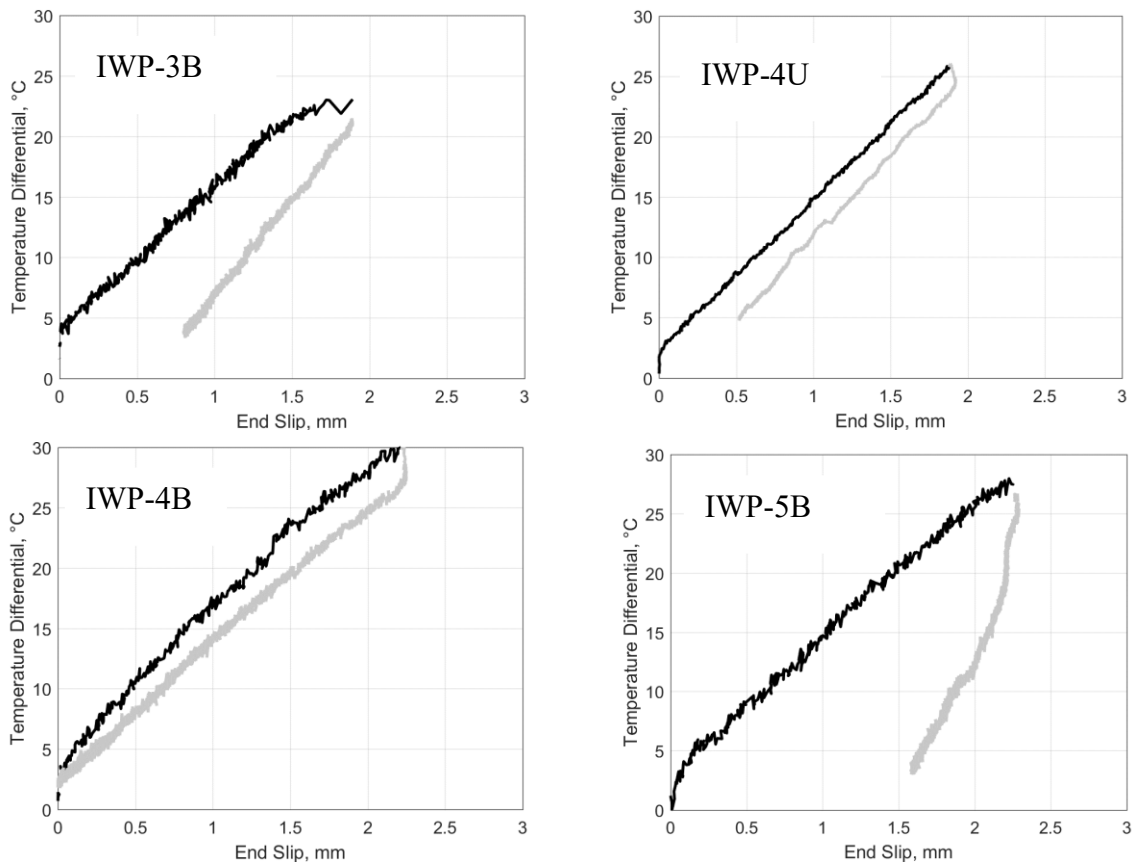


Figure 4.12 IWP total end slip for heating (black) and cooling (gray) phases

The cooling residual result of IWP-5B was due to prior heating cycling which caused the wall to lose stiffness. This loss of stiffness led to higher end slip results on IWP-5B. IWP-4U also showed higher end slip compared to the other panels through its pseudo-steady state heating (Section 4.7.1). This caused additional expansion of the hot wythe leading to a higher end slip compared to other panels. More discussion including impact of stiffness is discussed in section 4.7.4.

Table 4.3 Summary of Total End Slip during Heating Phase

Temperature Difference, ΔT , °C	Slip location	IWP-3B, mm	IWP-4B, mm	IWP-4U, mm	IWP-5B, mm
5	Total	0.071	0.11	0.209	0.191
	North	0.034	0.051	0.139	0.174
	South	0.037	0.059	0.071	0.016
10	Total	0.521	0.486	0.626	0.621
	North	0.249	0.231	0.441	0.527
	South	0.271	0.254	0.185	0.093
15	Total	0.940	0.829	1.02	1.02
	North	0.406	0.387	0.675	0.788
	South	0.533	0.442	0.347	0.234
20	Total	1.33	1.32	1.43	1.49
	North	0.563	0.587	0.924	1.15
	South	0.772	0.735	0.508	0.34
25	Total	^a –	1.65	1.81	1.94
	North	^a –	0.74	1.13	1.48
	South	^a –	0.911	0.673	0.456
30	Total	^a –	2.21	^a –	^a –
	North	^a –	0.955	^a –	^a –
	South	^a –	1.25	^a –	^a –
MAX	Total	1.73 @ 23 °C	2.21 @ 30 °C	1.81 @ 25 °C	2.11 @ 27 °C
	North	0.671 @ 23 °C	0.955 @ 30 °C	1.13 @ 25 °C	1.61 @ 27 °C
	South	1.05 @ 23 °C	1.25 @ 30 °C	0.673 @ 25 °C	0.501 @ 27 °C

^a – Temperature differential not reached during these tests

Table 4.4 Summary of Total End Slip during Cooling Phase

Temperature Difference, ΔT , °C	Slip Location	IWP-3B, mm	IWP-4B, mm	IWP-4U, mm	IWP-5B, mm
5	Total	0.953	0.310	0.574	1.70
	North	0.187	0.186	0.336	1.364
	South	0.765	0.124	0.238	0.331
10	Total	1.28	0.757	0.951	1.95
	North	0.350	0.354	0.552	1.518
	South	0.935	0.402	0.399	0.429
15	Total	1.58	1.16	1.32	2.12
	North	0.491	0.515	0.745	1.64
	South	1.09	0.647	0.573	0.483
20	Total	1.88	1.60	1.69	2.21
	North	0.676	0.698	1.01	1.68
	South	1.20	0.901	0.682	0.533
25	Total	^a –	2.12	2.37	2.46
	North	^a –	0.926	1.18	1.75
	South	^a –	1.19	1.19	0.709
30	Total	^a –	2.21	^a –	^a –
	North	^a –	0.956	^a –	^a –
	South	^a –	1.26	^a –	^a –
MAX	Total	1.88 @ 20 °C	2.21 @ 30 °C	1.88 @ 25 °C	2.27 @ 27 °C
	North	0.675 @ 20 °C	0.955 @ 30 °C	1.18 @ 25 °C	1.75 @ 27 °C
	South	1.20 @ 20 °C	1.25 @ 30 °C	0.709 @ 25 °C	0.527 @ 27 °C

^a – Temperature differential not reached during these tests

Table 4.5 Summary of end slip slope

	End slip slope, mm/°C							
	IWP-3B		IWP-4B		IWP-4U		IWP-5B	
	Heating	Cooling	Heating	Cooling	Heating	Cooling	Heating	Cooling
Total	0.0868	0.0235	0.0851	0.0936	0.0843	0.0589	0.0788	0.0732
North	0.0655	0.0144	0.0369	0.0396	0.0303	0.0290	0.0485	0.0475
South	0.0213	0.0090	0.0482	0.0540	0.0540	0.0299	0.0303	0.0257

4.7.4 Thermal Bowing of IWP

Thermal bowing at midspan of the wall was measured throughout heating and cooling of the panels. The ability of the connectors to resist relative wythe slip determines the magnitude of bowing. Resistance is dependent on the temperature differential and shear connector stiffness. Higher bowing is expected for more composite panels and vice versa.

All panels showed an initial spike in ΔT before any noticeable deflections due to thermal lag of the concrete. After this stage, all panels showed linear bowing-temperature response. Table 4.6 summarized the results of the four walls with respect to their maximum temperature differential, ΔT_{max} , achieved. Deflections were measured at quarter points along the length of the wall to create a bowing profile, see Figure 4.14 (b). The results showed curvature and thermal bowing increased every 5°C increment. In Figure 4.14 (b), IWP-4U showed similar midspan bowing to IWP-5B as it was subject to higher temperature loads from pseudo-steady state heating. IWP-4U's different temperature profile is reflected by it having a slightly different deflected shape than the other three panels.

Table 4.6 Summary of midspan deflection and end slip

Specimen ID	Maximum Temperature Difference, ΔT_{max} , °C ¹	Midspan Deflection (bow) at ΔT_{max} , mm	Midspan Deflection at $\Delta T = 20^\circ\text{C}$, mm	End Slip at ΔT_{max} , mm	Total End slip at $\Delta T = 20^\circ\text{C}$, mm
IWP-3B	23	7.93	6.55	3.02	1.33
IWP-4B	30	11.5	7.13	2.96	1.32
IWP-4U	26	9.53	7.18	1.98	1.43
IWP-5B	28	10.8	7.48	2.47	1.49

¹ Temperature difference defined as the hot concrete wythe minus the cold concrete wythe (Equation (11))

Table 4.6 showed the maximum bow of each IWP at maximum temperature differential reached. This bow is less than the allowable deflection of 16.9 mm ($l/360$), which accounted for 46% to 63% (at ΔT_{max} for IWP-3B and IWP-5B) of the acceptable service load deflections in the panels.

Figure 4.13 showed the thermal bowing at midspan for all panels. All the panels experienced support movements that needed to be considered when determining bowing. To account for this, the IWP bowing profiles were multiplied by a transformation matrix by the degree of rotation to zero movement at the panel supports. This allowed for bowing to be compared across the panels. Note that IWP-5B was the first to be tested and movements at the support were not recorded using LVDTs for that panel. DIC was used to account for movement at the support during heating but was unavailable for the cooling down cycle since the camera batteries were unable to last the required 48 hours to cool down.

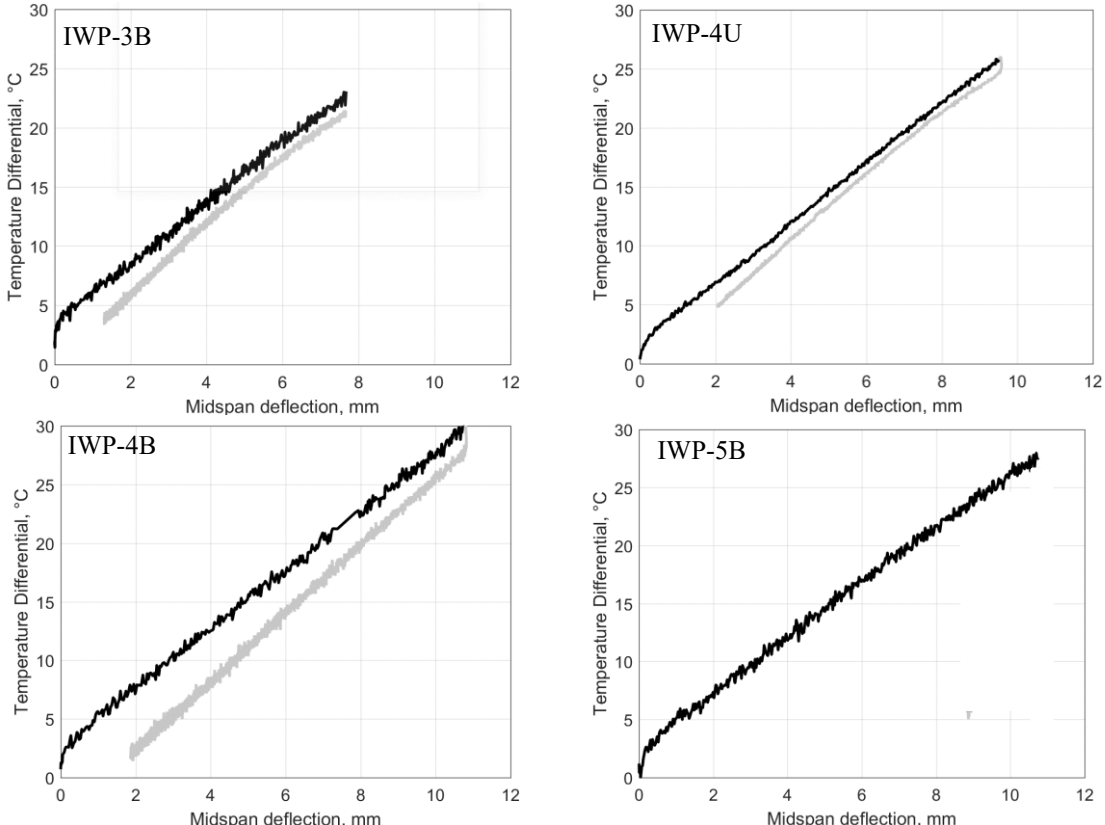


Figure 4.13 IWP midspan deflection (bow) versus temperature differential heating (black) and cooling (gray) cycle.

Figure 4.14 (a) showed the midspan deflection (i.e. bow) through the heating and the cooling phase for all IWP. This thermal lag behaviour was also observed during the cooldown cycle. At a ΔT of 10°C , the bow in IWP-3B, IWP-4B, and IWP-5B was 2.57, 3.05, and 3.16 mm respectively; At a ΔT of 20°C the midspan deflections of IWP-3B, IWP-4B, and IWP-5B was 6.55, 7.13, and 7.48 mm respectively. The cooling cycle also showed an increase in residual midspan deflection of IWP-4B compared to the less stiff panels. The bow during the IWP-5B cooldown could not be calculated as support displacement data was not available.

A general trend seen is that the higher composite panels show more bowing. The exception was IWP-4U, however it was seen from temperature plots that the pseudo-steady state induced a larger temperature load onto IWP-4U. With more of a temperature load, this magnified the force transfer that IWP-4U connectors must resist, leading to additional curvature and bowing for this specimen and a slightly different deflected shape than the other panels.

It is noted as IWP-5B was the first specimen, an initial thermal test to a ΔT of 30°C was conducted to verify the functionality of the thermal enclosure. Based on the observed end slips seen in the thermal testing (discussed in section 4.7.3), several of IWP-5B's connectors deformed beyond their proportional limit and may have had permanent loss of stiffness as a result. This would lead to IWP-5B having smaller bow than expected and may show less midspan deflection in subsequent testing as a result.

Table 4.7 reported the inverse slope ($\text{mm}/^{\circ}\text{C}$) of all panels from the heating and cooling phase. The slope was calculated using 50 and 80 percent of the max midspan deflection, a similar approach used for end slip. This avoided the initial temperature spike, and the tapering off that occurs at final temperatures. The slopes showed an increasing trend from IWP-3B towards the stiffer IWP-5B.

Table 4.7 Thermal bowing slope of IWP

Thermal bowing slope, mm/°C							
IWP-3B		IWP-4B		IWP-4U		IWP-5B	
Heating	Cooling	Heating	Cooling	Heating	Cooling	Heating	Cooling
0.368	0.343	0.412	0.347	0.394	0.372	0.427	^a

^a – Data unavailable for the cooling phase of IWP-5B

Table 4.8 Summary of midspan deflection (bow) for different temperature differentials

Temperature differential, ΔT , °C	IWP-3B, mm	IWP-4B, mm	IWP-4U, mm	IWP-5B, mm
5	0.477	0.942	1.25	1.15
10	2.57	3.05	3.33	3.16
15	4.54	4.89	5.21	5.11
20	6.55	7.13	7.18	7.48
25	- ^a	8.86	9.15	9.55
30	- ^a	10.7	- ^a	- ^a

^a – Temperature differential not reached during these tests

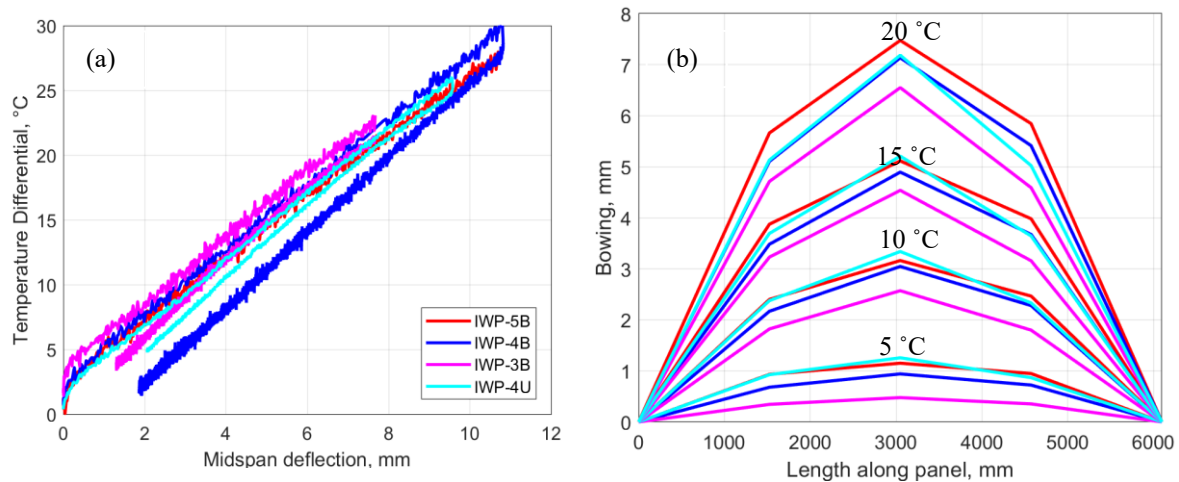


Figure 4.14 Deflections from thermal differential for (a) midspan deflection (b) bowing profile at 5 °C increments

4.7.5 Strains

Strains in the longitudinal 10M reinforcement and concrete surface were measured at midspan of all IWP and presented in Figure 4.15. This figure gives an idea of what the strain profile is like throughout the cross section of the IWP.

The cracking moment strain was calculated as $64 \mu\epsilon$ using the modulus of rupture to compare strain results. Compared to the hot wythe strain, cracking occurred on the hot wythe. This

was confirmed after the tests as cracks near midspan of the panels were noticed during visual inspections.

Table 4.9 reported the strain at five-degree increments throughout the cross section of the IWP. At ΔT of 20 °C, the strain of the hot wythe ranged from 90 $\mu\epsilon$ (IWP-3B) to 158 $\mu\epsilon$ (IWP-5B). All hot wythe rebar strains at 20°C were similar, ranging between 25 $\mu\epsilon$ for IWP-3B to 28 $\mu\epsilon$ for IWP-5B. The cold wythe at this differential showed negative (compression) strains (exception of IWP-5B). The strain readings indicated that curvature is occurring throughout the panels (Figure 4.15) which agrees with the bowing results. All strains were shown to be essentially linear with respect to ΔT , except for IWP-4U which may be caused by cracking near the strain gauge.

Table 4.9 Summary of strains on hot wythe, hot wythe rebar, and cold wythe

Temperature Difference, ΔT , °C	Strain Location	IWP-3B	IWP-4B	IWP-4U	IWP-5B
5	Hot Wythe	31	22	11	53
	Hot Rebar	17	17	-4	-1
	Cold Rebar	-2	0	-5	0
	Cold Wythe	-2	-8	-34	4
10	Hot Wythe	59	28	86	68
	Hot Rebar	19	19	16	11
	Cold Rebar	-6	-4	-5	0
	Cold Wythe	-6	-19	-2	15
15	Hot Wythe	99	77	117	112
	Hot Rebar	25	25	26	28
	Cold Rebar	-7	-6	-6	0
	Cold Wythe	-7	-37	-22	14
20	Hot Wythe	90	117	158	158
	Hot Rebar	18	18	47	47
	Cold Rebar	-5	-9	-8	-2
	Cold Wythe	^a –	-57	-26	10
25	Hot Wythe	^a –	124	186	226
	Hot Rebar	^a –	^a –	85	52
	Cold Rebar	^a –	-12	^a –	-2
	Cold Wythe	^a –	-68	-52	-7

^a – Data not available for these points

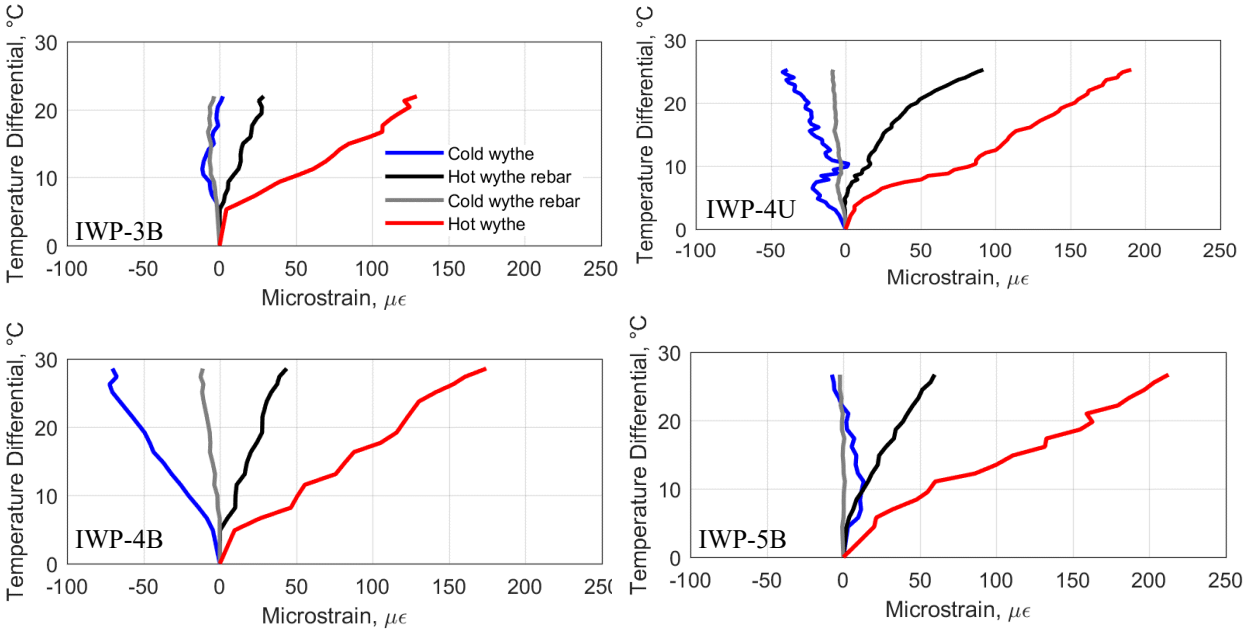


Figure 4.15 IWP midspan strain gauge on hot concrete wythe (a) IWP-3B (b) IWP-4U (c) IWP-4B (d) IWP-5B

4.7.6 Thermal Coefficient of Expansion

Two $850 \times 83 \times 160$ mm concrete beams were cast in the same batch as the IWP. One of the beams contained a WWM, and the other is plain concrete. The temperatures were measured from the hot wythe face of the IWP. Table 4.10 summarizes the strain results of all concrete gauges and reported a coefficient of thermal expansion for all the IWP and beam specimens. Using the reported strain, the thermal expansion coefficient was calculated using Equation (12).

$$\alpha = \frac{\epsilon}{\Delta T} \quad \text{Equation (12)}$$

Where ϵ is the microstrain of the hot wythe surface, and ΔT is the temperature differential. Thermal coefficient of expansion was higher for IWP ($9.0 \mu\epsilon / ^\circ\text{C}$ for IWP-5B) compared to the beams (4.2 to $4.6 \mu\epsilon / ^\circ\text{C}$). The differences resulted from temperature differential measurement, and strain resulting from curvature. The panels are subject to curvature from the thermal bowing which caused additional strain, whereas the beams were inside the enclosure and only exposed to expansion of the concrete.

Table 4.10 Summary of coefficient of thermal expansion

Specimen	Temperature Difference, °C	Strain, $\mu\epsilon$	Thermal Expansion Coefficient, $\mu\epsilon/^\circ\text{C}$
IWP-3B	23	150 ¹	6.5
IWP-4U	26	200 ¹	7.7
IWP-4B	30	150 ¹	5.0
IWP-5B	27	225 ¹	9.0
Reinforced-Beam	26	120	4.6
Plain-Beam	26	110	4.2

¹ – Strains incorporate bending from thermal bowing

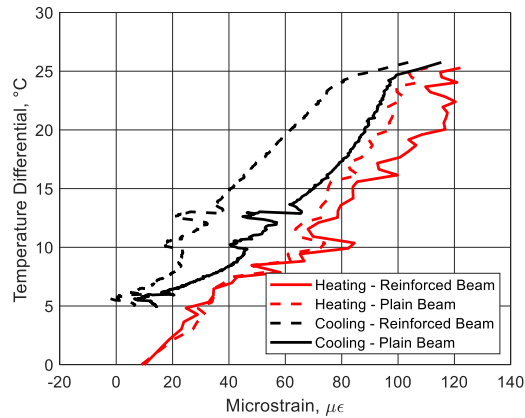


Figure 4.16 Strain at midspan for a WWM beam, and an unreinforced beam

4.7.7 Thermal Bowing Comparison

The following section compares the IWP together to understand overall trends and behaviours. End slip was discussed and used to estimate the force that transfers into the connectors. Connector force transferred into a strain, curvature, and bowing of the panel.

The slopes of the bowing profile shown in Table 4.7. Figure 4.17 indicated that bowing increased with connector stiffness (IWP-3B slope of 0.368 mm/ °C and IWP-5B slope of 0.427 mm/ °C). IWP-5B has about double the connector stiffness as IWP-3B but only had 16% more intense bowing (slope of bowing versus temperature). For comparison, the secant stiffness (found in Chapter 3) for the 5B and 3B connectors was 49.5 kN/mm and 27.1 kN/mm respectively. IWP-4U showed similar results as IWP-4B but had slightly higher deflections due to its pseudo-steady state temperature load. The slope response suggested non-linear behaviour is evident; a panel with zero connector stiffness would not be able to transfer shear and would result in only longitudinal expansion and no bowing.

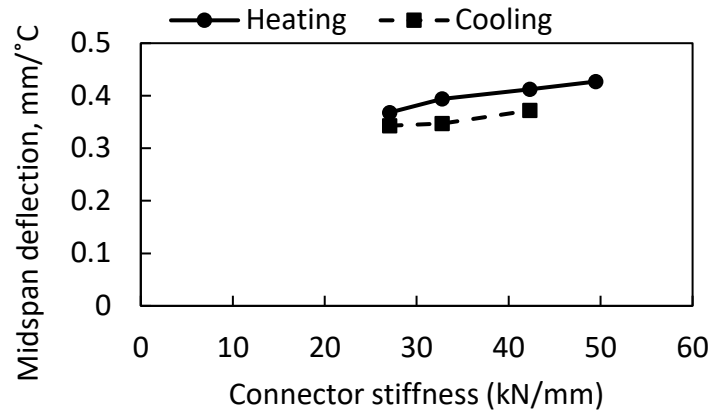


Figure 4.17 Midspan deflection with respect to connector stiffness of IWP

4.7.7.1 Total End Slip Behaviour

End slip behaviour in terms of connector stiffness is shown in Figure 4.18. IWP-3B slopes the least, however, is followed closely with IWP-4U, IWP-4B, and IWP-5B from inverse slope values (Table 4.5). Despite IWP-5B controlling behaviour in the north end slip, end slip in the less stiff connector, IWP-3B, still has more of an impact. IWP-5B showed the lowest end slip on the south end of 0.340 mm at 20°C. However, on the north end IWP-5B had considerably more end slip of 1.15 mm at 20 °C, which skewed the total end slip higher than the other IWP. Overall the less stiff panels resulted in more end slip. For comparison, IWP-3B total end slip slope was 0.087 mm/ °C, and IWP-5B was 0.079 mm/ °C, which represented a 9.2% decrease from IWP-3B to IWP-5B for the effect on end slip as stiffness doubles from IWP-3B to IWP-5B. Compared to the 16% effect on bowing, the end slip effect was approximately half in comparison. The expected end slip at zero stiffness depends on the hot wythes' coefficient of expansion. The slope of the end slip behaviour would be expected to be more linear compared to the non-linear behaviour the bowing showed.

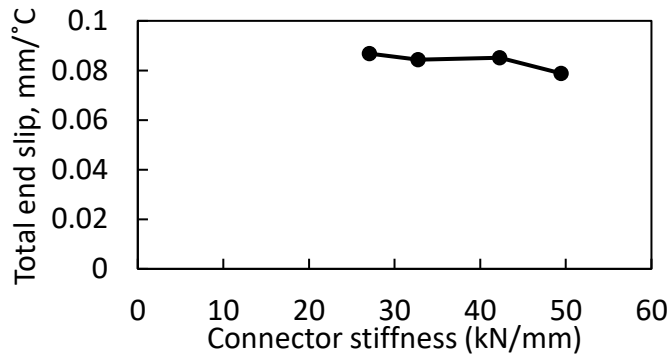


Figure 4.18 End slip with respect to connector stiffness of IWP

4.7.7.2 Stiffness Behaviour

The total stiffness for the panels was calculated by isolating the panel into “north” and “south” end slips. To estimate the forces carried by the connectors, a linear relation of the degree of end slip was assumed from midspan of the panel to the end. Previous work (Naito et al, 2012; Bai and Davidson, 2016) utilized a parabolic shape that closely matches a linear shape. For each connector, a percentage of end slip is assumed based on its location, shown in Figure 4.2. This estimated slip at each connector location was then used to interpolate forces (Figure 4.19) induced in the connectors at that slip using the average push-through results from Chapter 3 (Figure 3.7). Note that the forces from Chapter 3 (Figure 3.7) was divided by two as the push-through specimens were for two sets of shear connectors. Once the force was found, a secant was taken by dividing the force with the end slip at its north or south end. The total stiffness reported is the sum of the results from all connectors along the panel.

Figure 4.20 reported the stiffness of all IWP with respect to its end slip and midspan deflection. The stiffness of IWP-5B decreased 34% over a 20 °C increment (1017 to 682 kN/mm), whereas other connectors maintained their stiffness. The loss of stiffness was a result of the low proportional limit of 5B compared to the other connectors. Based on this result, using 5B connectors in this form may be inadvisable given the cyclic nature of temperature loads.

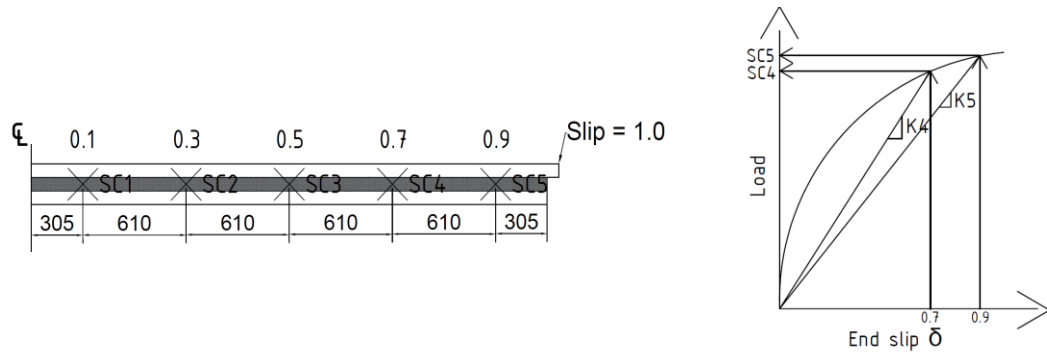


Figure 4.19 Retrieving force and stiffness, K , of each shear connector using total end slip

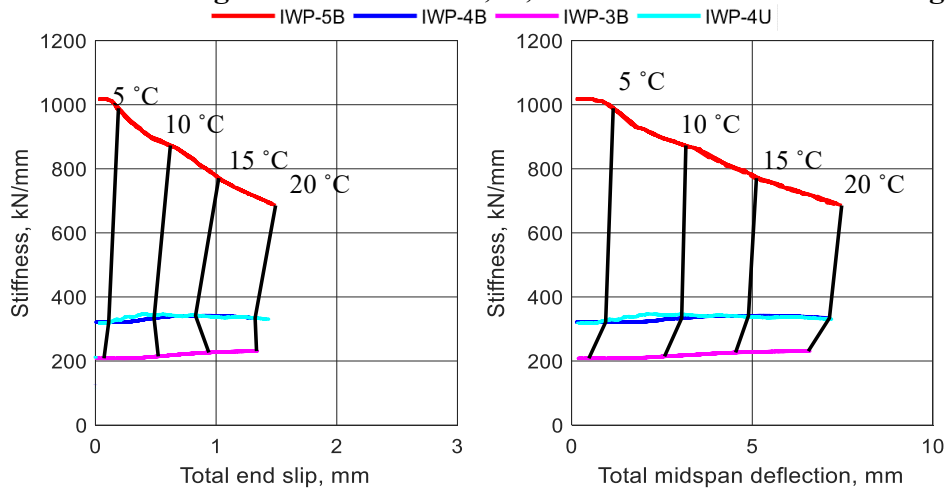


Figure 4.20 End slip and midspan deflection with respect to stiffness up to ΔT 20 °C

4.8 Force on Shear Connectors

The estimated force demand on the shear connectors is examined in this section. Thermal expansion of the concrete causes the concrete in the hot wythe to expand when it is heated, resulting in slip between the two wythes (accumulating from zero at midspan to greatest at their end). As connectors resisted slip, the force passes through the connectors into the cold wythe (see Figure 4.2). This transfer creates curvature and thus bowing depending on the connector stiffness.

The results of forces carried by the shear connectors to resist thermal bowing is shown in Figure 4.21. The trend showed more non-linear behaviour as stiffness increases. The residual forces of IWP-3B and IWP-5B were a result of these panels being exposed to an initial heating cycle prior to their test being recorded. Forces at ΔT of 20 °C for IWP-3B, IWP-4B, IWP-4U, and

IWP-5B was 18 kN, 26 kN, 27 kN, and 33 kN respectively. These values were above the proportional limit but less than the peak load. Based on this, the connectors at high temperature loads are subject to non-linear behaviour and deformations, as seen in end slip deformations (Figure 4.11). For design, it is more efficient to use connectors that are 12.7 mm in diameter or less to maintain elasticity of connectors when considering the cyclic nature of temperature loads for exterior IWP.

Figure 4.22 shows the estimated total force when all connector contributions are summed. The total longitudinal shear demand in the connectors increased 128% from IWP-3B (80 kN) to IWP-5B (182 kN) at a temperature differential of 20 °C. This indicates that a significant increase in internal forces developed as connector stiffness increased from IWP-3B to IWP-5B.

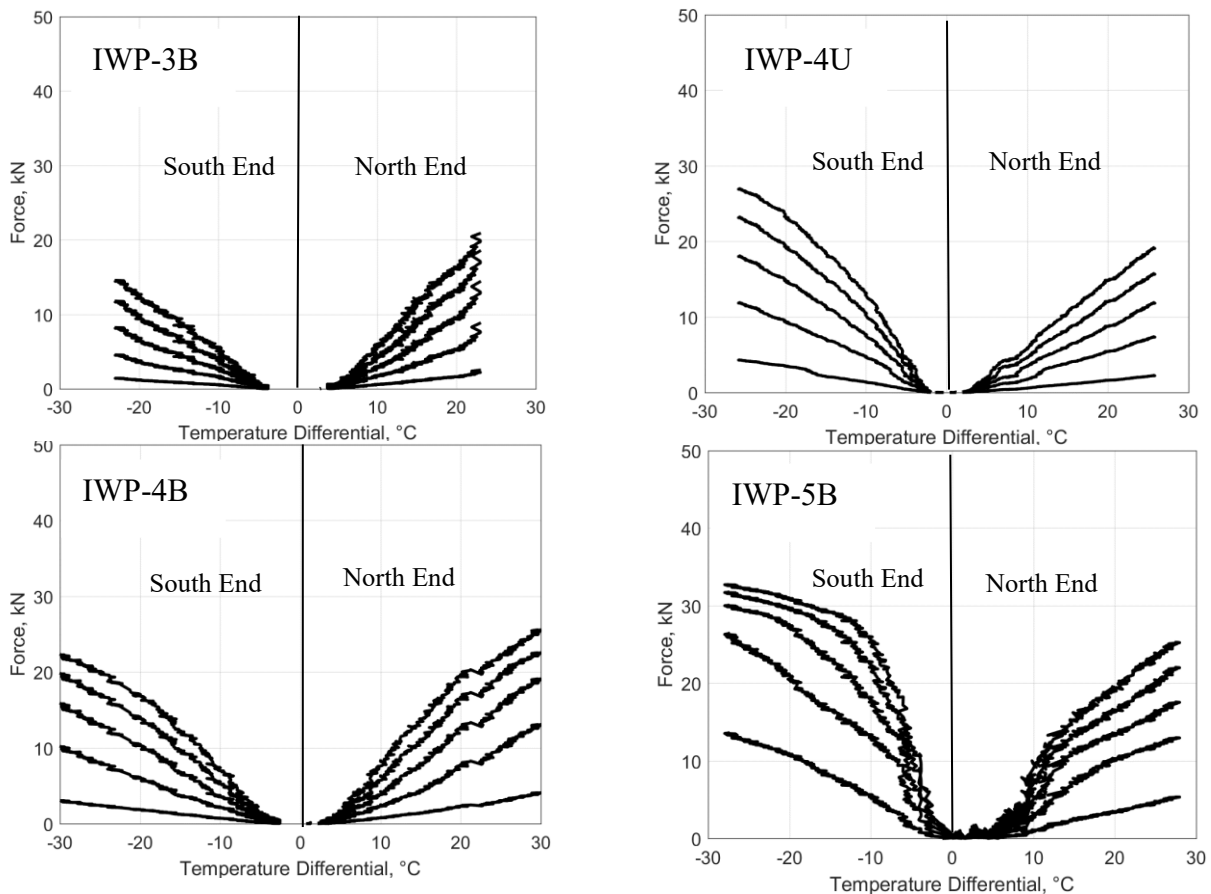


Figure 4.21 Estimated shear connector force on north side and south side of panel

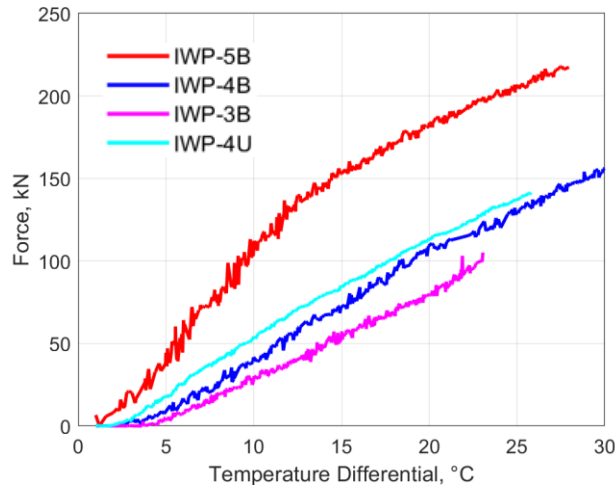


Figure 4.22 Total estimated shear connector force with temperature differential

The maximum thermal load of IWP-5B reached 218 kN. This load is considerably higher than 10.4 kN expected demand from the maximum factored wind load (2.9 kPa) from the National Building Code of Canada. However the maximum thermal load is comparable to typical service axial load ranges of 150 kN to 300 kN for load bearing panels of this width (Tomlinson, 2015). The thermal load put into the connectors for stiffer (i.e. 5B) panels may be a design concern since it may cause earlier than expected connector failure in load-bearing panels.

4.9 Limitations of Results

The following are considerations to be made when discussing the results:

1. In this study a simply-supported panel free to rotate at its ends was used, however in a realistic panel there will be some degree of fixity to consider. For instance, a fixed-fixed support has more resistance to end slip, but also resists the bowing. This causes additional stresses to be applied at the support and would affect how forces flow through the connectors. In the case of this experiment, the steel bearing supports and ball bearings are not frictionless and slight variations in supports led to slight fluctuations in panel response.
2. Humidity is a factor that contributes towards bowing of panels. A humidity sensor was used to measure the humidity in the laboratory but having a second sensor inside the

thermal enclosure is recommended to find relative humidity of the IWP wythe faces. Controlling humidity is best done with an environmental chamber but this was not available for this project.

3. Transient temperature control was important. Appendix C shows the temperature throughout the heating and cooling phase of all the IWP. These plots showed the panels transient heating phase. These profiles were similar in IWP-3B, IWP-4B, and IWP-5B but IWP-4U had a more severe thermal load that resulted from pseudo-steady state heating. Furthermore, between $\Delta T = 0$ °C and 5 °C, thermocouples showed an initial thermal lag through the concrete before it reached the transient temperature conditions experienced during the rest of the heating phase. This period consisted of variable amounts of slip and deflection for all IWP. To account for this when discussing bowing, the slope (bowing and end slip) was calculated after this initial phase.
4. Human error was another factor to consider. In this case it came from the fabrication of the panels as the thickness of the wythes were not perfectly 75 mm (3"). As they were cast vertically, sections along the length of the panel have slightly reduced or enlarged wythe thickness which impacted the longitudinal shear stiffness of the panel. This change in cross sectional area led to areas where concrete was thin and able to "hug" the insulation. This caused a pinching effect with the reinforcement, which can lead to insulation stiffness increase compared to that in the push through tests.

4.10 Chapter Conclusion

This chapter discussed the effect of inducing a thermal differential on four panels with varying connector stiffness. A thermal enclosure was constructed to heat up one face of the panels to

temperature differential of up to 20°C. Thermocouples, LVDT, and strain gauges were installed to investigate slip, thermal bowing, and strains. The following results are concluded:

1. Higher end slip was observed with panels of low stiffness. The inverse slope of temperature-slip showed a 9.2% decrease from IWP-3B to IWP-5B. Based on this, stiffer connectors are more efficient in resisting end slip; however, this come at the cost of losing elasticity in using higher size connectors (i.e. IWP-5B).
2. Thermal bowing increased with shear connection stiffness. There was a 16% increase from IWP-3B to IWP-5B for the effect of thermal bowing. This indicated stiffer connectors transfer the resistance of end slip, into a force that causes bowing. Considerations should be made on choosing stiffer connectors regarding allowable deflections as the stiffer connector (IWP-5B) was subjected to loads past the proportional limit.
3. Thermal loads induced significant loads to cause non-linear deformations in connectors. The loads showed a 65% increase from IWP-3B (20 kN) to IWP-5B (30 kN) connectors. These loads are past the proportional limit and resulted in permanent deformations of the connectors. Total longitudinal shear demand in the connectors ranged from 80 kN to 182 kN for IWP-3B and IWP-5B. In the case of IWP-5B, maximum thermal loads of 218 kN are significant and may cause premature connector failure if not accounted for in load-bearing panels.
4. Strains values on the surface of the hot wythe ranged from 90 $\mu\epsilon$ (IWP-3B) to 158 $\mu\epsilon$ (IWP-5B) at a temperature differential of 20°C. This strain was high enough to cause cracking of the wythes (confirmed with visual inspection at midspan of the hot wythe). Strains also confirmed presence of curvature through cross-sectional strain profile of cold wythe, cold rebar, hot rebar, and hot wythe.

4.11 Recommendations

Several recommendations are made based on the results of this Chapter:

1. Panels with smaller and larger connectors should be tested to confirm if the diminishing effect of bowing with varying stiffness is observed. IWP that have lower connection stiffness would expect to see less bowing, and in theory no bowing at zero stiffness. This trend predicts non-linear behaviour but requires more experimentation.
2. Use of an environmental chamber. This will limit results such as IWP-4U, where there was a pseudo-steady state temperature load induced, whereas other panels saw transient temperature response. As humidity differences from the faces of the IWP effect bowing, sensors to measure humidity inside and outside the chamber are recommended in future tests.
3. Cycling the load over a similar temperature differential. This will allow the effect of the connectors proportional limit and bowing to be understood better. It was found higher connector panels have considerably low proportional limit, which led to quicker loss of stiffness (i.e case of IWP-5B). As temperature is a cyclic load, this would be more representative of what panels would face in real systems.

5. SUMMARY AND CONCLUSIONS

This chapter provides a summary, conclusion, and recommendation from the experimental investigation of push-through specimens, and thermal bowing of several IWP.

5.1 Summary

Chapter 2 presented a literature review of insulated wall panels. Chapter 3 discussed details on the connectors used in thermal testing. Three connector sizes (9.5, 12.7, and 16.0 mm) and debonding effects are investigated through push-through testing. Factors such as proportional limit, peak loads, stiffness, and deformability were observed. Chapter 4 presents results and discussion of an experimental program that investigated the thermal bowing of IWP. A thermal enclosure was built to induce a temperature differential onto four panels of varying stiffness (Chapter 3 different bar diameters). The end slip, thermal bowing, strains, and resulting forces on connectors were discussed.

5.2 Conclusions

Several conclusions are made regarding the thermal bowing for panels with varying stiffness. The following conclusions are drawn from the experiments:

1. A literature review on the state of IWP, shear connectors, and previous thermal experimentation was provided in Chapter 2. This accomplished Task 1 of the research objective.
2. Chapter 3 provided an experimental investigation on evaluating the stiffness of GFRP connectors with push-through tests. The bonded specimen stiffness increased 56% (42.8 kN/mm) from 3B to 4B and increased 60 % (29.5 kN/mm) from 4B to 5B. For unbonded specimens, stiffness increased 17% (14.1 kN/mm) from 3U to 4U and increased 20% (25.1 kN/mm) from 4U to 5U. This chapter completed Task 2 of the research objective.

3. Four IWP were constructed using connectors from Chapter 3. The varied connector size allowed a comparison of thermal bowing for different panel stiffness. Furthermore, a thermal enclosure was constructed to investigate IWP bowing under temperature differentials up to 30° C. The enclosure's purpose was to create a temperature differential by heating one wythe ('hot wythe') while leaving the other exposed to lab ambient temperature ('cold wythe'). The fabrication is discussed in more detail in Chapter 4. This accomplished Task 3 and 4 of the research objective.
4. As the stiffness of the panel increases, the midspan deflection of the panel increases. The more composite IWP (IWP-5B) panels showed 16% more thermal bowing compared to the less composite panels (IWP-3B) from the results.

Conversely, the less shear connection stiffness a panel has, the more the end slip of the panel increases. The IWP with less stiffness and closer to non-composite behaviour showed behaviour that is controlled more by end slip than midspan. The end slip effect from IWP-3B to IWP-5B decreased by 9.2%. The shear connectors have less of an influence to resist the end slip.

In terms of stiffness, both total end slip and bowing show the panel with stiffest connector (IWP-5B) subject to non-linear behaviour. This led to a decrease of stiffness much quicker compared to the other connectors. This accomplished Task 5 of the research objective.

5. Thermal loads caused a 65% increase for IWP-3B (20 kN) to IWP-5B (30 kN). The loads surpassed the proportional limit found in Chapter 3, and in the case of IWP-5B led to permanent deformations. Total shear demand in the connectors ranged from 80 kN to 182

kN for IWP-3B and IWP-5B respectively. This accomplished *Task 6* of the research objective.

Overall, this thesis introduced experimentally evaluating the thermal bowing behaviour of IWP with varying shear connector stiffness. Trends such as positive correlation of bowing with stiffness were observed; however, with only four full-scale specimens there is still more experimentation to be done. The results indicate that thermal bowing can be significant in these types of panels. Bowing resulted in up to 63% of the acceptable service load deflections and about 72% of the expected load-bearing axial service loads on the connectors. The interaction between connection stiffness and bowing seems to be non-linear, but additional experimentation is required to confirm.

As a designer, considerations should be made towards the selection of connector stiffness. The advantage of using higher stiffness connector (i.e. more composite) in IWP is a higher wall strength as load-bearing members, and potential cost savings since thinner wythes may be used to resist the same load demands as a lower stiffness IWP. However, this comes at the disadvantage of increased thermal bowing, and in cases where out-of-plane deflections are critical, this should be considered. Another concern is that the shear connectors may exceed their proportional limit load due to their higher stiffness. In particular for this study, for connectors with stiffness similar to 5B, temperature differentials of 25° C were enough to subject these into non-linear behaviour, resulting in inefficiency of the connector system.

5.3 Recommendation for Future Work

This experimental program studied the effect of thermal bowing for various stiffnesses of IWP. As it is the initial work of more studies to come, there are several recommendations for future work that are based on the outcomes of this thesis.

1. Testing the panels under several thermal cycles. The cyclic temperature testing of the panels will represent what a typical IWP would go through weather cycles.
2. Construction of an environmental chamber. Performing the test under strict humidity conditions. Having an environmental chamber that can control humidity may be of use for controlling parameters effecting thermal bowing. Stricter control over the heat flow can also help reduce impact from transient to pseudo-steady state heating (i.e. IWP-3B, 4B, 5B vs IWP-4U).
3. Changing the end conditions of the panel to represent typical support conditions of panels used in industry to understand the effect of support conditions on thermal bowing.
4. Performing experiments with shear connectors of different stiffness. In particular, it may be of use to examine if the thermal bowing becomes less drastic with specimens less-stiff than IWP-3B. This thesis looked at connectors on the stiffer side compared to others in the literature. Panels with less shear connection stiffness would help identify trends such as the non-linear bowing behaviour with respect to stiffness that is suspected based on these results.
5. Cycling the push-through tests under slips similar to those seen in the thermal tests would better show the impact of exceeding the proportional limit on the connectors (e.g. is there permanent deformation). This will show if certain connection systems are more subject to loss of stiffness.

References

- Abid, S.R. 2018. Three-dimensional finite element temperature gradient analysis in concrete bridge girders subjected to environmental thermal loads. *Cogent Engineering*, 5(1). Cogent. doi:10.1080/23311916.2018.1447223.
- ASHRAE 90.1 - Energy Standard for Buildings Except Low-Rise Residential Buildings. (2010). American Society of Heating, Refrigerating and Air-Conditioning Engineers, Atlanta.
- ASHRAE. (2001). 2001 ASHRAE handbook : fundamentals. American Society of Heating, Refrigerating and Air-Conditioning Engineers, Inc., Atlanta, GA.
- ASTM C1611 / C1611M-18, Standard Test Method for Slump Flow of Self-Consolidating Concrete, ASTM International, West Conshohocken, PA, 2018
- ASTM C39. Standard test method for compressive strength of cylindrical concrete specimens, 2001.
- ASTM. (2011). “Standard test method for tensile properties of fiber reinforced polymer matrix.” ASTM D7205/D7205M-06, West Conshohocken, PA.
- Bai, F., and Davidson, J.S. 2016. Theory for composite sandwich structures with unsymmetrical wythes and transverse interaction. *Engineering Structures*, 116: 178–191. Elsevier Ltd. doi:10.1016/j.engstruct.2016.02.052.
- Benmokrane, B., et al. (2014). “Characterization and Comparative Durability Study of Glass / Vinylester , Basalt / Vinylester , and Basalt / Epoxy FRP Bars.” *Journal of Composites for Construction*. 10.1061/(ASCE)CC.1943-5614.0000564, 1–12.
- Choi KB, Choi WC, Feo L, Jang SJ, Yun HD. 2015. In-plane shear behavior of insulated precast concrete sandwich panels reinforced with corrugated GFRP shear connectors. *Composites Part B: Engineering*. 2015 Sep 15;79:419-29.

- Cuddihy, J., Kennedy, C., and Byer, P. 2005. Energy use in Canada: environmental impacts and opportunities in relationship to infrastructure systems. *Canadian Journal of Civil Engineering*, 32(1): 1–15. doi:10.1139/104-100.
- Destrebecq, J.F., Toussaint, E., and Ferrier, E. 2011. Analysis of Cracks and Deformations in a Full Scale Reinforced Concrete Beam Using a Digital Image Correlation Technique. *Experimental Mechanics*, 51(6): 879–890. doi:10.1007/s11340-010-9384-9.
- Dutton, M. 2012. Digital image correlation for evaluating structural engineering materials. doi:10.1016/S1369-7021(10)70235-2.
- Einea, A.; Salmon, D.C.; Tadros, M.K.; and Culp, T. (1994). “A New Structurally and Thermally Efficient Precast Sandwich Panel System,” *PCI Journal*, 39(4), 90-101.
- Ekenel, M. (2013). “Testing and Acceptance Criteria for Fiber-Reinforced Composite Grid Connectors Used in Concrete Sandwich Panels.” *Journal of Materials in Civil Engineering*, 0899-1561/06014004(5),1-5.
- Frankl, B. (2008). “Structural Behavior of Insulated Precast Prestressed Concrete Sandwich Panels Reinforced with CFRP Grid,” MSc Thesis, University of North Carolina, Raleigh, United States of America.
- Frankl, B.A., Lucier, G.W., Hassan, T.K., and Rizkalla, S.H. 2011. Behavior of precast, prestressed concrete sandwich wall panels reinforced with CFRP shear grid. *PCI journal*, 56(2): 42–54. doi:10.15554/pcij.03012011.42.54.
- Freeman, W. T., and Kuebler, G. C. (1974). "Mechanical and Physical Properties of Advanced Composites." *Composite Materials Testing and Design (Third Conference)*, ASTM STP 546, American Society for Testing and Materials, Williamsburg, VA, 435-456.
- Gleich, H. a. 2007. New Carbon Fiber Reinforcement Advances Sandwich Wall Panels. Product

- Watch, (April): 61–63.
- Gombeda, M.J., Trasborg, P., Naito, C.J., and Quiel, S.E. 2017. Simplified model for partially-composite precast concrete insulated wall panels subjected to lateral loading. *Engineering Structures*, 138: 367–380. Elsevier Ltd. doi:10.1016/j.engstruct.2017.01.065.
- Goudarzi N, Korany Y, Adeeb S, Cheng R. 2016. Characterization of the shear behavior of Z-shaped steel plate connectors used in insulated concrete panels. *PCI Journal*. 2016 Mar 1;61(2).
- Hassan, T.K., and Rizkalla, S.H. 2010. Analysis and design guidelines of precast , prestressed concrete , sandwich wall panels reinforced with CFRP grid. *PCI Journal*, Spring: 147–162.
- Hodicky, K., et al. (2014). “Experimental and Numerical Investigation of the FRP Shear Mechanism
- Kada, H. 2001. Determination of the coefficient of thermal expansion of high performance concrete from initial setting. *Materials and Structures*, 35(245): 35–41. doi:10.1617/13684.
- Kim, J., and You, Y.-C. (2015). “Composite Behavior of a Novel Insulated Concrete Sandwich Wall Panel Reinforced with GFRP Shear Grids: Effects of Insulation Types.” *Materials*, 8, 899–913.
- Kim, Y.J., and Allard, A. 2014. Thermal response of precast concrete sandwich walls with various steel connectors for architectural buildings in cold regions. *Energy and Buildings*, 80: 137–148. Elsevier B.V. doi:10.1016/j.enbuild.2014.05.022.
- Leabu, B. V. F. (1965). “Precast Concrete Wall Panels : Design Trends and Standards.” *ACI Special Publication*, 11, 31–44.
- Lecompte, D., Vantomme, J., and Sol, H. 2006. Crack Detection in a Concrete Beam using Two Different Camera Techniques. *Structural Health Monitoring*, 5(1): 59–68.

doi:10.1177/1475921706057982.

- Lee, B.-J., and Pessiki, S. (2004). “Analytical Investigation of Thermal Performance of Precast Concrete Three-Wythe Sandwich Wall Panels.” *PCI journal*, 49(4), 88–101.
- Lee, B.-J., and Pessiki, S. (2006a). “Thermal Behavior of Precast Prestressed Concrete Three-Wythe Sandwich Wall Panels.” *Building Integration Solutions*, American Society of Civil Engineers, Reston, VA, 1–15.
- Lee, B.-J., and Pessiki, S. (2006b). “Thermal Performance Evaluation of Precast Concrete Three-Wythe Sandwich Wall Panels.” *Energy and Buildings*, 38(8), 1006–1014.
- Lee, B.-J., and Pessiki, S. (2008). “Revised Zone Method R-Value Calculation for Precast Concrete Sandwich Panels Containing Metal Wythe Connectors.” *PCI Journal*, 53(5), 86–100.
- Leung, A. (1984). “Structural Design and Analysis of Concrete Sandwich Panels and their Practical Application.” M.Eng Thesis, Memorial University of Newfoundland, St. John’s, Canada.
- Losch, B.E. 2005. M.E. (April): 16–20.
- Losch, E. 2003. Bowing of Insulated Precast Concrete Wall Panels. *PCI Journal*, (November-December).
- Mallick, P. K. (2007). *Fiber-Reinforced Composites: Materials, Manufacture, and Design*. CRC Press, Boca Raton, FL.
- Mathieson, H. A. (2015). “Behavior of Sandwich Panels Subjected to Bending Fatigue, Axial Compression Loading, and In-Plane Bending.” Ph.D Thesis, Queen’s University, Kingston, Canada.
- McCall, W. C. (1985). “Thermal Properties of Sandwich Panels.” *Concrete International*, 7(1), pp. 35-41.

Naito, C., Hoemann, J., Beacraft, M., and Bewick, B. (2012). "Performance and Characterization of Shear Ties for Use in Insulated Precast Concrete Sandwich Wall Panels." *Journal of Structural Engineering*, 138(1), 52–61.

National Research Council of Canada. 2005. *National Building Code of Canada*. NBCC-2005. Ottawa, ON, Canada: National Research Council of Canada.

NRCan. (2016). *Energy Fact Book 2016 – 2017*. Office of Energy Efficiency, National Resources Canada, Ottawa, Ontario.

NECB 2011. (2011). "National Energy Code of Canada for Buildings 2011." Canadian Commission on Building and Fire Codes, National Research Council Canada, Ottawa, Ontario.

PCI Industry Handbook Committee (2010). "PCI Design Handbook – Precast and Prestressed Concrete, Seventh Edition." Precast/Prestressed Concrete Institute, Chicago, Illinois.

PCI Committee on Precast Concrete Sandwich Panels. 2011. State of the Art of Precast / Prestressed Concrete Sandwich Wall Panels. *PCI Journal*, 56(2): 131–176.

Pessiki, S., and Mlynarczyk, A. (2003). "Experimental Evaluation of the Composite Behavior of Precast Concrete Sandwich Wall Panels." *PCI Journal*, 48(2), 54–71.

Post, A.W. 2006. Thermal and fatigue Testing of Fiber Reinforced Polymer Tie Connectors used in Concrete Sandwich Walls.

Robert, M., and Benmokrane, B. 2010. Behaviour of GFRP reinforcing bars subjected to extreme temperatures. *Journal of Composites for Construction*, 14(4): 353–360.
doi:10.1061/(ASCE)CC.1943-5614.0000092.

- Rudd, D, 2017. A comprehensive review on the state of shear connector behaviour. University of Alberta (Edmonton, Alberta).
- Sakyi-Bekoe, K. 2008. Assessment of the Coefficient of Thermal Expansion of Alabama Concrete. : 213.
- Salmon, D.C.; Einea, A.; Tadros, M.K.; and Culp, T.D. (1997). “Full Scale Testing of Precast Concrete Sandwich Panels,” *ACI Structural Journal*, 94(4), 354-362.
- Sauter, J. E. (1991). “Insulated Concrete Sandwich Walls.” *Exterior Wall Systems: Glass and Concrete Technology, Design, and Construction*, ASTM STP1034, B. Donaldson, Ed., American Society for Testing and Materials, Philadelphia, Pennsylvania, pp. 170-186.
- Shi, J. W., Zhu, H., Wu, Z. S., and Wu, G. (2011). “Durability of BFRP and Hybrid FRP Sheets under Freeze-Thaw Cycling.” *Advanced Materials Research*, 163-167, 3297–3300.
- Sim, J., Park, C., and Moon, D. Y. (2005). “Characteristics of basalt fiber as a strengthening material for concrete structures.” *Composites Part B: Engineering*, 36(6-7), 504–512.
- Teixeira N, Fam A. Fatigue Behavior of Partially Composite-Insulated Concrete Sandwich Walls. *ACI Structural Journal*. 2017 Jan 1;114(1):125.
- Tomlinson, D., and Fam, A. (2014a). “Experimental investigation of precast concrete insulated sandwich panels with glass fiber-reinforced polymer shear connectors.” *ACI Struct. J.*, 111(3), 595–606.
- Tomlinson, D., and Fam, A. (2014b). “Performance of concrete beams reinforced with basalt FRP for flexure and shear.” *J. Compos. Constr.*, 10.1061/(ASCE)CC.1943-5614.0000491, 04014036.
- Tomlinson, D., and Fam, A. 2016a. Combined Loading Behavior of Basalt FRP–Reinforced Precast Concrete Insulated Partially-Composite Walls. *Journal of Composites for*

- Construction, 20(3): 4015060. doi:10.1061/(ASCE)CC.1943-5614.0000611.
- Tomlinson, D., and Fam, A. 2016b. Analytical approach to flexural response of partially composite insulated concrete sandwich walls used for cladding. *Engineering Structures*, 122: 251–266. Elsevier Ltd. doi:10.1016/j.engstruct.2016.04.059.
- Tomlinson, D.G., Teixeira, N., and Fam, A. 2016. New Shear Connector Design for Insulated Concrete Sandwich Panels Using Basalt Fiber-Reinforced Polymer Bars. *Journal of Composites for Construction*, 20(4): 1–13. doi:10.1061/(ASCE)CC.1943-5614.0000662.
- Tomlinson, D. 2015. Behaviour of partially composite precast concrete sandwich panels under flexural and axial loads.
- Van Geem, M. G., and Shirley, S. T. (1987). "Heat Transfer Characteristics of Insulated Concrete Sandwich Panel Walls." Rep. No. ORNL/Sub-79-42539/8, Oak Ridge National Laboratory, Oak Ridge, TN.
- White, D.J., Take, W.A., and Bolton, M.D. (2003), "Soil deformation using particle image velocimetry (PIV) and photogrammetry," *Géotechnique*, 53(7), 619-631.
- Woltman, G. 2014. Structural and Steady-State Thermal Experimental Investigations of an Insulated Sandwich Panel.
- Woltman, G., Noel, M., and Fam, A. 2017. Experimental and numerical investigations of thermal properties of insulated concrete sandwich panels with fiberglass shear connectors. *Energy and Buildings*, 145: 22–31. Elsevier B.V. doi:10.1016/j.enbuild.2017.04.007.
- Woltman, G., Tomlinson, D., and Fam, A. 2013. Investigation of Various GFRP Shear Connectors for Insulated Precast Concrete Sandwich Wall Panels. *Journal of Composites for Construction*, 17(5): 711–721. doi:10.1061/(ASCE)CC.1943-5614.0000373.

Xia, J., Xi, Y., and Jin, W. 2017. Temperature-Dependent Coefficient of Thermal Expansion of Concrete in Freezing Process. 143(8): 1–8. doi:10.1061/(ASCE)EM.1943-7889.0001256.

Appendix A – Formwork and Specimen Construction Process



Figure A.1 Push-through formwork

Plywood of 19 mm (3/4 in) thickness is cut and then assembled into formwork for push-through samples. Three push-through formwork were created that contained six samples each for a total of eighteen push-through specimens.



Figure A.2 Push-through specimen preparation

Each push-through specimen is prepared with chairs (National Concrete Accessories, 38.1 mm, 1.5”) holding in place minimum WWM reinforcement. Pilot holes were drilled were 1/8th inch (3

mm) diameter less than the connector at 45° through the foam. GFRP shear connectors were then inserted to create an “X” shape. The same process was used for the full scale IWP.



Figure A.3 Formwork preparation

Prior to pouring, the formwork was prepared in a space that allows worker access on all sides. Two longitudinal two-by-four pieces are placed and screwed on top to prevent insulation from displacing upwards during pour.



Figure A.4 Formwork preparation of IWP

A similar process is followed for the IWP. Two pieces of formwork were created that contained two walls each. The insulation, WWM, and shear connectors were assembled in one piece and then craned into the formwork. Vertical chairs were used to keep the concrete thickness consistent throughout the formwork for the concrete pour. Lateral braces are placed every 610 mm (2 ft) to maintain proper straightness of the wall and resist lateral pressure from the concrete.



Figure A.5 Formwork preparation

Two-by-fours are placed along the top of the wall at 1220 mm (4 ft) spacing to prevent insulation from displacing up during pour. The ends of the IWP were capped off with 19 mm (0.75 in) plywood.



Figure A.6 Concrete pour

One mix (volume of 3.5 m^3) of 40 MPa concrete was ordered for all the IWP and push-through specimens. Care was ensured to place the concrete evenly (filling both wythes at the same rate) throughout the pour. Thirty cylinders for compressive testing and two beams for coefficient of thermal expansion tests were also cast.



Figure A.7 Finishing

After pouring the concrete, trowels were used to finish off the concrete. Since a self-consolidating mixture was used, no vibrators were required to consolidate the concrete.



Figure A.8 Specimens immediately before curing (a) push through formwork (b) full panel formwork

The specimens were left to cure for a minimum of 28 days under lab conditions. Water was added on top of the concrete for 10 days following the pour to facilitate the curing process. During this process, a vapour barrier was placed on top to maintain as much moisture in the specimen.

Appendix B – Push-through specimen load and stiffness plots

Figure B.1 shows the load deflection curves, and Figure B.2 shows the stiffness plots of all 18 push-through specimens from a deflection of 0 mm to 1 mm. The plots are separate into three top, centre, and bottom rows showing the #3, #4, and the #5 bar diameter specimens respectively. The left side of the subplots show the bond load deflection response, and the right subplots show the unbonded load deflection response. The LVDT and the DIC curves are shown as black and red respectively. It can be noted that as the bar diameter increases, the variability in the stiffness becomes greater. The #3 bar stiffness show narrower ranges as compared to the #4 #5 bar. The DIC data also consistently reports a lower stiffness value compared to the LVDT data for all plots.

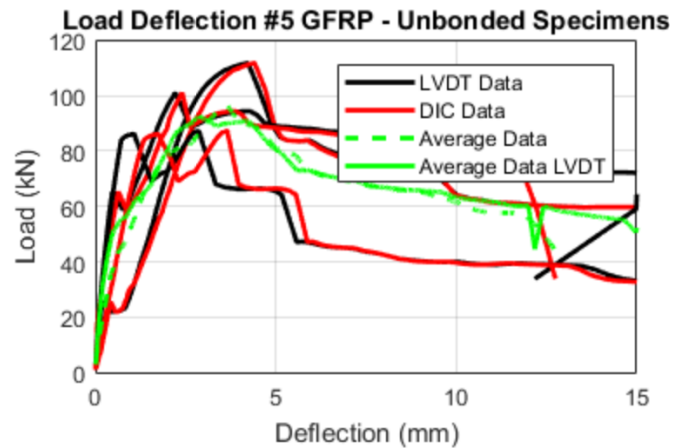
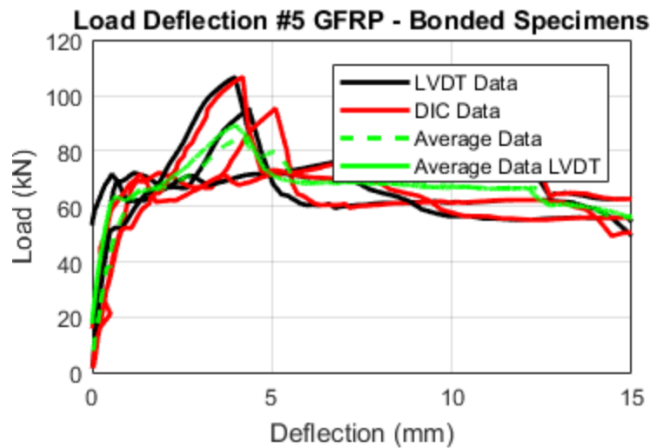
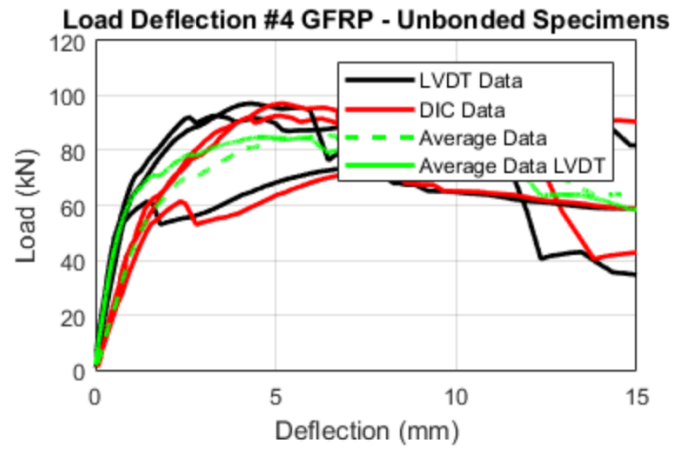
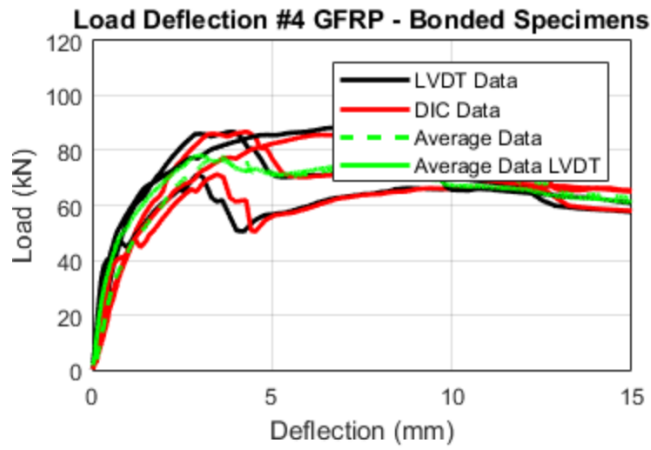
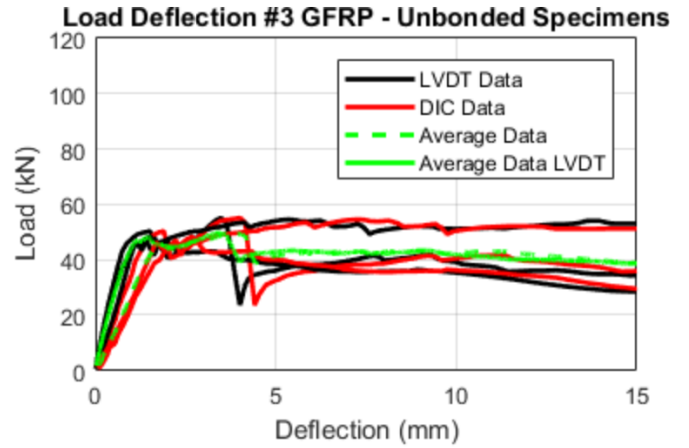
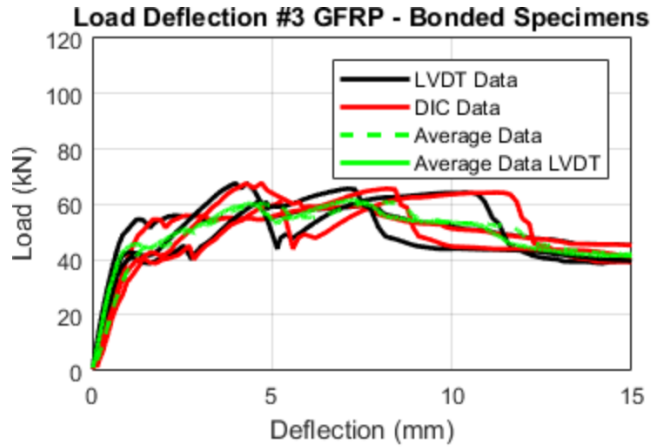


Figure B.1 Push-through test summary of 18 specimens

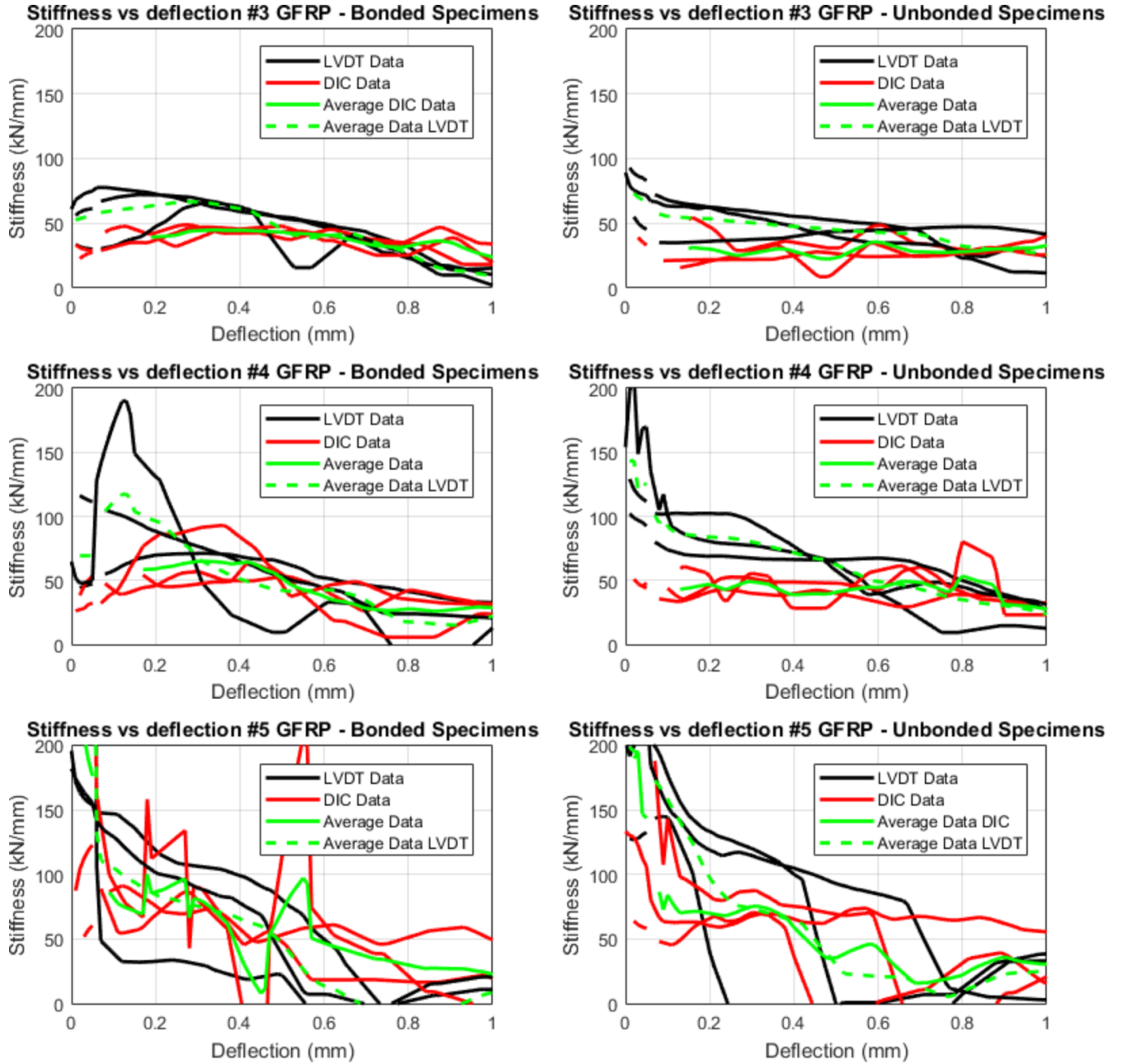


Figure B.2 Stiffness overview of all 18 push-through specimens

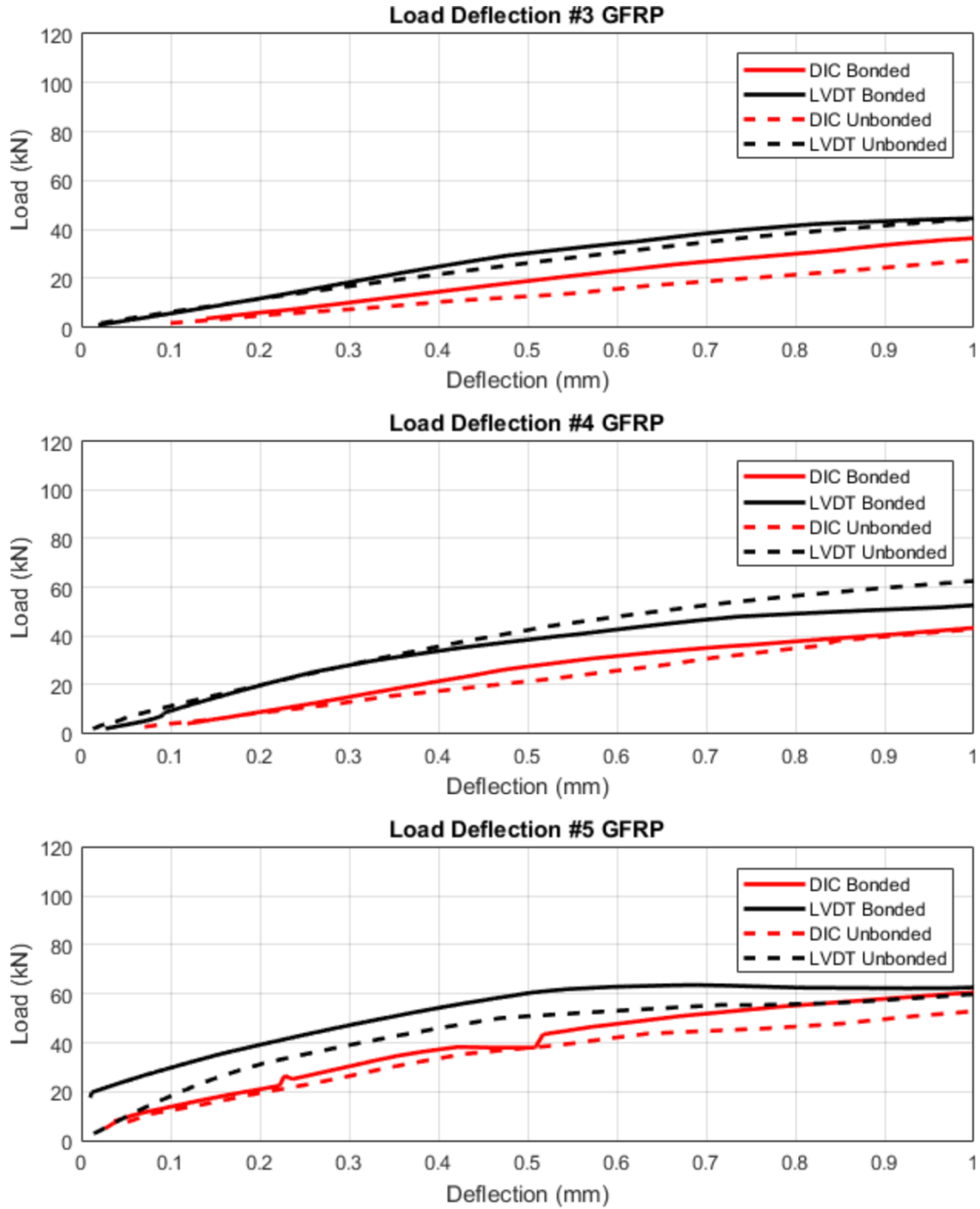


Figure B.3 Push-through average load deflection curves through 1 mm of deflection

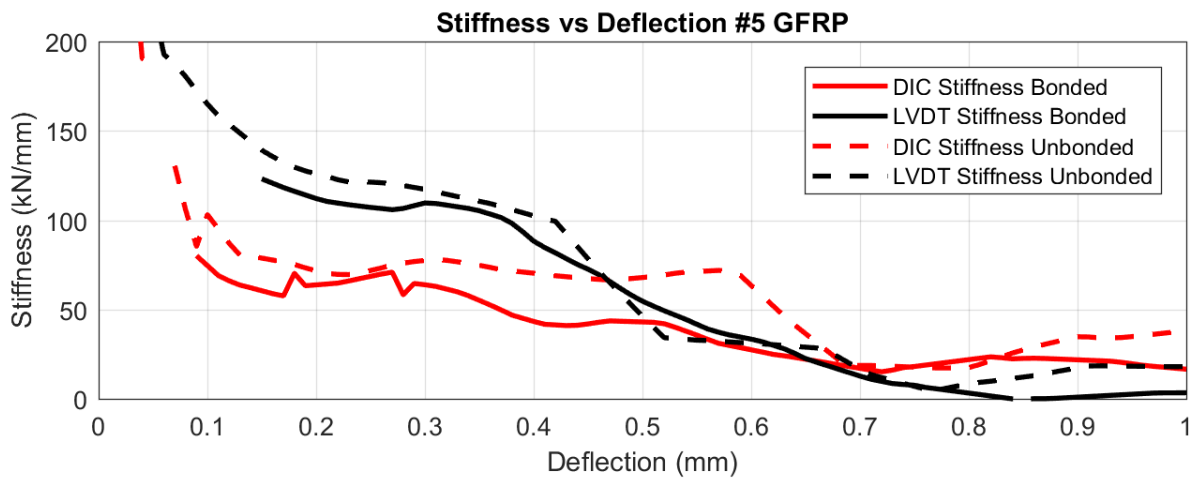
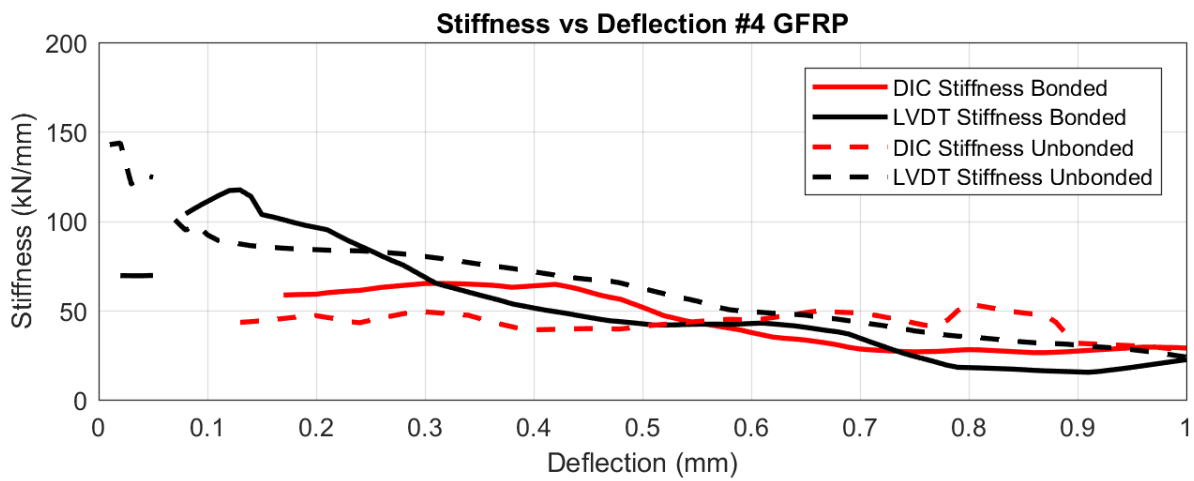
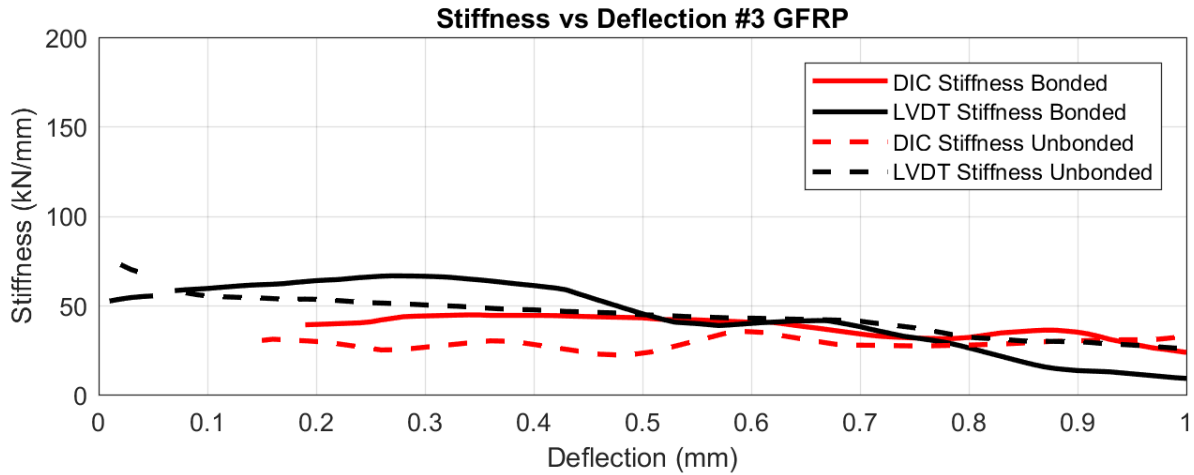


Figure B.4 Push-through average stiffness curves through 1 mm of deflection

Appendix C – Temperature plots

Temperature of all IWP specimens were recorded during the heating and cooling phase of the thermal tests. Thermocouples were placed at three locations as shown in Chapter 4, at midspan, and at the ends of the panel. The surface of the hot wythe, and the concrete to insulation interface were recorded. The following figures show the recorded temperature for the duration of the IWP tests.

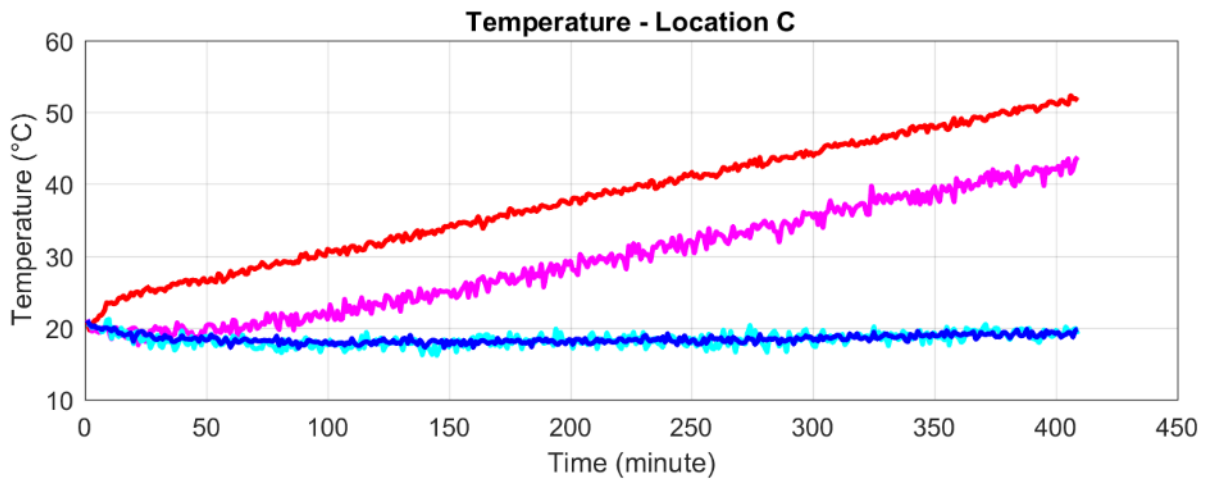
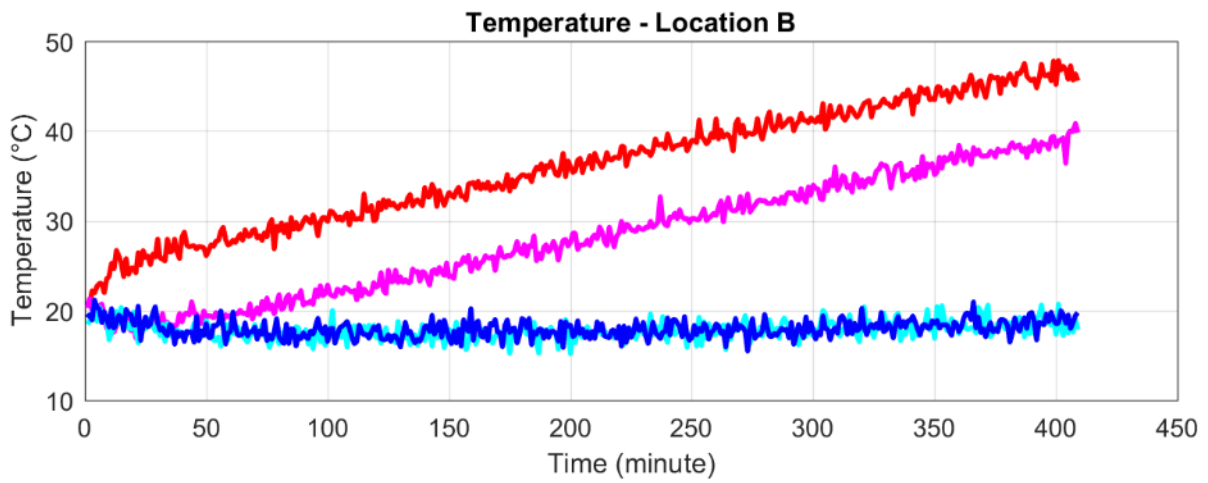
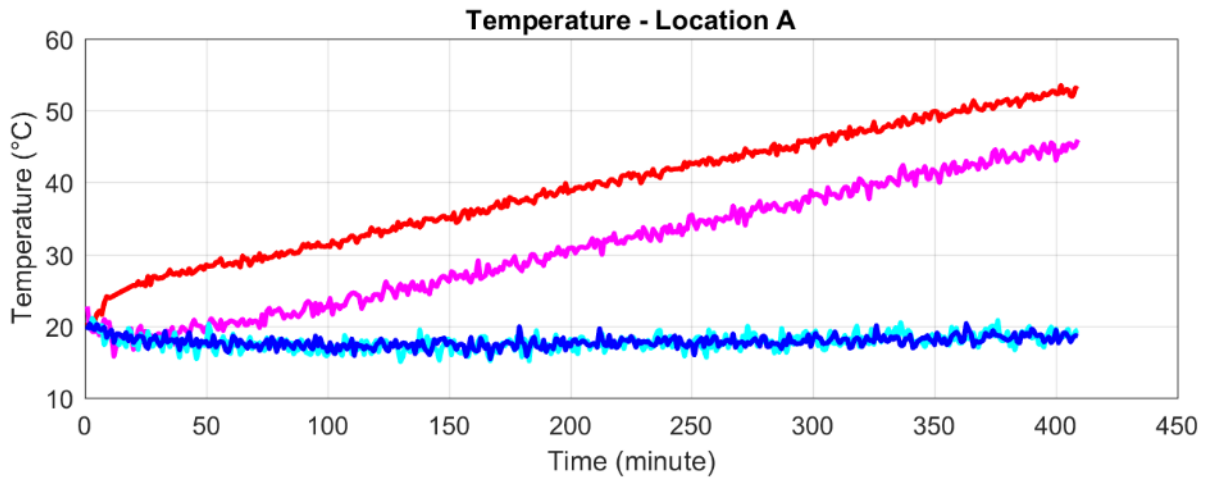


Figure C.1 IWP-5B Heating cycle

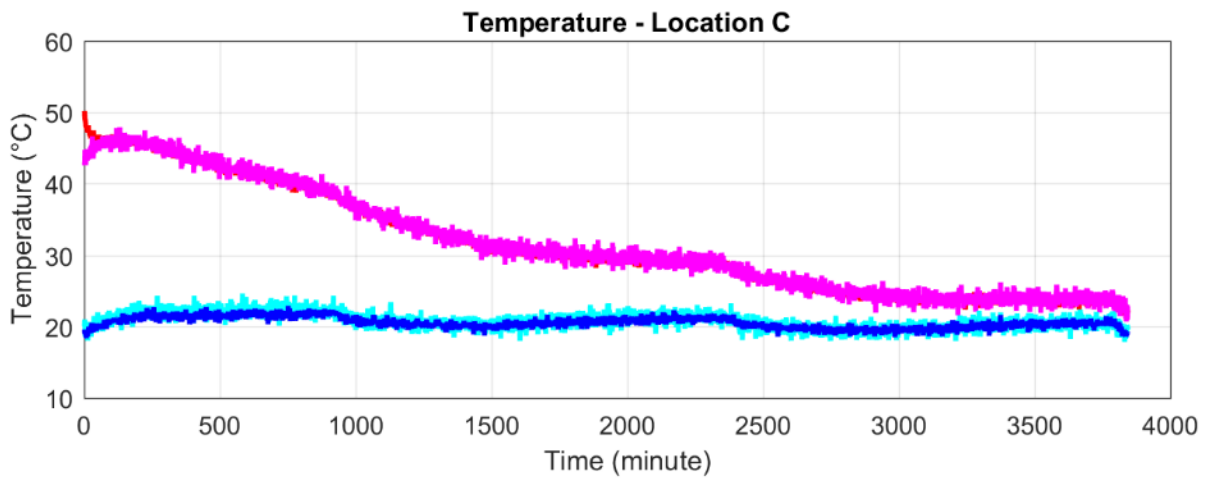
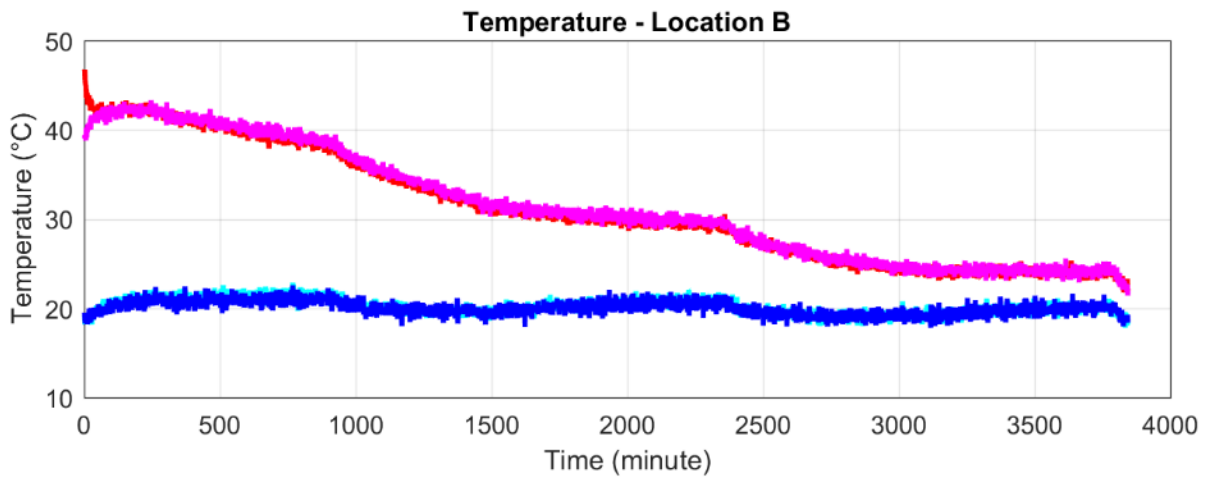
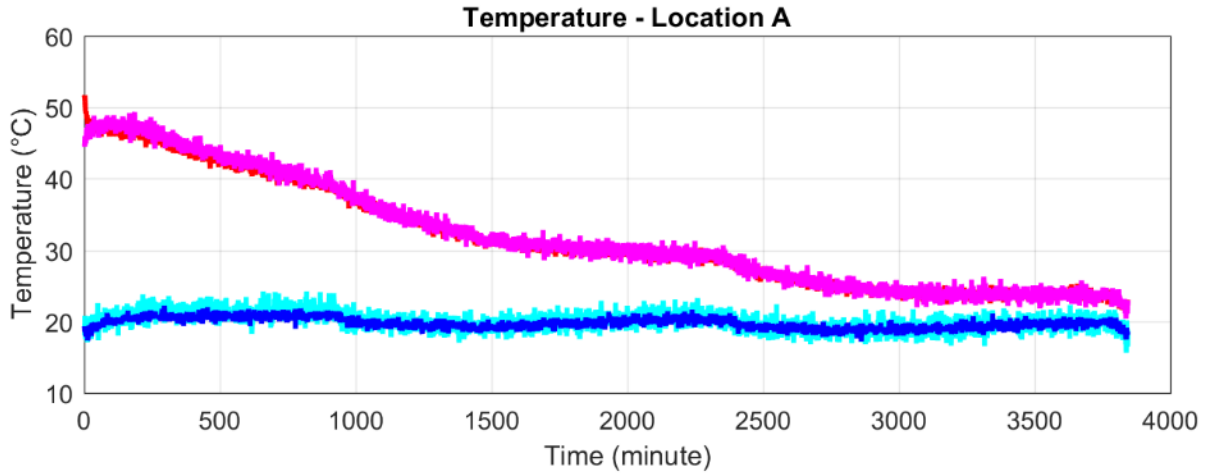


Figure C.2 IWP-5B Cooling cycle

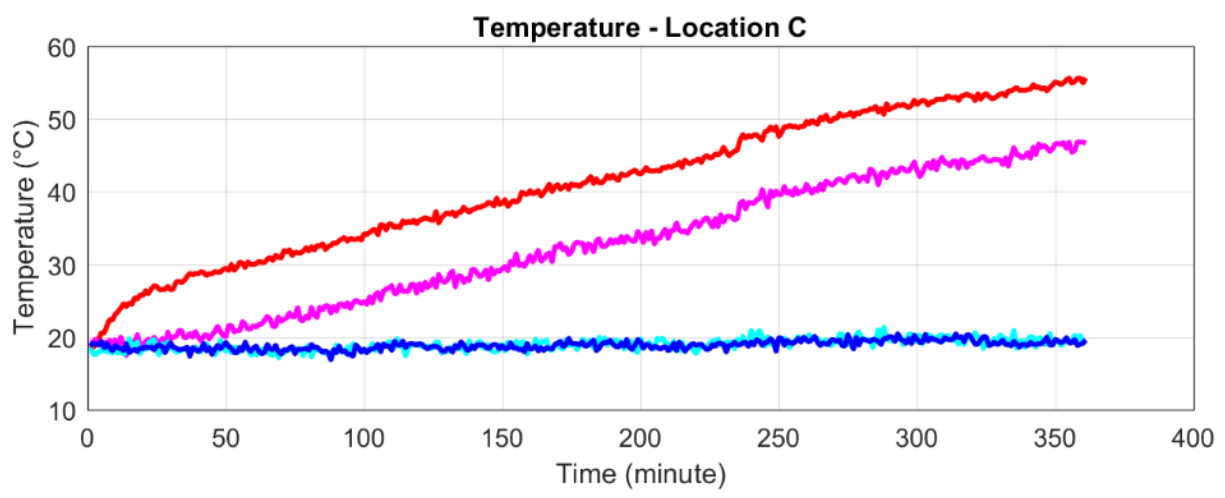
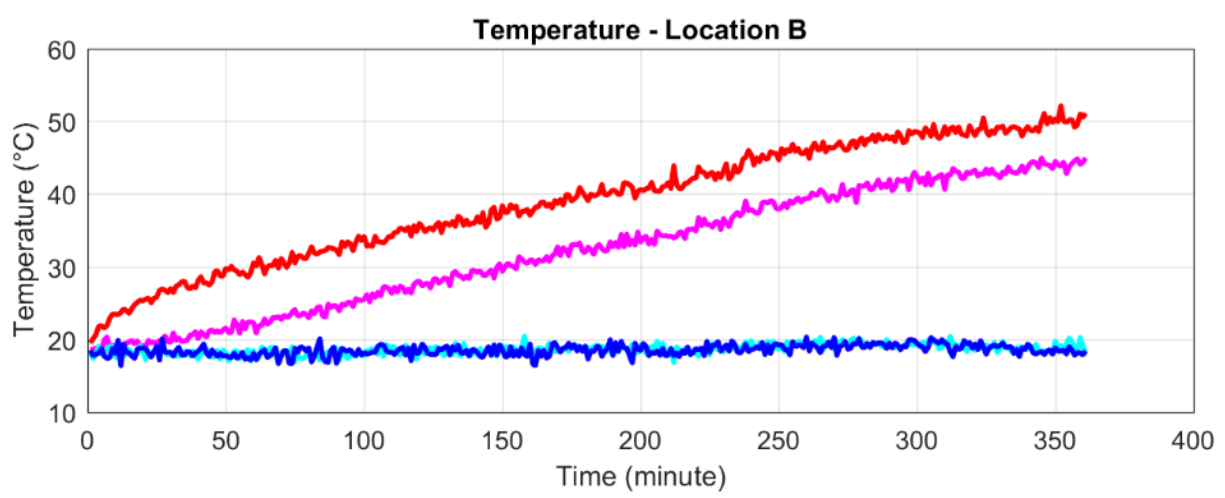
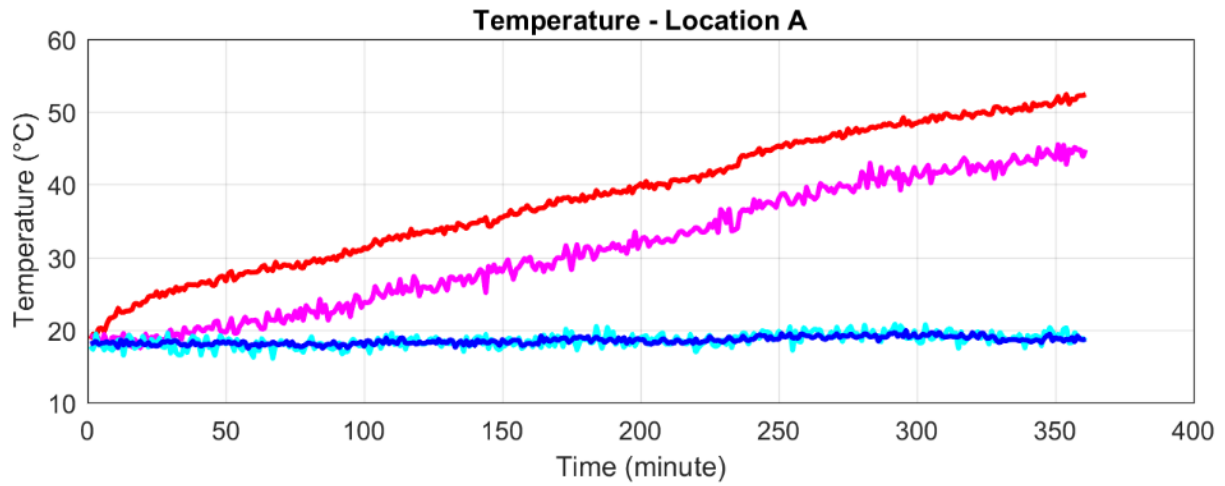


Figure C.3 IWP-4B Heating cycle

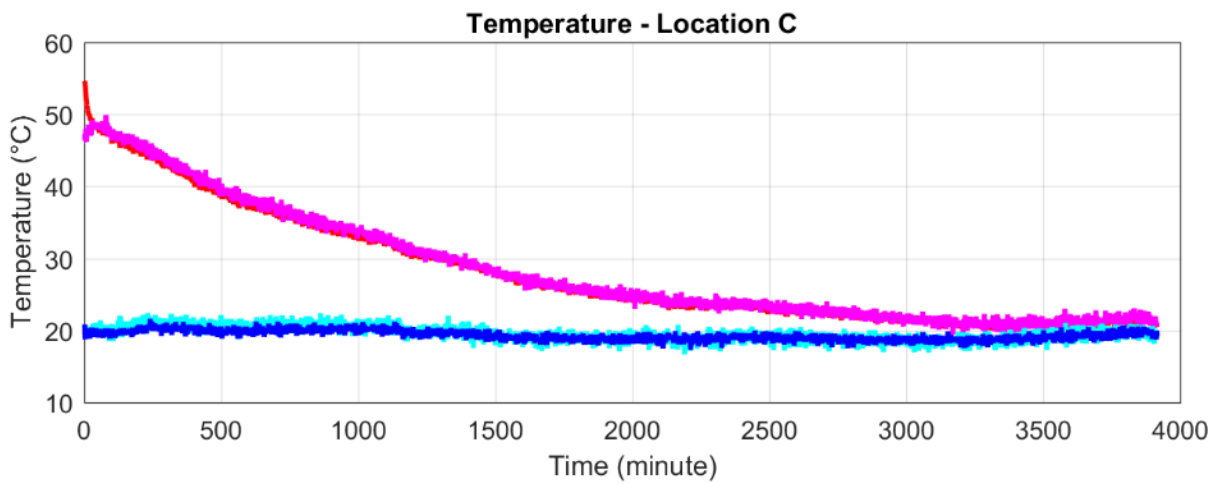
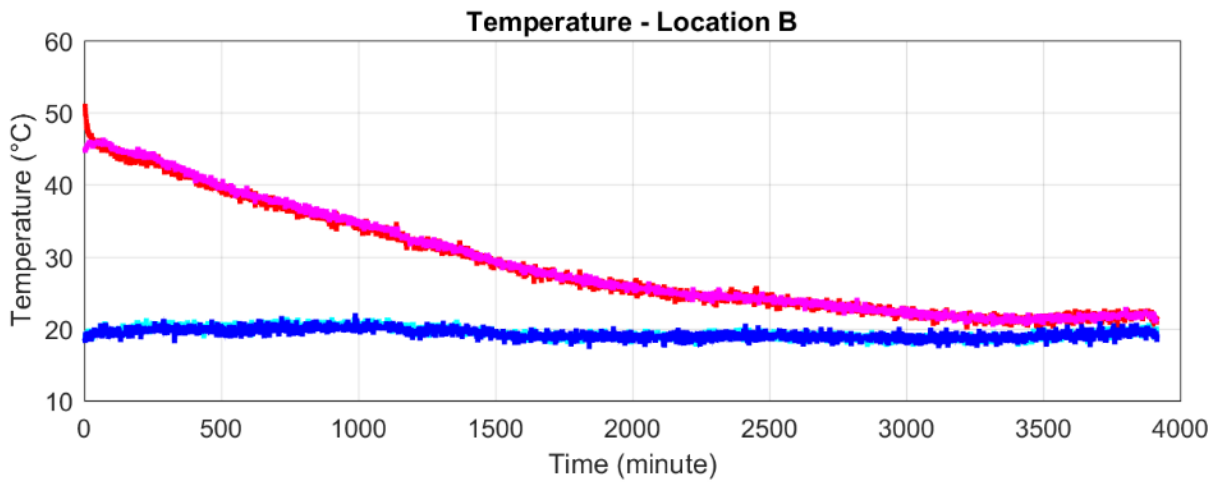
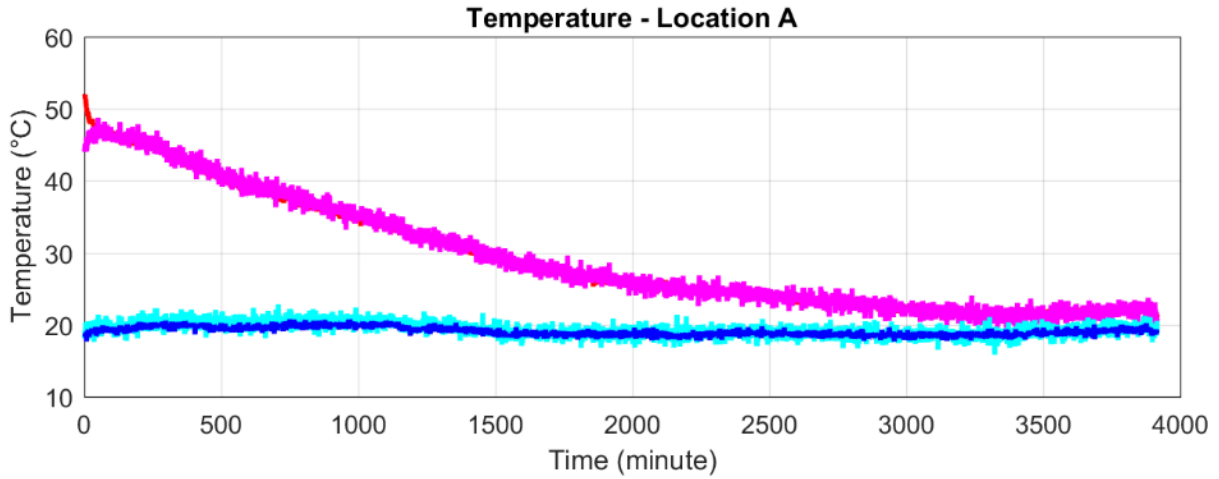


Figure C.4 IWP-4B Cooling cycle

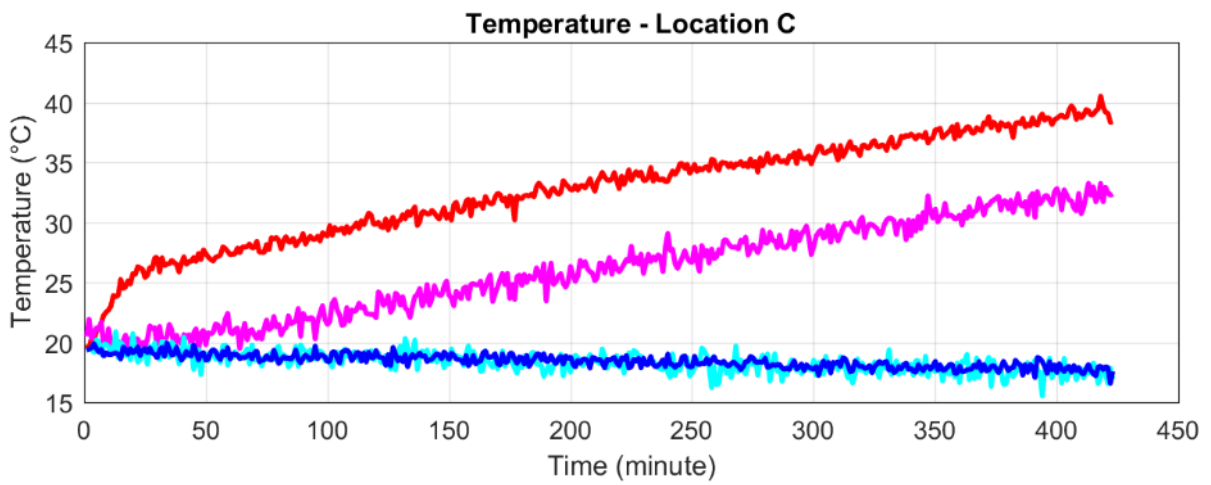
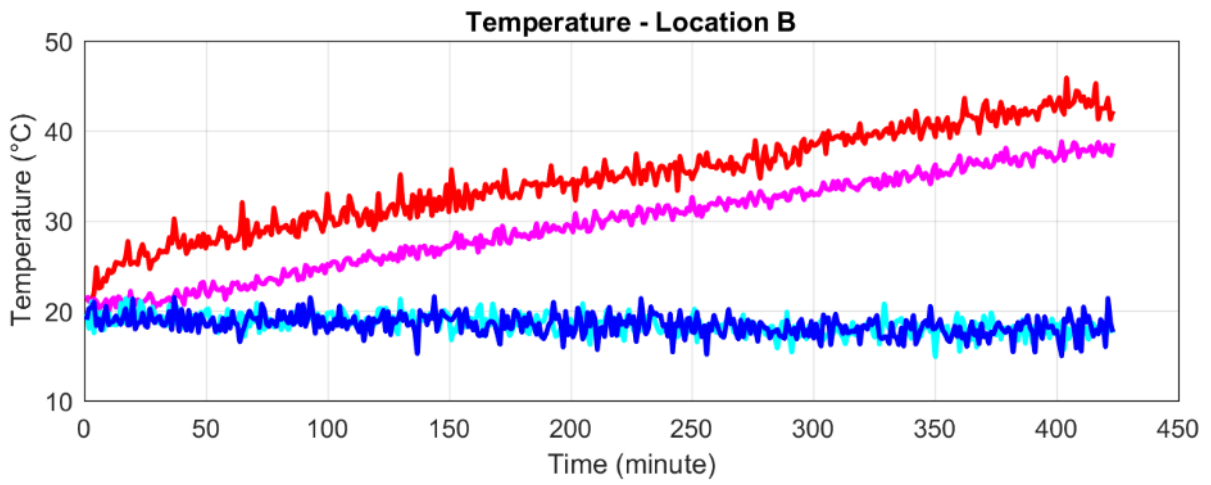
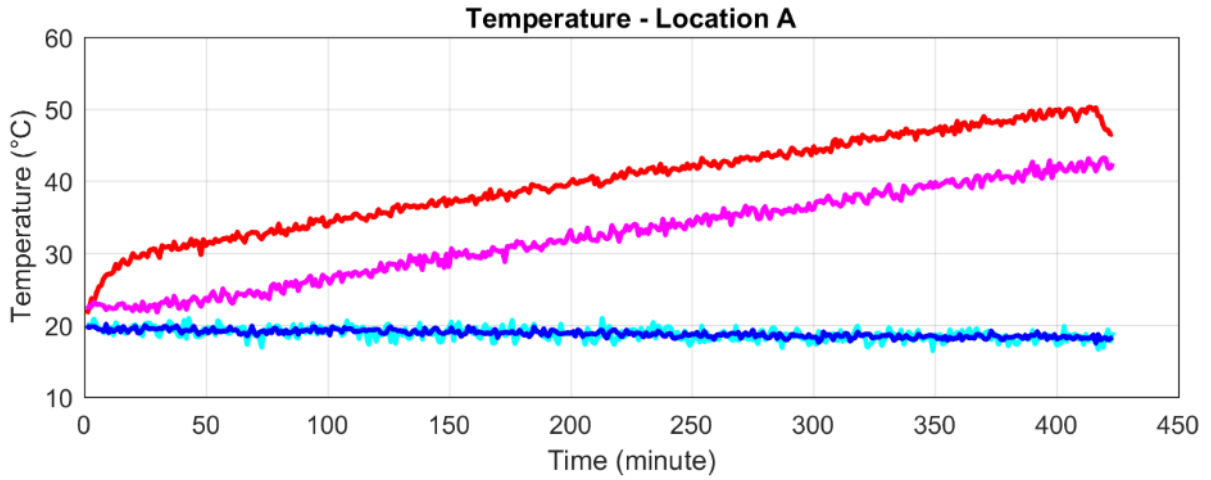


Figure C.5 IWP-3B Heating cycle

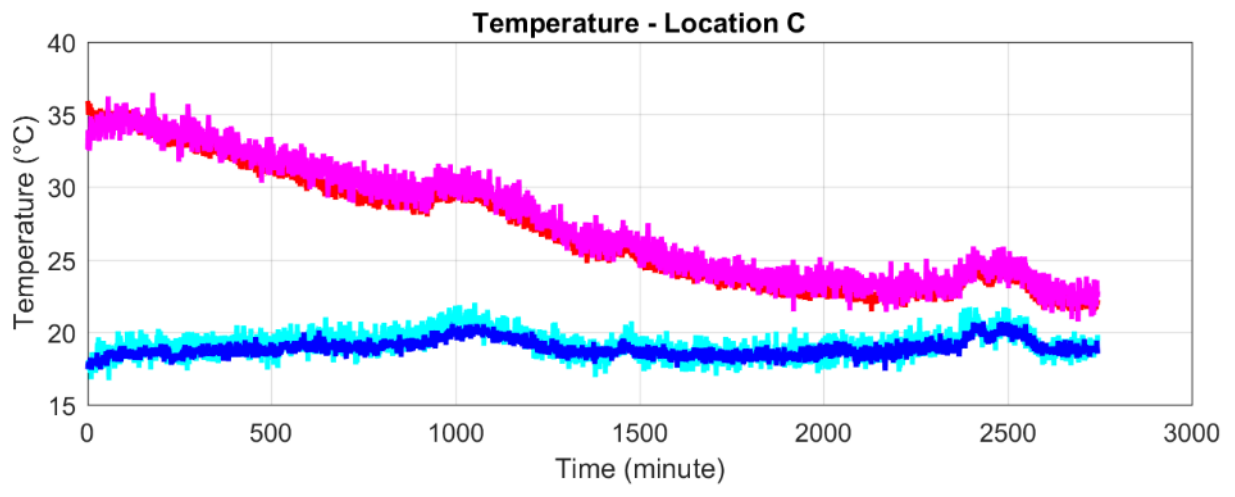
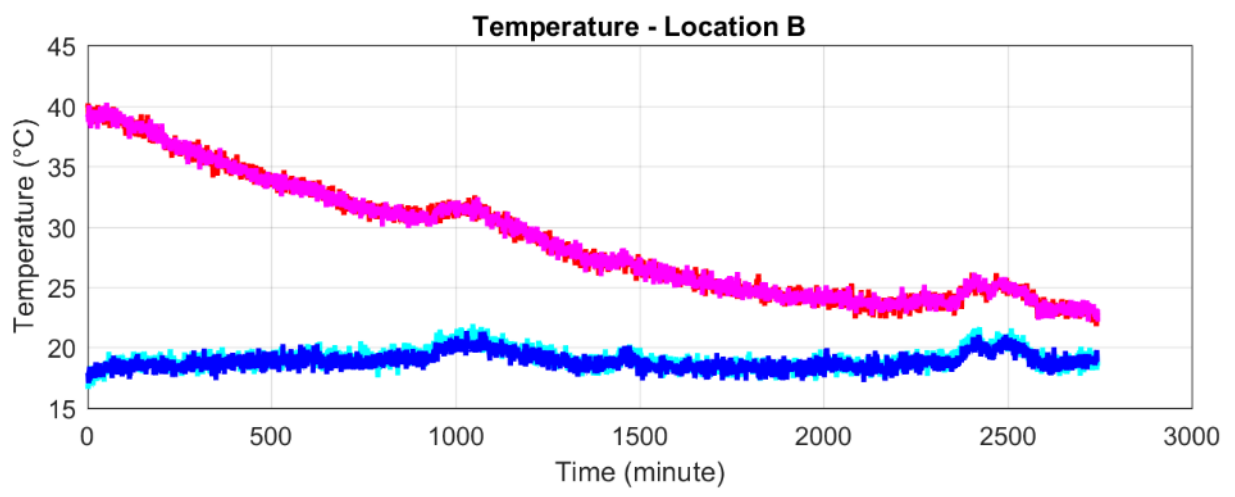
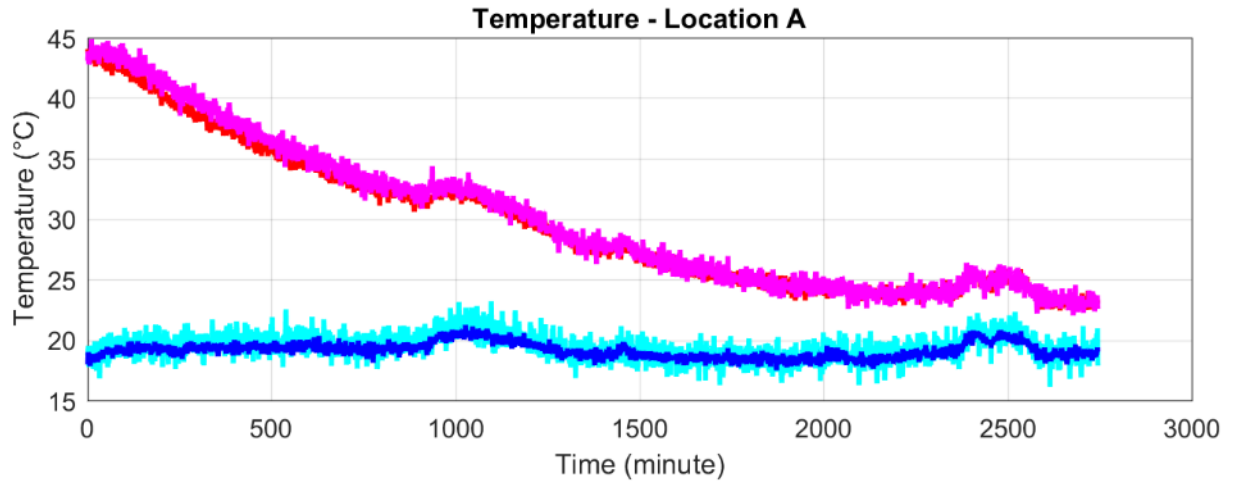


Figure C.6 IWP-3B Cooling cycle

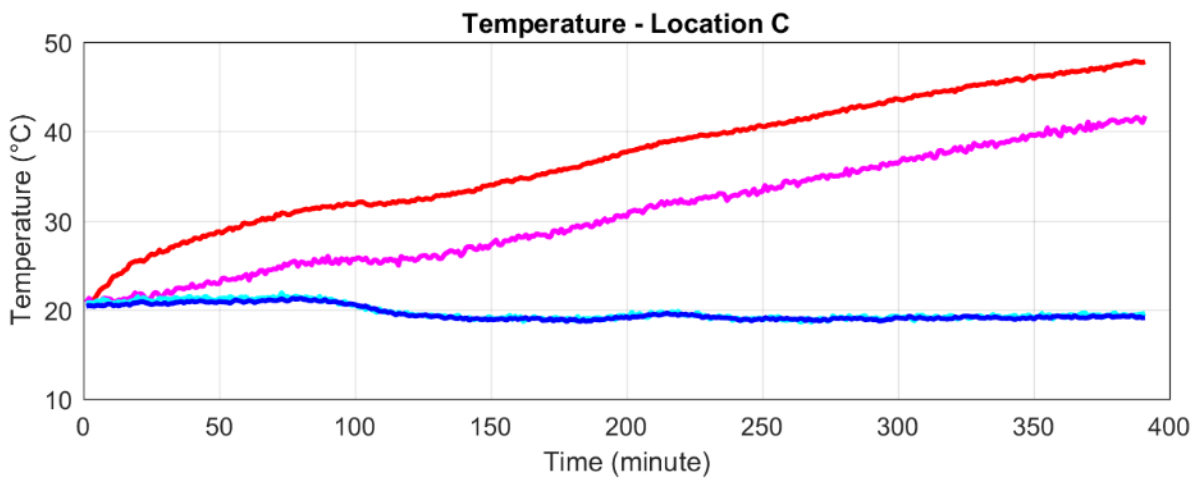
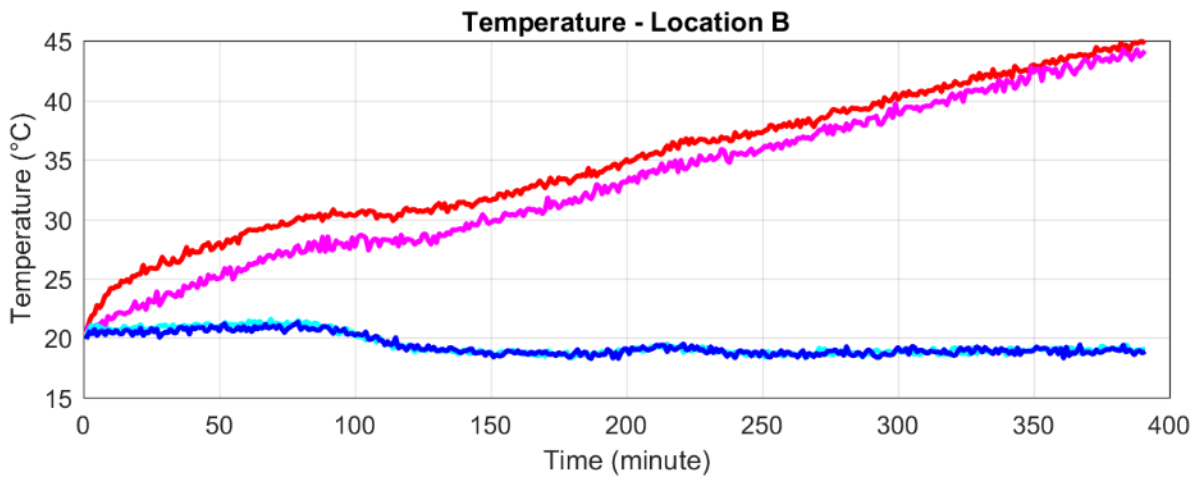
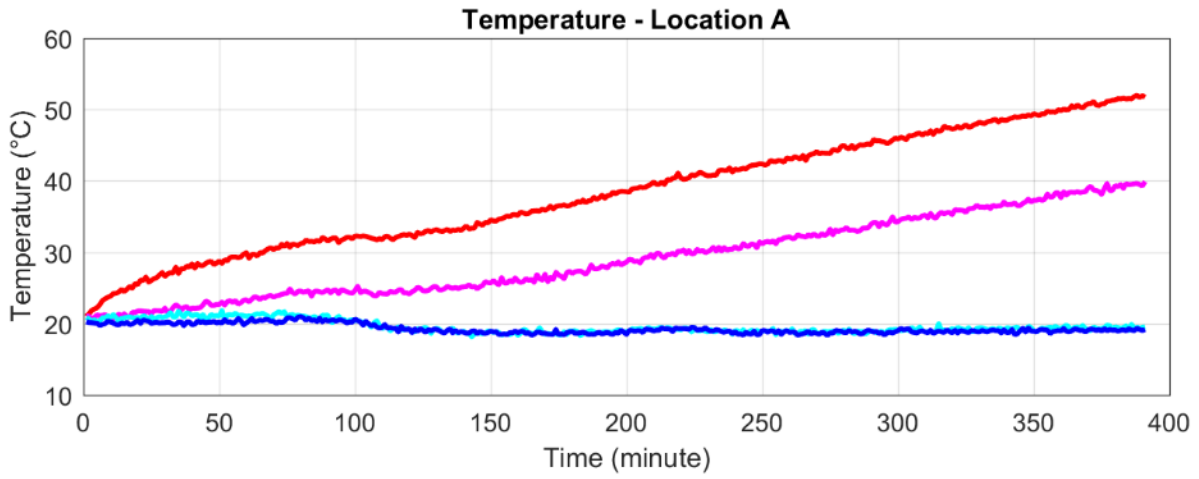


Figure C.7 IWP-4U Heating cycle

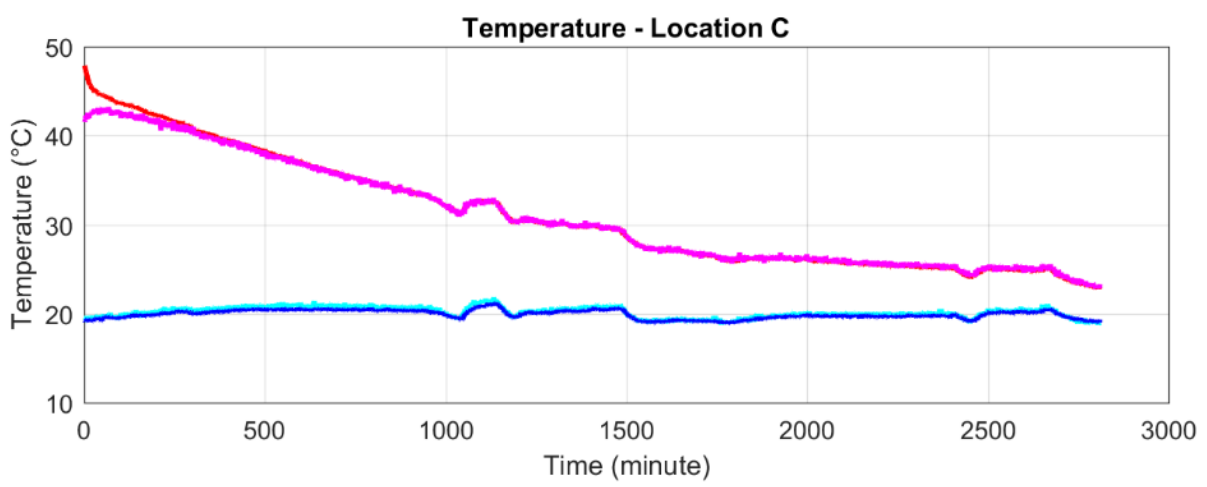
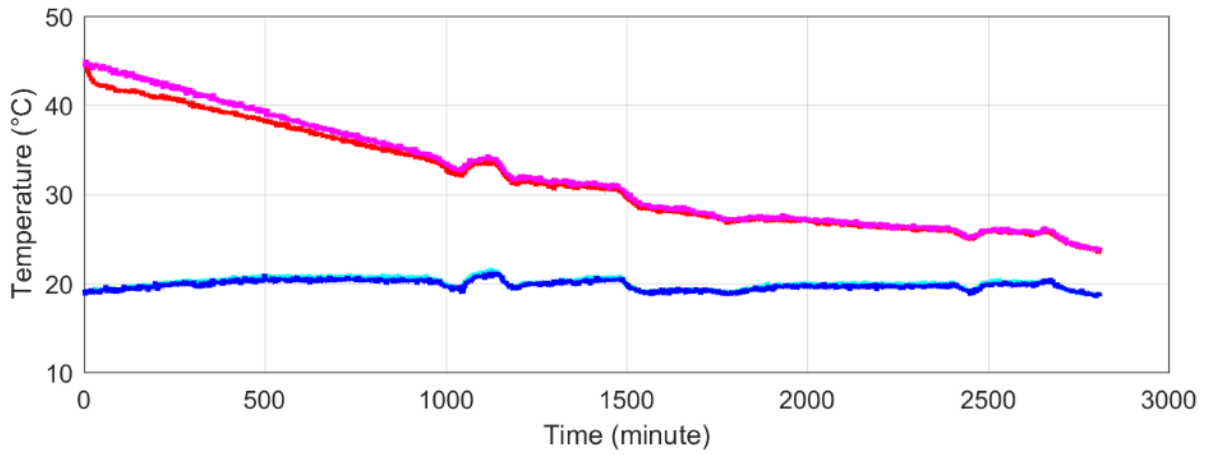
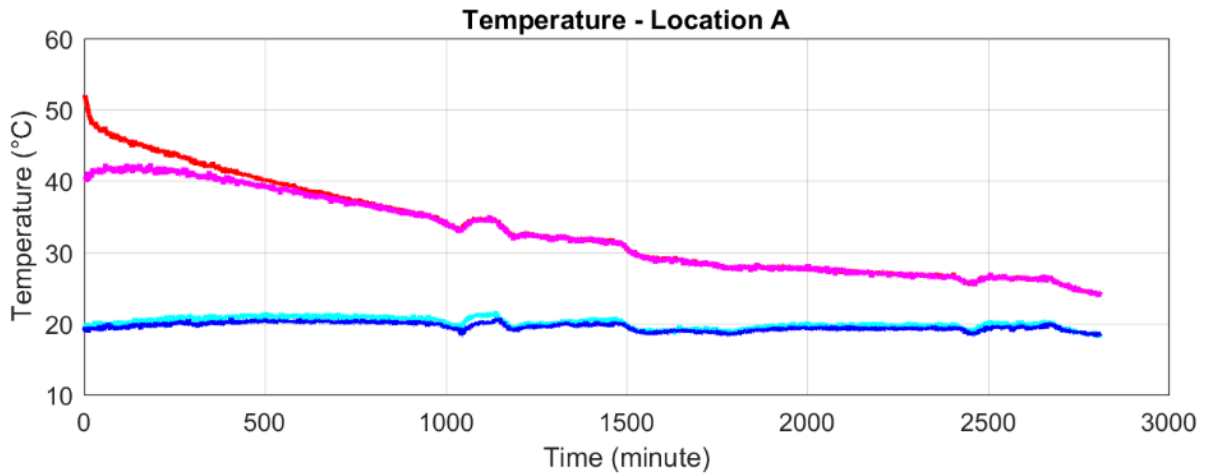


Figure C.8 IWP-4U Cooling cycle

Appendix D – Material properties

Material properties used through the push-through and thermal experimentation are found here. ASTM tests were done on 10M bar, WWM, Insulation, and concrete cylinders. Results such Young’s Modulus, yield stress, compressive strength are presented with their average and standard deviations for all test specimens. The manufactures data sheet for the XPS insulation is also attached.

10M Bar						
	Specimen 1	Specimen 2	Specimen 3	Specimen 4	Average Value	SD
E (GPa)	199	194	201	204	200	4.07
f_y (MPa)	403	414	414	431	415	11.8
f_u (Mpa)	616	609	621	619	616	5.12
Diameter (mm)	11.3	11.3	11.2	11.2	11.3	0.06
Area (mm ²)	100	100	98.5	98.5	99.4	1.02
WWM						
	Specimen 1	Specimen 2	Specimen 3	Specimen 4	Average Value	SD
E (GPa)	195	202	206	199	201	4.54
f_y (MPa)	485	498	506	490	495	9.31
f_u (Mpa)	505	519	535	492	513	18.8
Length (mm)	203	203	203	203	203	0.00
Diameter (mm)	6.30	6.30	6.30	6.40	6.33	0.05
Area (mm ²)	31.2	31.2	31.2	32.2	31.4	0.50
Insulation						
	Specimen 1	Specimen 2	Specimen 3	Average Value	SD	
Thickness (mm)	76.2	76.2	76.2	76.2	0.00	
Length (mm)	139	139	139	139	0.00	
Area (mm ²)	3548	3548	3548	3548	0.00	
f_c (MPa)	0.253	0.251	0.255	0.253	0.01	
Concrete Cylinders 28 Days						
	Specimen 1	Specimen 2	Specimen 3	Average Value	SD	
E_c (GPa)	25990	23223	21151	23455	2427.80	
f_c (Mpa)	52.10	52.10	52.15	52.12	0.03	

Property and Test Method*	Value
Density, ASTM D1622, lb/ft ³	1.8
Compressive Strength ⁽¹⁾ , ASTM D1621, psi, min., vertical	20
Tensile Strength, ASTM D1623, lb/in ² , min., vertical	50
Shear Strength, ASTM C273, lb/in ² , min.	25
Shear Modulus, ASTM C273, lb/in ² , min.	300
Flexural Strength, ASTM C203, lb/in ² , min., extruded	40
Flexural Modulus, ASTM C203, lb/in ² , min., extruded	1,500
Water Absorption, ASTM C272, % by vol., max.	0.3
Water Vapor Permeance ⁽⁴⁾ , ASTM E96, perm, max.	1.5
R-Value ⁽²⁾ per inch (25 mm), ASTM C518, °F•ft ² •h/Btu, fresh @ 55°F (13°C) min	7.2 **
per inch (25 mm), ASTM C518, °F•ft ² •h/Btu, fresh @ 20°F (-7C) min.	8.0 **
Surface burning characteristics ⁽³⁾ , ASTM E84	
Flame Spread Index	15
Smoke Developed Index	165

⁽¹⁾Vertical compressive strength measured at 10 percent deformation or at yield, whichever occurs first.

⁽²⁾R means resistance to heat flow. The higher the R-value, the greater the insulating power.

⁽³⁾This numerical flame spread rating is not intended to reflect hazards presented by this or any other material under actual fire conditions.

⁽⁴⁾Actual water vapor permeance for 1" thick material. Value decreases as thickness increases

* Properties shown are representative values for 1" thick material

** Per DOE-10 CFR Appendix B to Subpart R of Part 431. For foam produced as board stock "final chemical form" means after extrusion and ready for assembly into a panel or after assembly into a panel.

Figure D.1 Dowchemical XPS Panelmate information (url:

http://msdssearch.dow.com/PublishedLiteratureDOWCOM/dh_09ae/0901b803809ae2ae.pdf?file_path=styrofoam/pdfs/noreg/179-08123.pdf&fromPage=GetDoc)

Appendix E – Time plots

Plots of deflection and end slip with respect to time are found here. The time is recorded in minute increments for both the heating and cooling phase. End slip in this section is split into north, south, and total end slip.

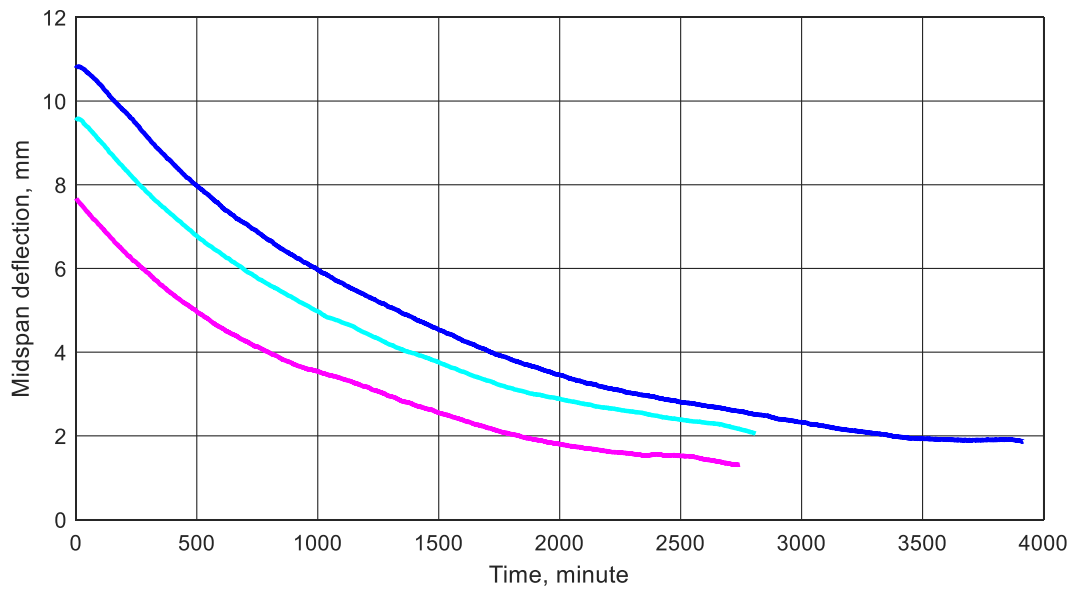
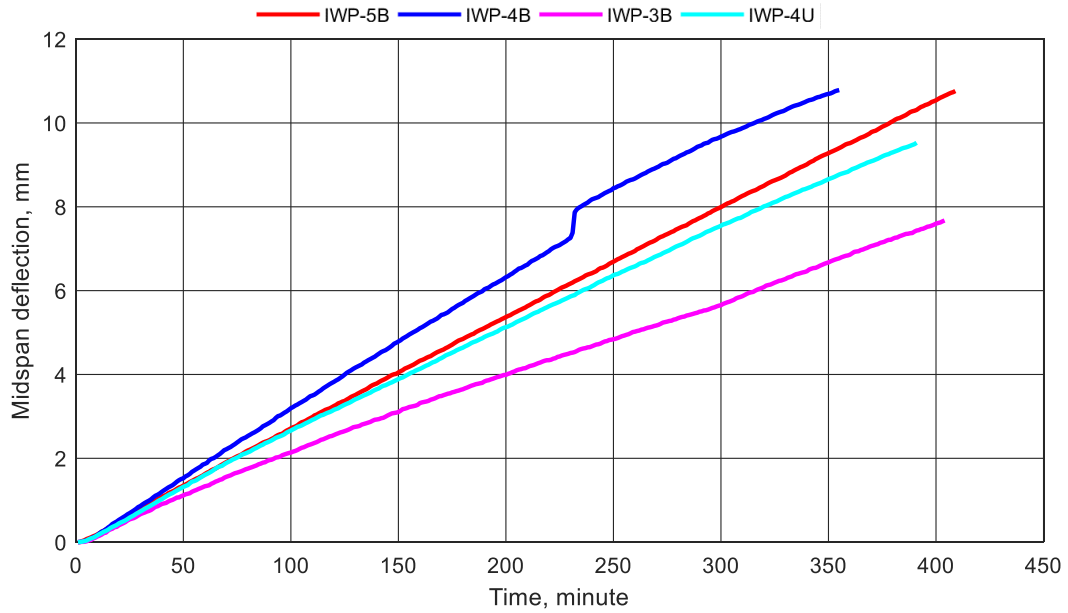


Figure E.1 Midspan deflection with respect to time

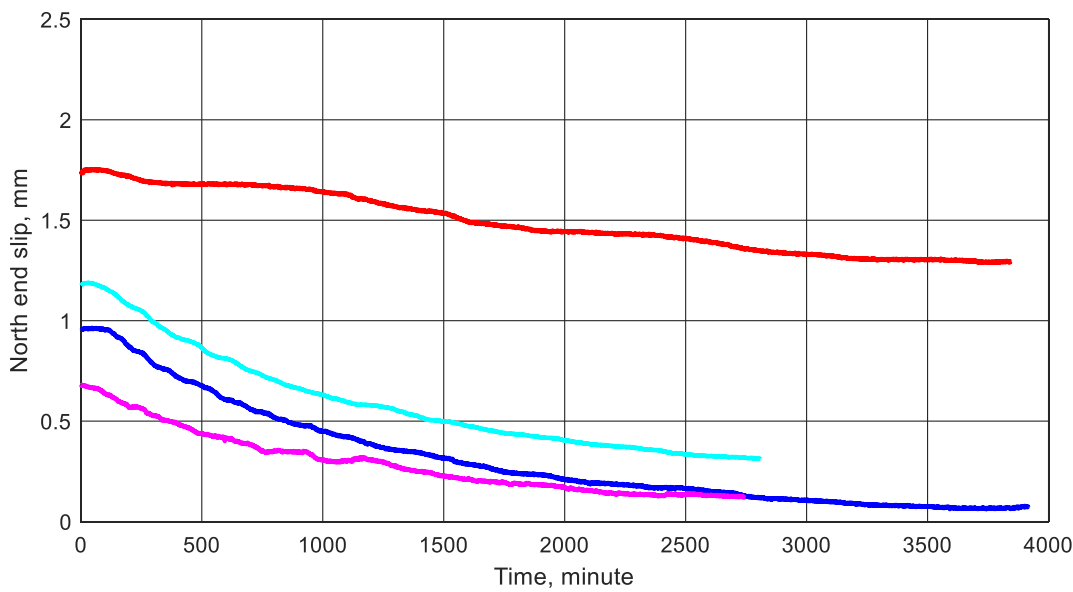
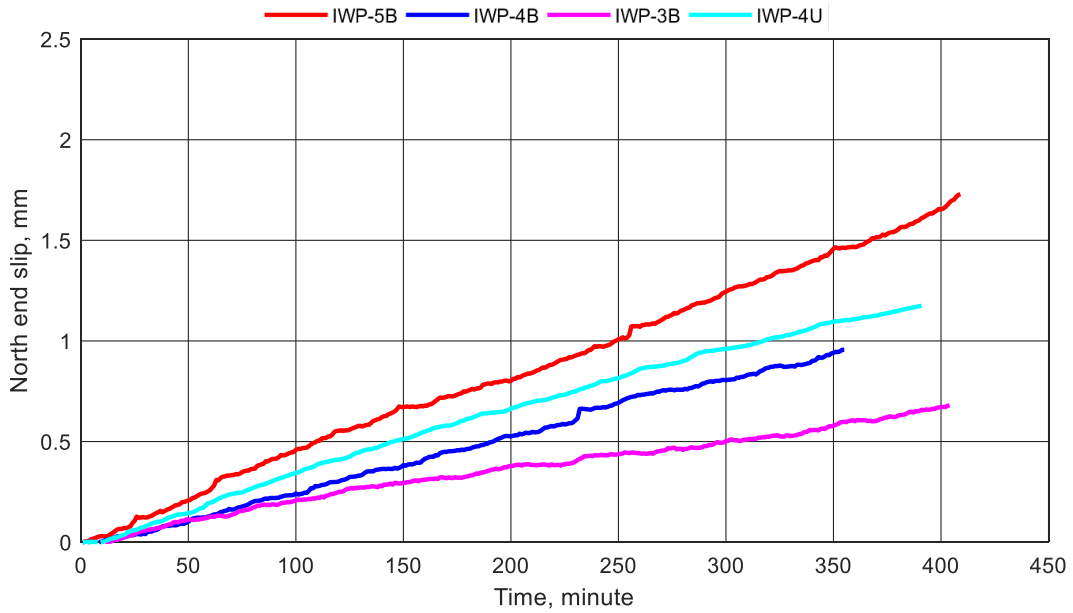


Figure E.2 North end slip with respect to time

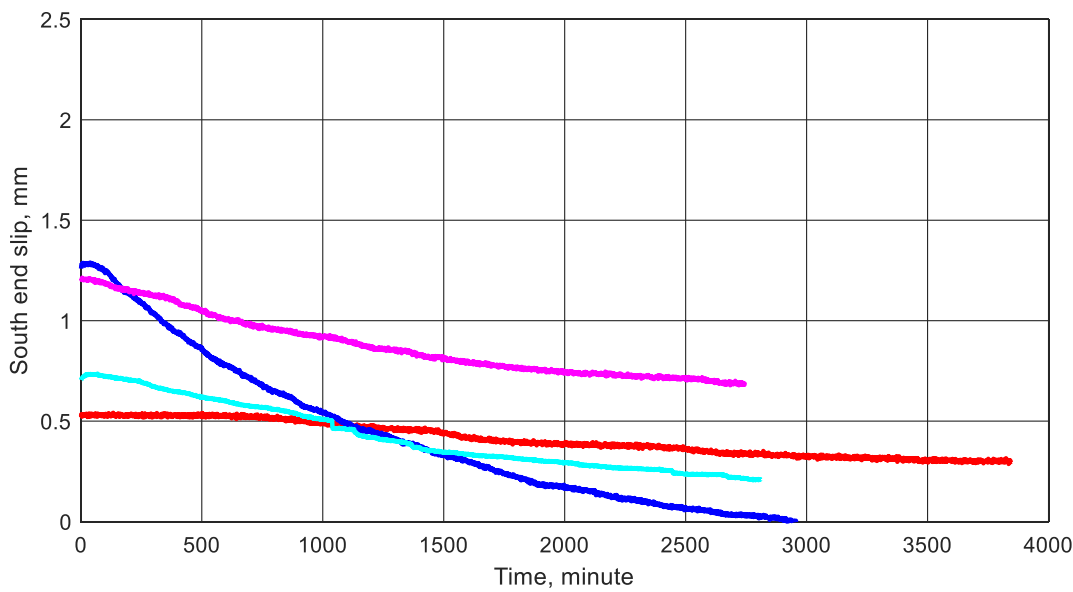
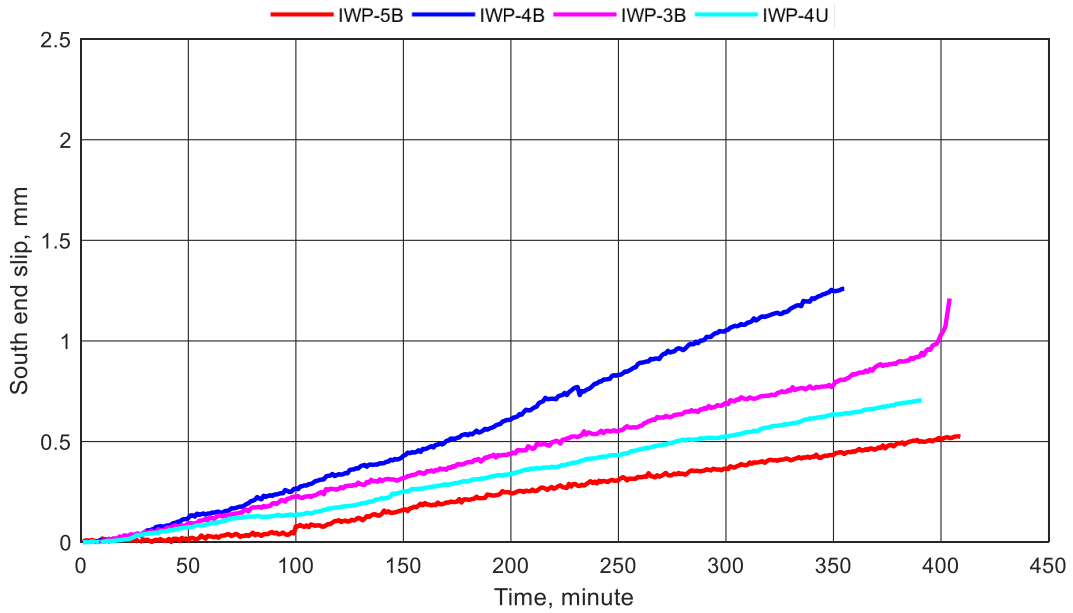


Figure E.3 South end slip with respect to time

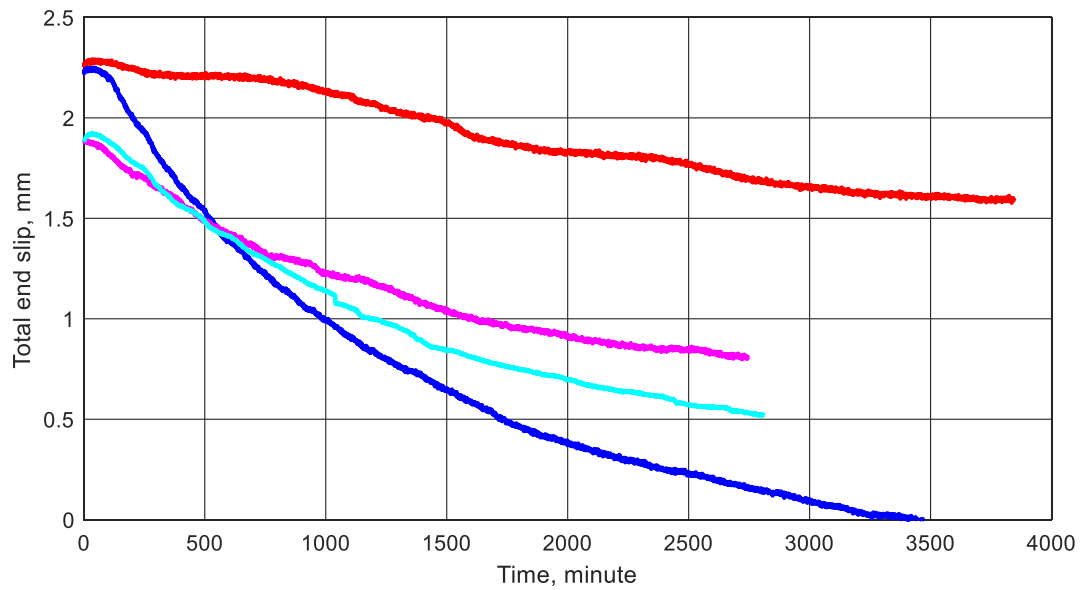
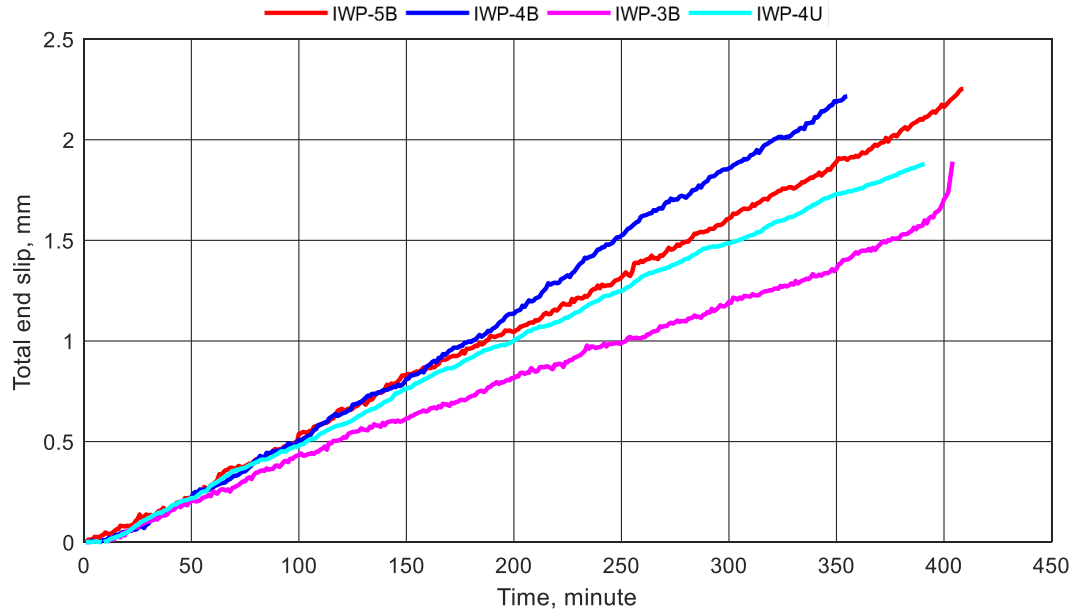


Figure E.4 Total end slip with respect to time